The Characterization of TiC and Ti(C,N) Based Cermets with and without Mo_2C

by

Tyler Stewart

Submitted in partial fulfillment of the requirements
for the degree of Master of Applied Science

at

Dalhousie University
Halifax, Nova Scotia
February 2014

Table of Contents

List of Tables

List of Figures

Abstract

Titanium carbide (TiC) and titanium carbonitride (Ti(C,N)) are both common components in hard, wear resistant ceramic-metal composites, or cermets. In this study the intermetallic nickel aluminide (Ni_3Al) has been used as a binder for the production of TiC and Ti(C,N) based cermets. These cermets offer several improved characteristics relative to conventional WC-based 'hardmetals', such as lower mass and improved oxidation resistance, which are also combined with high fracture resistance, hardness and wear resistance. The cermets were produced using an *in-situ*, reaction sintering procedure to form the stoichiometric Ni_3Al binder, with the binder contents varied from 20 to 40 vol%. However, for high N content Ti(C,N) cermets, the wettability of molten Ni_3Al is relatively poor, which leads to materials with residual porosity. Therefore various amounts of Mo_2C (1.25, 2.5, 5 and 10 vol%) were incorporated into the $Ti(C_{0.3},N_{0.7})$-Ni_3Al cermets, with the aim of improving the densification behaviour. Mo_2C was found to improve upon the wettability during sintering, thus enhancing the densification, especially at the lower binder contents. The tribological behaviour of TiC and Ti(C,N) cermets have been evaluated under reciprocating sliding conditions. The wear tests were conducted using a ball-on-flat sliding geometry, with a WC-Co sphere as the counter-face material, for loads from 20 to 60 N. The wear response was characterised using a combination of scanning electron microscopy, energy dispersive X-ray spectroscopy, and focused ion beam microscopy. Initially, two-body abrasive wear was observed to occur, which transitions to three-body abrasion through the generation of debris from the cermet and counter-face materials. Ultimately, this wear debris is incorporated into a thin tribolayer within the wear track, which indicates a further transition to an adhesive wear mechanism. It was found that Mo_2C additions had a positive effect on both the hardness and indentation fracture resistance of the samples, but had a detrimental effect on the sliding wear response of the cermets. This behaviour was attributed to increased microstructural inhomogeneity with Mo_2C additions.

List of Abbreviations and Symbols Used

CIP Cold Isostatic Press

EDS Energy-dispersive X-ray Spectroscopy

SEM Scanning Electron Microscope

XRD X-ray Diffraction

UMT Universal Micro-Tribometer

CVD Chemical Vapour Deposition

PVD Physical Vapour Deposition

PVB Polyvinyl Butyral

SHS Self-propagating High temperature Synthesis

SPS Spark Plasma Sintering

Acknowledgements

I would like to thank those that guided me throughout this project, especially my supervisor Dr. Kevin Plucknett. As well as the other students in the research group that are directly supervised by Dr. Plucknett. I would also like to thank Patricia Scallion for her assistance on both the SEM and FIB, along with Dean Grijm for help with manufacturing lab equipment. Furthermore, great appreciation is directed towards Boeing for the provision of funding for the project.

Finally, I would like to thank my family for their help in getting me where I am today.

1 Introduction

Titanium carbonitride (Ti(C,N)) is a ceramic material that has gained a lot of attention in recent years due to its excellent properties such as high hardness, chemical inertness, high thermal conductivity and high melting temperature. All the properties listed make Ti(C,N) an ideal candidate to be used in the ceramic-metal composite (or cermet) based family of materials, especially when coupled with the intermetallic nickel aluminide (Ni_3Al). Ni_3Al has many attractive properties including excellent oxidation resistance up to relatively high temperatures (~1100°C) due to the formation of a protective Al_2O_3 surface layer, along with the ability to retain its strength at elevated temperatures. Ti(C,N)-Ni_3Al based cermets borrow the attractive properties from their constituents to give materials that are relatively low in mass, very hard, and have good corrosion and wear resistance characteristics.

The purpose of this project is to develop the bulk cermet material that is to be later used as a base material in thermal spray coatings. The cermets were manufactured through a reaction sinter process to create samples with 20 to 40 vol% Ni_3Al, coupled with TiC, $Ti(C_{0.7},N_{0.3})$, $Ti(C_{0.5},N_{0.5})$, or $Ti(C_{0.3},N_{0.7})$ as the ceramic matrix. For the high N ceramic phase (i.e. $Ti(C_{0.7}N_{0.3})$), Mo_2C was also added as an alloy addition from 1.25 to 10 vol% in order to correct the poor wettability those samples experienced. To characterize the various samples, the Vickers hardness and indentation fracture resistance (IFR) were assessed. For the main emphasis of the thesis, the specific wear rates of the cermets were determined, through application of reciprocating wear tests, using a ball on flat sliding geometry with a tungsten carbide-cobalt (WC-Co) counter face sphere.

The present thesis is divided into seven chapters, which display the various stages of work completed throughout the project. In Chapter 2 the theory and literature review needed in order for the reader to fully comprehend the material presented in later chapters is presented. In Chapters 3 and 4 the materials, methods and results that are not presented in Chapters 5 and 6 are displayed. In Chapters 5 and 6 the manuscripts that are submitted for publication are presented, these manuscripts have not been altered in any way other than to display the correct page number in sequence with the remainder of the thesis. Chapter 7 provides an overview of all the work presented through the thesis, highlighting

several of the main conclusions, and also presents an outline of selected future work that should be considered for studies in similar areas.

2 Literature Review

In the following chapter the background information that is needed to provide a basic understanding of the results presented in Chapters 4 and 5 is outlined. A brief overview of cermets and their applications is discussed, along with the properties of the constituents of the cermets used in this particular study, including the microstructural features and typical alloy additions added to the cermets. The basic theory of how such samples are manufactured is also provided, including powder compaction and sintering. The methods used to characterize the materials upon fabrication, which include the hardness, indentation fracture resistance and wear response are discussed in detail, with the typical response seen in Ti(C,N)/TiC based cermets also presented. Finally, since the overall goal of this study is to produce bulk materials that will ultimately be developed as thermal spray coatings, a general background for thermal spray coatings is also presented.

2.1 Introduction to Cermets

Today's aerospace manufacturing industry is demanding better materials constantly in order to increase productivity and reliability of their equipment, and thus lower maintenance costs. In addition, there is a strong drive to lower operating mass and therefore make aircraft more fuel efficient. There are several key attributes that are desirable in the materials that will help realize these goals, such as high wear and corrosion resistance, good hardness and toughness, being environmentally friendly, high performance at extreme temperatures and relatively low manufacturing costs.

Having high wear and corrosion resistance is crucial for a part to survive long periods of time in the high wear environments that the landing gear of aircraft are subjected to. If the part is able to continually successfully survive during use at these conditions it not only reduces costs in repairing and replacement but it also increases the safety factor of the structure as a whole. Although having a highly corrosive resistant material is very important, having a mechanically sound material is equally as essential. Two key characteristics that one must consider when selecting a suitable material is therefore the hardness and toughness behaviour because without having respectable performances in these areas the integrity of the structure would quickly be compromised, especially at the extreme working conditions they are immersed in. Finally, environmentally friendly

processes and materials are important, so as to not cause unneeded contamination to the working environment and to meet the strict rules and regulations set by the industry.

There are many different types of materials that meet some combination of the required properties, but there are very few that meet all of the requirements together. One family of materials that meets essentially all of these needs is ceramic-metal composites, which are often referred to as ‘cermets’. These composites were first developed by the allies during the Second World War in the search for a material that had the high temperature resistance of ceramics along with the toughness and ductility of cemented carbides (i.e. WC-Co). The term ‘cermet’ comes from the combination of a relatively brittle but hard ceramic matrix with a tough metallic 'binder'. Typical applications of cermets include use as a protective coating layer on the inside of pipelines that carry oil and gas, machining and tooling purposes (including cutting tools and compaction/forming dies), high performance braking systems for cars, and also as a form of ballistic protection for equipment and personnel in the military. However the main focus of this study will be to study a cermet that is to be used as a replacement for the hard chrome components currently used in the landing systems of aircraft.

There are numerous types of cermet systems that have had extensive research conducted upon them, including those based on titanium carbide (TiC) or titanium carbonitride (Ti(C,N)) as the ceramic phases. Traditional ‘hardmetals’, which are tungsten carbide (WC) embedded into a cobalt binder, serve the same purpose as cermets but have relatively poor oxidation and corrosion resistance, together with a high density, which prevents them from being used for most structural applications at high temperatures. Therefore they are primarily used for cutting and machining applications because of their combination of high strength, toughness and hardness, which leads to good wear resistance.[1] For that reason a more promising base for a cermet system to be used as an aerospace coating are the lighter, more heat resistant TiC and Ti(C,N) families. In Ti(C,N) based cermets, the hardness and toughness of the materials can be controlled considerably by the amounts of TiC and TiN present, because the hardness increases with TiC content, while the toughness increases with the fraction of TiN. Typical metallic binders that have been used in these cermets include nickel, cobalt, stainless steels and

most recently nickel aluminide (Ni_3Al).[2] Ni_3Al is of particular interest because of its high temperature resistance and high strength retention at elevated temperatures.

2.2 Titanium Carbonitride

Titanium carbonitride (Ti(C,N)) is a binary solid solution of titanium carbide (TiC) and titanium nitride (TiN). Since both TiC and TiN are isomorphs of one another, the two can be substituted in the lattice framework while causing minimal strain on the system, therefore the behaviour of Ti(C,N) is very similar to that of TiC and TiN.[3]

TiC has attracted a large amount of interest for a great number of structural applications because of its inherit physical properties as a refractory ceramic. These properties include high hardness, good electrical conductivity, high chemical resistance and a relatively low density.[4] These attractive properties make TiC an ideal choice for applications such as cutting tools, grinding wheels, wear resistant coatings and high temperature heat exchangers.[4] It has also been employed as an additive to cemented carbides in order to make them harder. Although TiC is ideal for the previously listed applications, it cannot be used on its own in most cases because it is highly brittle and would simply fail under many circumstances. Therefore it is usually coupled with a relatively more ductile, tough material.

TiN is very similar to TiC, in the sense that it is a very hard, light and a highly temperature resistant ceramic, with an electrical conductivity comparable to that of steel. Although it does have a rather high melting temperature of around 2400°C it begins to form oxides in air at temperatures close to 800°C. Similar to TiC, TiN is chemically resistant and thermally stable but unlike TiC it is an excellent diffusion barrier.[3] It is also used as an additive to plastics like polyethylene terephthalate (PET), up to a certain content, because it improves the thermal properties of PET bottles.[5]

2.2.1 Production of Titanium Carbonitride

For the most part, refractory carbides and nitrides such as TiC and TiN do not exist in a natural state. In addition, their synthesis is generally expensive and time consuming since these materials are highly refractory and inert, with strong covalent bonds that decompose or sublime upon melting. As a result they cannot be obtained through the

more traditional paths. It is because of this issue that they have not been extensively used until recently.[3] In general, refractory carbides and nitrides are available in several different forms including powders, monolithic shapes, coatings, fibers or whiskers. However, the form that is to be discussed further in the present work is the powdered TiC, TiN and Ti(C,N) materials, and there are presently several techniques that are used to produce them.

TiC, TiN and Ti(C,N) can be produced by direct carbonization or nitridation of elemental titanium metal or hydride. This process is very energy intensive because it requires temperatures between 1900°C and 2900°C, and times from 5 to 20 hours.[3] The final product is an extremely agglomerated powder, which requires further milling to produce fine particles, so additional chemical purification is then necessary to remove impurities picked up from the milling equipment.[6] Therefore, this method is very costly not only because of the price of pure titanium but also from being extremely energy intensive.[7]

The oldest and most common process that is used to produce TiC and TiN is to use TiO_2 as the starting reactant. Carbothermal reduction produces large quantities of powder, while making use of relatively inexpensive stating materials. If TiN is desired, a carbothermal reduction of TiO_2 is conducted in a nitrogen rich atmosphere, while if TiC is required, the reduction is performed with excess carbon.[8] These reactions are typically very slow, taking between 10 to 20 hours to go to completion; the chemical reaction equations for the reduction to produce TiC and Ti(C,N) are presented below:[8,9]

$$TiO_2(s) + 3C(s) = TiC(s) + 2CO(g) \qquad \text{Eqn 1}$$

$$TiO_2(s) + 3C(s) + 0.5N_2(g) = 2CO(g) + Ti(C,N)(s) \qquad \text{Eqn 2}$$

However, much like direct carbonization this method produces particles that are not uniform in size, and there is currently no commercial process that produces consistent submicron particles.[9] Therefore further milling is required to obtain fine particles. In addition, since oxygen is present in the starting material, it always contaminates the final product.[8]

Another technique that can be used to produce TiC powder can be to avoid the reaction step with TiO_2 and actually go directly to the source of it. Ilmenite ($FeTiO_3$) is the main source of TiO_2, which by itself is a useful material that is used in paint pigments and welding rod coatings.[10] Work has been done to test the feasibility of the carbothermal reaction of carbon with ilmenite and it was proven that it is possible to produce fine particles of TiC at a size around 12.8µm.[4] The reaction that takes place between the carbon and ilmenite can be seen in the equation below.

$$FeTiO_3(s) + 4C(s) = Fe(s) + TiC(s) + 3CO(g) \quad \text{Eqn 3}$$

The previously described techniques, which are used to produce TiC, TiN and Ti(C,N) powders, have several key flaws in the products they produce; mainly the large particle size and high amounts of impurities present in the final product. To tackle these problems another technique has been devised that produces oxygen-free powder particles that are consistently between 0.1µm and 0.5µm in size. This is done by a gas phase reaction that consists of a mixture of titanium halide ($TiCl_4$), a reductant vapour (Na or Mg) and a reactive gas (CH_4 or N_2) between the temperatures of 800°C and 1100°C.[8] The chemical formation of the TiC, TiN and Ti(C,N) powders can be seen below in several different examples:

Carbide Formation:[8]

$$TiCl_4 + 2Mg + CH_4 = TiC + 2MgCl_2 + 2H_2 \quad \text{Eqn 4}$$

$$TiCl_4 + 4Na + CH_4 = TiC + 4NaCl + 2H_2 \quad \text{Eqn 5}$$

Nitride Formation:[8]

$$TiCl_4 + 2Mg + 0.5N_2 = TiN + 2MgCl_2 \quad \text{Eqn 6}$$

$$TiCl_4 + 4Na + 0.5N_2 = TiN + 4NaCl \quad \text{Eqn 7}$$

Carbonitride Formation:[8]

$$TiCl_4 + 2Mg + CH_4 + 0.5N_2 = Ti(C,N) + 2MgCl_2 + 2H_2 \quad \text{Eqn 8}$$

$$TiCl_4 + 4Na + CH_4 + 0.5N_2 = Ti(C,N) + 4NaCl + 2H_2 \quad \text{Eqn 9}$$

Another widely used technique to produce titanium carbonitride powders that are essentially free of impurities is self-propagating high temperature synthesis (SHS). There are two types of combustion reactions, either propagating or bulk reactions.[11] In propagating reactions powered compacts are ignited, usually near the top, which in turn creates a combustion wave that then passes through the entire compacted sample. While in a bulk reaction scenario the compact is heated very rapidly in a furnace until the combustion reaction occurs simultaneously throughout the entire sample. Bulk reactions, also known as thermal explosions, are usually only used to synthesize intermetallic compounds because of their low ignition temperatures, whereas propagating reactions can be used to synthesize ceramic powders such as Ti(C,N).[11] During SHS reactions very high temperatures can be reached in extremely short periods of time (e.g. 2 to 3 seconds) because of the highly exothermic nature of the reactions. It is due to the extremely fast heating time that it can be assumed that there is no time for the heat to disperse to the surroundings; therefore the maximum temperature reached is the 'adiabatic temperature' of the material.[12] One of the reasons why there are so few impurities found in the final products that are produced by SHS is because the high temperatures are believed to burn off any impurities that may contaminate the final powder.

During the production of Ti(C,N) by SHS, titanium and carbon black powders are first mixed and compacted in the appropriate proportions to create the various final mixtures of Ti(C,N) powders. The compacts are then placed in a sample chamber while nitrogen gas is flowed through where the combustion takes place.[13] To calculate the ratios needed for each separate type of powder the following equation was used:[14]

$$Ti + xC + (y/2)N_2 = TiC_xN_y \qquad \text{Eqn 10}$$

where x+y=1.

A schematic diagram of the setup used to perform the above reaction can be seen in Figure 1 below.[13]

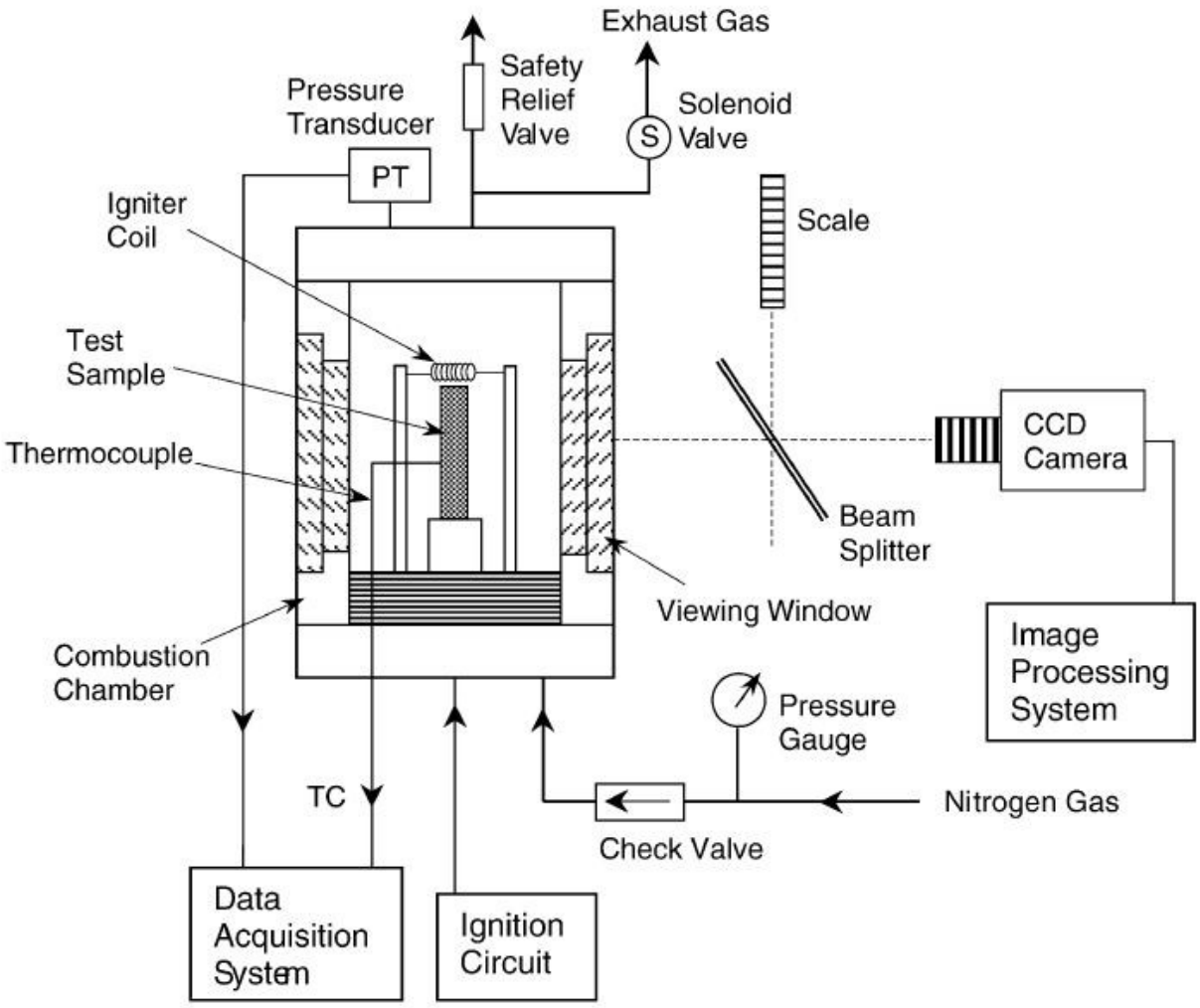

Figure 1. Diagram of the experimental arrangement used to produce Ti(C,N) by SHS.[13]

2.2.2 Physical Properties of Titanium Carbonitride

Refractory carbides and nitrides such as TiC and TiN are hard, wear resistant, chemically inert and have high melting temperatures; these attractive properties have made them become a very important material in engineering applications. Both TiC and TiN have the basic sodium chloride crystal structure, meaning the corners of the face centered cubic (fcc) are filled by either carbon for TiC or nitrogen for TiN, while the (0.5,0,0) position of the superlattice is occupied by Ti atoms.[14] As mentioned previously, Ti(C,N) is simply a binary solid solution of TiC and TiN, where C and N atoms can interchange easily throughout the structure; the crystal lattice of Ti(C,N) can be seen below in Figure 2.[14]

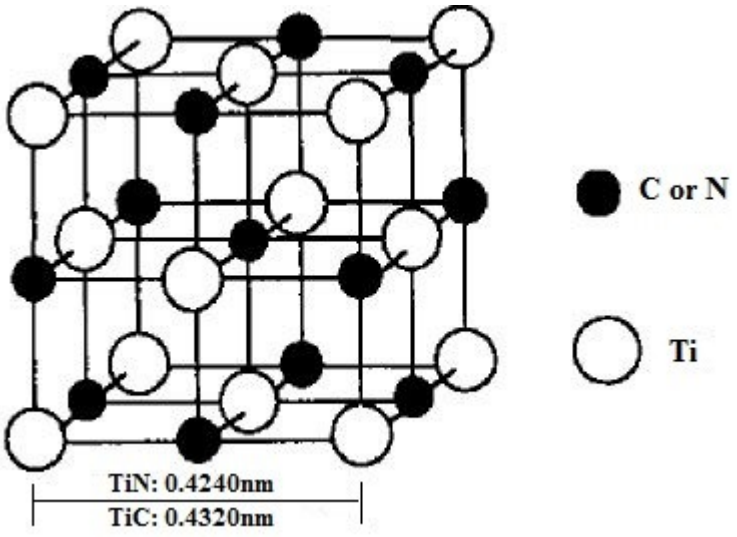

Figure 2. The crystal lattice structure of Ti(C,N).[14]

As seen from Figure 2, the lattice parameter of TiN is slightly smaller than TiC, but it is not enough of a difference to cause any significant amount of strain within the lattice structure. However, as the amount of N present in the crystal structure increases, the lattice parameter decreases in a linear fashion.[14] Similarly, as the amount of N increases in Ti(C,N) the micro- and nano-hardness of the material decreases, as shown in Figure 3.[15]

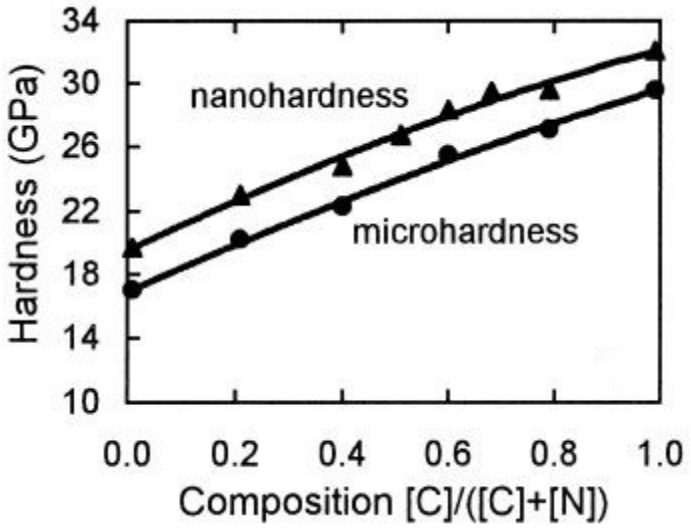

Figure 3. Hardness of Ti(C,N) as a function of C and N.[15]

A variance between the microhardness and nanohardness can be seen in Figure 3, which is most likely due to micro-cracking throughout the material as the hardness is measured, and since the micro scale is larger than that of the nano, more of these cracks will contribute to the resulting decreased hardness measurement.[15] The elastic properties can also be characterized as a function of the nitrogen content in Ti(C,N) and, as can be seen in Figure 4, the Young's (E), bulk (B) and shear (G) modulus values and do not vary greatly as the composition changes.[15]

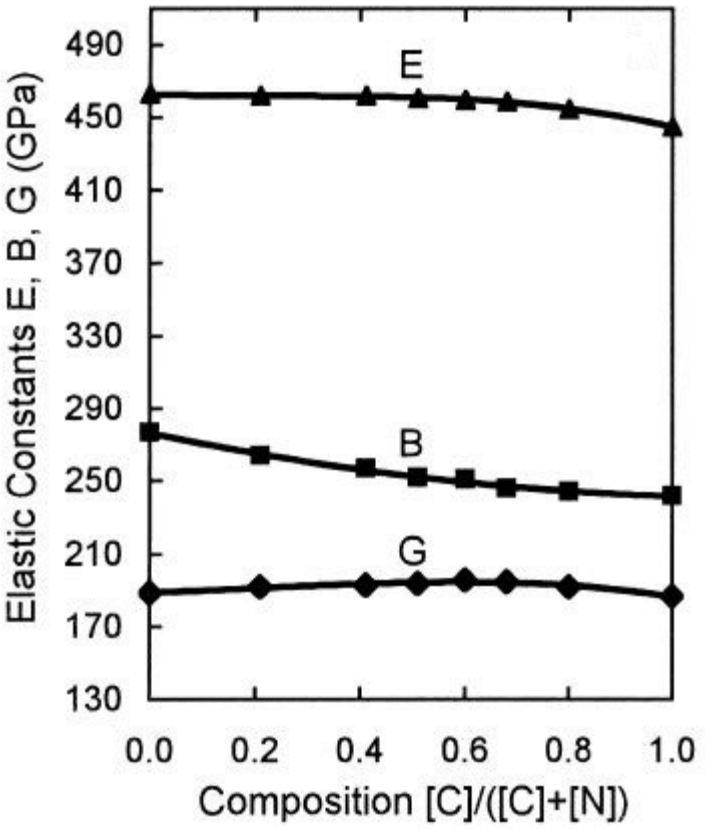

Figure 4. The elastic properties of Ti(C,N).[15]

2.3 Nickel Aluminide (Ni_3Al)

Intermetallic compounds are often developed unintentionally in steels/stainless steels during normal use and service. However, they are intentionally formed in nickel based alloys, such as nickel aluminide (Ni_3Al), as a new class of high temperature resistant alloy.[16] They have been considered for a variety of high temperature structural applications for many years because of their very good oxidation and corrosion resistance. Intermetallic compounds can be described as an ordered phase formed between two or more metallic elements to create a new structured alloy, where multiple sublattices are needed to describe its atomic structure. The excellent elevated temperature properties exhibited by these compounds are a result of their long-range ordered superlattice, which reduces dislocation movement along with diffusion properties at higher temperatures.[16]

Aluminides of transitional metals such as nickel have high enough quantities of aluminum to form a continuous, fully adherent alumina (Al_2O_3) layer on the surface of the material when exposed to an air or oxygen atmosphere.[17,18] In nickel aluminides, it is this alumina layer on the surface that gives the excellent oxidation and carburization resistance, even at temperatures up to 1100°C. In addition to the high corrosion and oxidation resistance, Ni_3Al also maintains its high yield strengths and high stiffness between 650-1100°C, as opposed to many nickel based superalloys.[17] It is because of these attractive properties that Ni_3Al has been extensively used as a strengthening agent in the form of precipitation hardening of many nickel based superalloys.[19]

At ambient conditions polycrystalline Ni_3Al is very brittle, suffering from intergranular fracture. Conversely, single crystals of Ni_3Al are extremely ductile.[18] The brittle nature of the polycrystalline materials has been proposed to be a result of several different factors, one of which is poor grain boundary cohesion, resulting from large differences in electronegativity between the Ni and Al atoms.[20,21] Other suspected reasons for the brittle nature of Ni_3Al are the difficulty of slip transmission across grain boundaries, arising from the need for chemical order at the boundaries, and also the presence of microcracks at the boundaries which cause premature failure.[21] Finally, perhaps the most important factor that causes the embrittlement of the aluminide was found to be due to the moisture content in air, through the generation of atomic hydrogen which enters the material and causes embrittlement. It has been shown that the problem of poor ductility in the polycrystalline Ni_3Al materials can be corrected by microalloying with boron additions, and the benefits of this method will be discussed in more detail in a later section.[22,23] Similar to the brittleness at ambient conditions, Ni_3Al alloys are also brittle in nature at elevated temperatures, meaning their ductilities are somewhat sensitive to the temperature of the test environments.[22] The material shows significantly lower ductility in air at temperatures reaching 300°C, with the worst embrittlement occurring at around 600 to 850°C, where there is a transition from transgranular to intergranular fracture. This effect is caused by air, and most likely gaseous oxygen since the same results were observed in conditions with pure O_2 and when the test was repeated in a vacuum the ductility remained. During elevated temperature use oxygen is chemisorbed onto the nickel aluminide surface, and weakening of atomic bonding occurs across grain

boundaries.[22] Then the localized areas of high stresses created during the early stages of plastic deformation nucleate and propagate microcracks along grain boundaries, causing premature failure. To combat this, it has been found that adding small amounts of chromium to Ni_3Al will rapidly form a protective Cr_2O_3 layer that will effectively block oxygen from embrittling the material.

Nickel aluminide remains fully ordered up to a temperature near its melting point and is capable of taking rather large amounts of other elements into solid solution.[24] With increasing temperature the overall yield stress of Ni_3Al increases up to a maximum, reached at ~800°C, contrary to more conventional materials. This response gives Ni_3Al great potential to have high strength retention in extreme working conditions. Most studies have shown that many solutes do not provide significant hardening effects at temperatures as high as 800°C, but some Group IV-A elements do, mainly Hf and Zr. It is for that reason Ni_3Al is commonly alloyed with those elements at low concentrations.[18]

2.3.1 Physical Properties of Ni_3Al

Intermetallic aluminides such as Ni_3Al have relatively high melting temperatures, good corrosion and oxidation resistance, moderately low densities ($7.50 g/cm^3$), along with the ability to retain rather high strengths and stiffness at high temperatures.[16] The phase diagram of the Al-Ni system can be seen in Figure 5, where the melting temperature is displayed as 1360°C.[25]

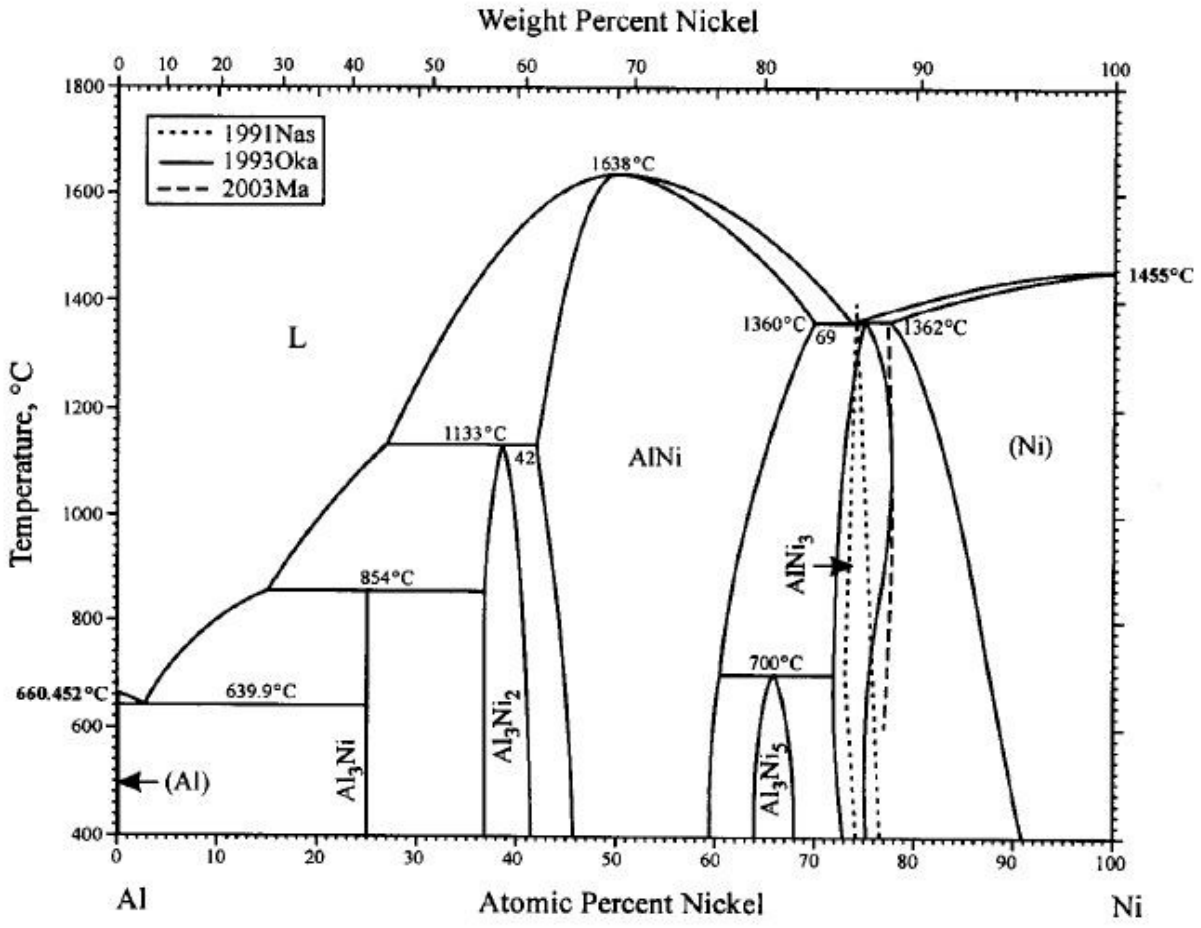

Figure 5. The Al-Ni phase diagram.[25]

Nickel aluminide has a basic FCC crystal structure, with a lattice parameter of 0.357nm.[26] A simple schematic of the unit cell can be seen in Figure 6, with the face center atoms being Ni and the corner atoms being Al.[19]

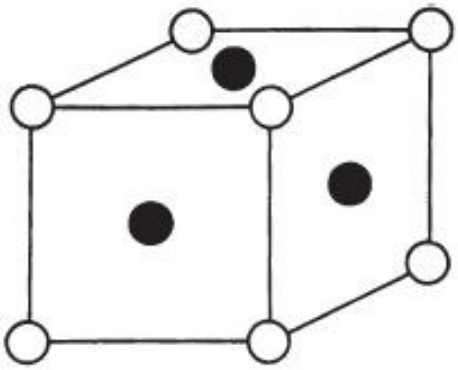

Figure 6. The Unit Cell of Nickel Aluminide (Ni_3Al).[19]

In Figure 7 the elastic modulus, along with the heat capacities of polycrystalline Ni_3Al are shown as a function of temperature between 25 and 400°C. [26] It is interesting to note that near room temperature the modulus of Ni_3Al is very similar to that of Ni, but as temperature increases the rate at which the modulus of Ni_3Al decreases is about half of the rate at which Ni decreases.[26]

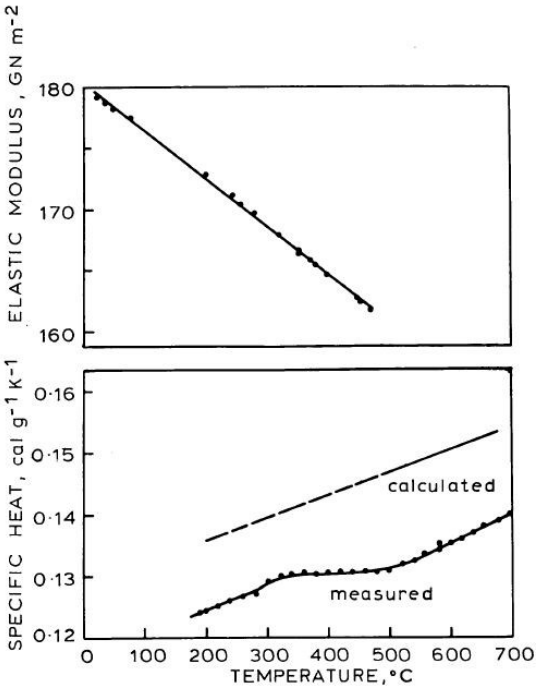

Figure 7. The elastic modulus and specific heat capacity of nickel aluminide (Ni_3Al).[26]

2.4 Titanium Carbonitride Cermets

The first TiC based cermets produced were predominately TiC with a Ni binder, and potentially Mo as a further alloying addition; these cermets were very hard but also brittle in nature. It was later found that the addition of nitrogen to the TiC lattice structure would enhance the ductility of the cermets.[27] The hardness of the cermets increases with increasing amounts of TiC, while the wear resistance properties are increased through increasing amounts of TiN. Titanium carbonitride cermets have very good creep and wear resistance because of their high hardness and the thermal stability of their phases.[28] In addition, TiN has superior thermal conductivity than TiC, which makes Ti(C,N) based cermets more thermal shock resistant than those based solely on TiC.[14] The addition of nitrogen is believed to be more effective if it is added to the microstructure in the form of Ti(C,N), instead of TiN, because it produces better homogeneity and consequently improved structural performance.[29] Therefore the properties and microstructure of the cermets depend largely on the characteristics of the precursor materials; mainly the carbon-nitrogen ratio, the stoichiometry of the hard phase and the percentage of binder present.

Ti(C,N) cermets combine the high hardness properties generally associated with TiC, with the good toughness attributes of TiN, but can suffer from poor wetting with some metallic binder systems as the fraction of TiN is increased. The contact angle that exists between the ceramic and the liquid metal during sintering is a measure of the wettability of the system. Contact angles greater than 90° are considered to be non-wetting, while if the angle is 0° it is referred to as a perfectly wetting system. For strong bonding to occur there must be a combination of both good wetting and the ability for small amounts of the carbide phase to dissolve into the binder.[14] If a system experiences poor wettability then the final structure will have a poor densification response, with retained porosity that will act as stress raisers, resulting in a cermet with poor physical properties. For a given cermet system alloy additions can be made that alter the interaction between the carbide and metallic phases, in such a fashion that a poor wetting system can be transformed into one that densifies fully upon sintering.

Zhang investigated the effects of the C:N ratio in Ti(C,N) based cermets, by manufacturing samples with various amounts of C and N in solid solution.[30] The optimal composition in terms of the hardness was found to be at a ratio of 1:1, where the cermets had the ideal combination of hardness from the TiC phase and toughness from the TiN phase. In two separate studies on Ti(C,N) cermets the effects of both TiC and TiN were further confirmed, where as the amount of TiC was increased the hardness also increased, and with rising amounts of TiN present the indentation fracture resistance (IFR) improved.[27,31] The rise in hardness from the higher amounts of TiC present is caused by the higher modulus of elasticity of TiC compared to that of TiN. The Ti(C,N) based cermets were consequently able to achieve hardness and IFR values comparable to that of the more traditional cemented carbides.[27]

2.4.1 Microstructural Characteristics

When characterizing the microstructures of cermets the two primary tasks that are to be completed are to quantify the size and volume fraction of the microstructural features and to determine their compositions. The grains of Ti(C,N) cermets are often divided into three distinct phases: the core, the inner rim and the outer rim. The core is composed of undissolved Ti(C,N), while the rim phases are based upon Ti(C,N) with somewhat high concentrations of heavier elements such as W, Ta and Mo if they are present in the material.[32] The core is primarily created by undissolved powder grains, but it can also be formed in the very early stages of sintering.[33] Conversely the inner rim is formed upon solid-state sintering, before the eutectic temperature is reached, and the outer rim is re-precipitated during liquid phase sintering.[34] In Figure 8 a typical microstructure of a Ti(C,N) based cermet can be seen.[27]

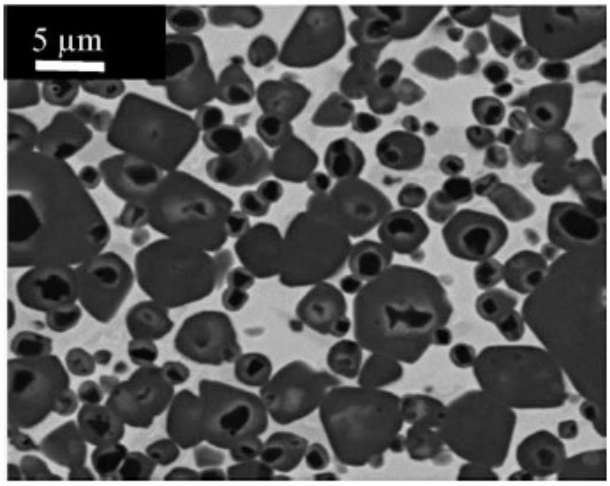

Figure 8. SEM micrograph of a Ti(C,N)-Mo_2C-Ni cermet.[27]

The nitrogen content in the Ti(C,N) phase has a strong effect on the thickness of the rim in the core/rim structure, and is an indication of the extent of carbide dissolution and precipitation in the Ti(C,N) system.[35]

Upon densification there are several microstructural properties that are observable that determine specific properties of the cermets. One such feature is the contiguity of the carbide phase, which is the ratio of the carbide/carbide interfacial area to the total interface surface area.[36,37] It has a range of values from 0 (totally dispersed) to 1 (fully agglomerated). As the contiguity increases, hardness increases and the fracture toughness simultaneously decreases. The equation used to calculate the contiguity is:

$$C = \frac{2Ncc}{2Ncc+Nbc} \qquad \text{Eqn 11}$$

where N_{cc} is the average number of intercepts per unit length of a test line which intersects carbide/carbide boundaries and N_{bc} is the number of intercepts of binder/carbide interfaces.[38] Another observable feature is the binder mean free path, which is a measure of the characteristic ligament dimension of ductile binder phase between the brittle carbide particles. The equation used to calculate this parameter is:

$$\lambda = d * \frac{1-fc}{fc*(1-C)} \qquad \text{Eqn 12}$$

where d is the average carbide particle size and f_c is the volume fraction of the carbide phase. In general as the mean free path increases so too does the IFR.

2.4.2 Alloy Additions

When manufacturing Ti(C,N) cermets there are a number of issues that arise that can result in samples not being suited for practical industrial use. When the nitrogen content of Ti(C,N) is at higher concentrations the cermets have potential sintering issues, which can result in a cermet that has inherent flaws in the microstructure, thus creating a material that has relatively poor mechanical properties. To address these problems previous research has been carried out on cermets similar to the Ti(C,N)/Ni_3Al system, in search of alloying additions that will improve their properties. The two that will be the focus of future studies are molybdenum (Mo) and boron (B), with each providing different benefits to the system if used in correct quantities.

2.4.3 Molybdenum

Elemental molybdenum, or molybdenum carbide (Mo_2C), is used as sintering aid in TiC or Ti(C,N) based cermets to help improve the wettability of the metallic phase on the ceramic, while improving other mechanical properties like fracture toughness, simultaneously.[39] Improved wettability of the phases results in a reduction of the detrimental processing issues, including microstructural defects such as voids and binder micro-cracks, while there also is an increase in the interphase bond strength and phase uniformity.[40] The addition of Mo in the initial powder decreases the final carbide grain size in the sintered cermet by decreasing the solubility of Ti(C,N) in the binder, thus limiting grain growth by solution precipitation during sintering.[41] The specific mechanism that limits the solubility is the formation of a Mo rich shell around the Ti(C,N) particles, which is far less soluble in the binder phase than the original Ti(C,N) ceramic.[41] Since grain growth is limited in the microstructure, a slight increase in the transverse rupture strength (TRS), or flexure strength, is often observed. The carbonitride grain size determines an important characteristic in the cermet system. Firstly, the *in-situ* hardness, which sets the upper limit of the hardness increases with decreasing grain size. Secondly, the binder MFP, which is proportional to the grain size, is reduced. Consequently, there is an increase the binder hardening effect by the

reduction of the MFP.[42] The increase in TRS values can be also partially explained by Mo forming a solid solution with the binder phase of the material and the improved wetting behaviour, which reduces the amount of pre-existing flaws like micro-cracks in the structure of the material.[40]

As previously stated, typical microstructures of Ti(C,N) based cermets consist of a core/rim morphology. The core is usually undissolved ceramic phase along with heavier elements, the rim is usually a solid solution of Mo and Ti(C,N) while the matrix is the metallic binder phase. If the addition of Mo becomes too high the rim will grow too large thus creating larger grain sizes, and at the same time Mo forms a solid solution with the binder making it inhomogeneous.[43] It is the larger grain sizes and the inhomogeneity of the binder that causes cermets to lose their mechanical properties with the addition of too much Mo.[39,43] However, it was also found that the addition of Mo initially increases the hardness of the cermets up to 10 wt%, but then as the amount is increased up to around 15 wt% detrimental effects are observed. This can be explained by the sharp reduction of grain size in the cermets with the addition of Mo up to 10 wt%, while further additions do not affect the grain size too dramatically, but the soft Mo dilutes the hard Ti(C,N) ceramic thus decreasing the hardness.[39] The fracture toughness (K_{IC}) was also improved by the addition of Mo up to 5 wt%, and with additional amounts the value was lowered. .[39] The addition of Mo up to 5 wt% hardens the binder phase of the cermet, thus resulting in a tougher material. However, as the amount of Mo is increased the grain size generally decreases, which results in lower toughness values, since a material is generally tougher with larger grain sizes and hence larger binder ligament dimensions.[39]

2.4.4 Boron

The addition of small quantities of boron (B) has been shown to significantly improve the ductility of Ni_3Al based alloys. It is important to note that these improvements are only seen in Ni rich compositions, where the atomic ratio of Ni/Al is greater than three.[16]

There has been a great deal of research conducted on the utilization of borides in cermet samples through the reaction sintering process, but the formation of a brittle third phase in the metal matrix has caused many attempts to fail. Therefore there are several key

characteristics that one must consider when choosing to add B to a cermet. Mainly it involves selecting a suitable metal matrix that will not form a brittle third phase with the addition of B, and to form a liquid phase between the boride and the metal matrix to obtain full densification of a sintered product while preventing grain growth.[44] Due to the brittleness of polycrystalline Ni_3Al the use of Ni_3Al based alloys as a structural material is somewhat limited. However, it was observed that small quantities of B would result in a material with high ductility values with mostly transgranular fracture.[45] The extent of the improvement in ductility was later determined for Ni rich alloys, which can be seen in Figure 9.[46]

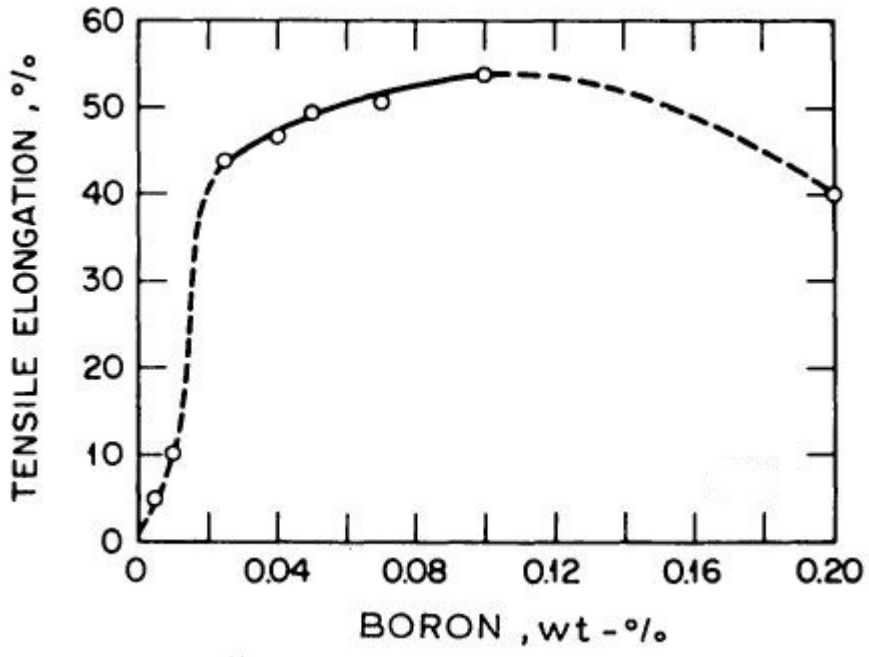

Figure 9. The effects of boron on Ni_3Al ductility.[46]

There are several different theories as to why B increases the ductility of polycrystalline Ni_3Al, they include: (i) increasing the grain boundary cohesive strength;[23] (ii) facilitating slip accommodation at grain boundaries to reduce the stress created by dislocation pile up;[47] (iii) causing compositional disordering by attracting Ni to grain boundaries;[48] (iv) minimizing moisture induced embrittlement by reducing the rate of hydrogen diffusion at grain boundaries;[49] or (v) B clustering at constitutional vacancies

occurs in Ni rich alloys, leaving a reduced amount of B available for segregation to grain boundaries.[26] All of the reasons listed are attributed to a modification involving grain boundary properties, however it was also shown that B increases ductility of single crystals of Ni_3Al meaning it also affects the bulk material as a whole. In addition, as the amount of Al is increased in Ni_3Al alloys the benefits gained from the B addition are somewhat minimized, with the fracture mode changing from transgranular to more intergranular in nature.

The addition of B also provides a strengthening mechanism for single and polycrystalline Ni_3Al through solid solution strengthening, with the effects maximized as Al and B levels rise. If the strengthening from B doping is a linear function, as reported by some researchers, the rate of change is around 997 MPa/at% B for single crystals, which is much higher than the reported 250 MPa/at% B in polycrystalline Ni_3Al.[23,50] However, there has also been a softening effect observed as a result of B addition.[51] It was found that boron doping would soften the fine grained Ni_3Al, but harden the coarse ones. This is because of the competition between the softening at the grain boundaries and the hardening in the interiors.[52] Therefore the softening/hardening effect of B in Ni_3Al is largely dependent on grain size, with smaller grains increasing softening and coarser grains increasing hardness.

2.5 Powder Compaction

A very common technique used to process cermets is by utilizing powder metallurgical methods. Once a uniform powder blend is obtained it must be pressed into a green body before the final product can be sintered. The green bodies created after pressing have a consistency of chalk, meaning they are very brittle, therefore they need to be handled with great care. The green body strengths are dependant on the material being pressed, and also directly proportional to the compaction pressure used. There are numerous compaction methods currently utilized for processing, which is determined by the size, shape and complexity of the final product desired. The final mechanical properties of the compacts depend greatly on the ability to obtain a strong green body.

2.5.1 Single Action Compaction

In the pressing of powders, die compaction is the most widely used technique. It involves rigid dies that are used in either hydraulic or mechanical presses. While pressing a powder a uniform density is not achieved throughout the compact. This is due to the frictional forces created between the powder and the die wall as well as the forces between particles themselves. In die compaction there are two basic types to choose from, either single or double action compaction. The two different types of die compaction techniques create compacts that are slightly different from one another, and are classified according to the movement of the individual tool elements, as outlined in Figure 10. In single action compaction the lower punch and the die remain stationary, while the upper punch is lowered to compact the powder. This creates a sample that has a density gradient from the top to the bottom. While in double action compaction only the die is stationary with the upper and lower punches compacting the powder, which results in a sample that has a much more uniform density throughout.[53] Usually single action compaction is used only on thin samples, while double action is used for samples that are thicker and are in need of better density control.

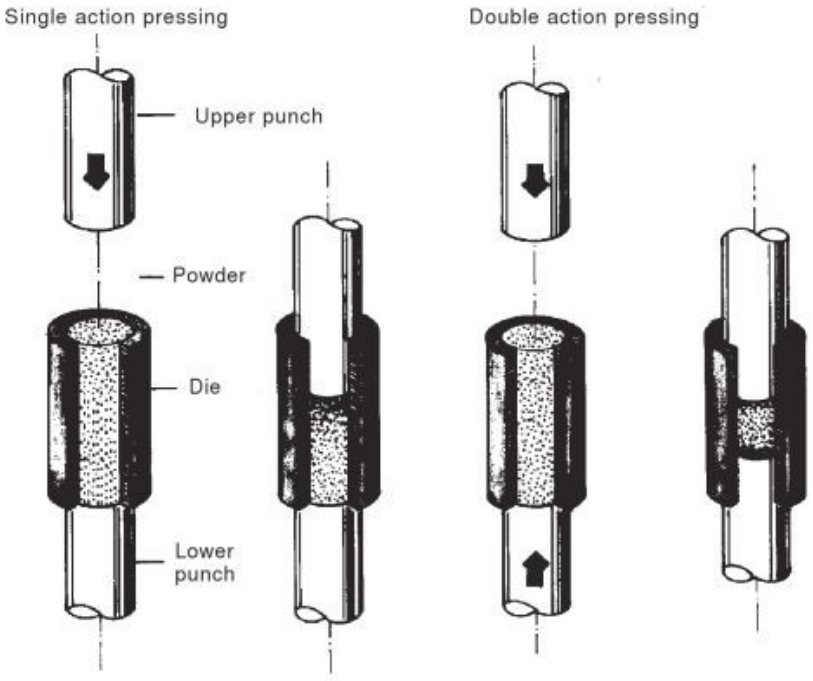

Figure 10. A comparison of single vs. double action compaction.[53]

2.5.2 Cold Isostatic Pressing

Cold isostatic pressing (CIP) involves the compaction of powders enclosed within a flexible mould, by using fluids such as oil or water, at pressures between 200 and 700 MPa. The use of flexible moulds allows for the ability to press rather complex shapes with a uniform density, while achieving high green strengths. However, the dimensional control over the compacted samples is not as precise as die compaction, so CIP generally produces samples with a rougher surface, while the moulds used do not last as long as rigid dies. A simple schematic of a CIP process is shown in Figure 11.[53]

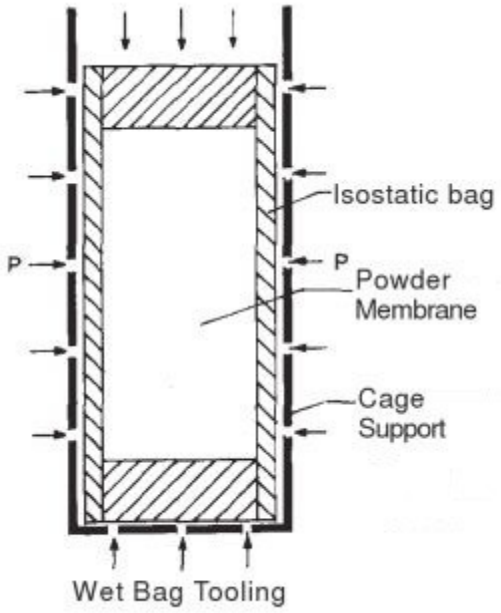

Figure 11. Simple schematic of the CIP process.[53]

2.6 Sintering

Liquid phase sintering is a powder metallurgical process where at least a small portion of a compact being sintered is in a liquid state, and is of particular interest because it usually leads to practically fully dense materials.[34] During the sintering of cermets it is the metal binder phase, along with a small amount of dissolved ceramic (typically a carbide or carbonitride) phase that forms the liquid portion of the system. In the "heavy alloy" theory the solubility of the solid phase into the liquid plays a huge role in determining the final microstructure of the sintered compact.[54] The heavy alloy theory states that if the solid has a high solubility into the liquid phase grain growth will be maximized, while if there is low solubility the amount of grain growth will be limited. However, in heterogeneous systems such as cermets the heavy alloy theory does not fully explain the dispersion of the two phases throughout the microstructure. It was found that in cermets the main factor that determines the distribution of the various phases was the relative surface energies of the interfaces with respect to one another.[55]

The final microstructure of a liquid phase sintered material, such as a cermet, has a large effect on the mechanical properties.[34] The main microstructural features that can be observed in a cermet system include the grain size and shape, contiguity of the dispersed

phase, volume fraction of the binder phase as well as the mean free path of the binder (a measure of the mean binder ligament dimension). In this instance contiguity is defined as the average fraction of the surface area shared by one grain of a phase and all other adjacent grains of the same phase, while the mean free path of the binder phase is the uninterrupted intercept length of the binder phase in a random direction. In order to control the resulting microstructure upon sintering, the three main process parameters that can be varied are the sintering time, temperature, and atmosphere, along with any alloying additions that may be present.[34]

2.7 Cermet Property Characterization

To quantify the various mechanical parameters exhibited by cermets, several key tests are commonly performed that measure mainly interrelated properties of cermet materials. These properties include the flexure strength, hardness, fracture resistance and wear behavior. All of the tests listed measure key aspects that are usually desired while selecting the appropriate cermet for a particular purpose.

2.7.1 Vickers Hardness

Indentation hardness testing is a relatively straightforward method that is used to characterize the mechanical properties of a rather small volume of the material. A typical hardness test is performed by simply applying a fixed load on a material using a predetermined geometry for the indenter. The Vickers diamond pyramid hardness test is one of the most widespread techniques used to quantify a material, especially hard ceramics.[56] In order to compare various materials in terms of their hardness, the Vickers hardness number (H_V) is used, which is the ratio of the applied load "P" to the pyramidal contact area "A" of the indentation. The area can then be further simplified down in terms of the diagonal length of the impression and "α", a constant which is equal to 1.8544.[56]

$$H_V = P/A = \alpha P/d^2 \qquad \text{Eqn 13}$$

Diamond indenters make it possible for the Vickers hardness test to be used to evaluate the hardness of any material, while giving the ability to place all the hardness values on one continuous scale, as opposed to the Rockwell test which has several scales. The indentation impact itself is one smooth motion, where the applied load is held in place for

10 to 15 seconds, as opposed to an impact like in Rockwell test, which happens almost instantaneously.[57] A schematic diagram of a typical Vickers hardness indentation in a sample, together with the diamond tip geometry is shown in Figure 12.[57]

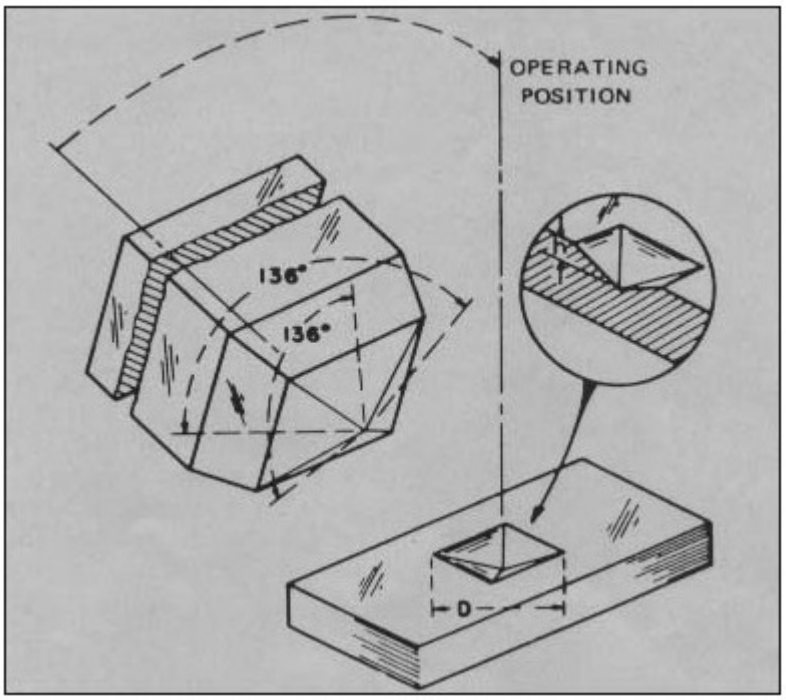

Figure 12. A schematic diagram of the Vickers indentation Test.[57]

2.7.2 Indentation Fracture Resistance

In cermet systems the bulk mechanical properties, such as toughness, are determined by the binder volume fraction, composition, and microstructural parameters such as the binder mean free path and ceramic (i.e. carbide) grain size.[58] The bulk hardness increases, while the fracture toughness decreases with both decreasing binder volume fraction and binder mean free path, all the while maintaining a constant carbide grain size.[59] The analysis of the crack patterns that relate to the toughness of more brittle materials, such as ceramics, was first conducted by using the Hertzian cone crack geometry produced by spherical indenters.[60] However, the concept of relating the size of indentation cracks to the toughness of a material was first proposed by Palmqvist, while working with metal carbides and using the Vickers hardness test as seen in Figure 13.[61,62]

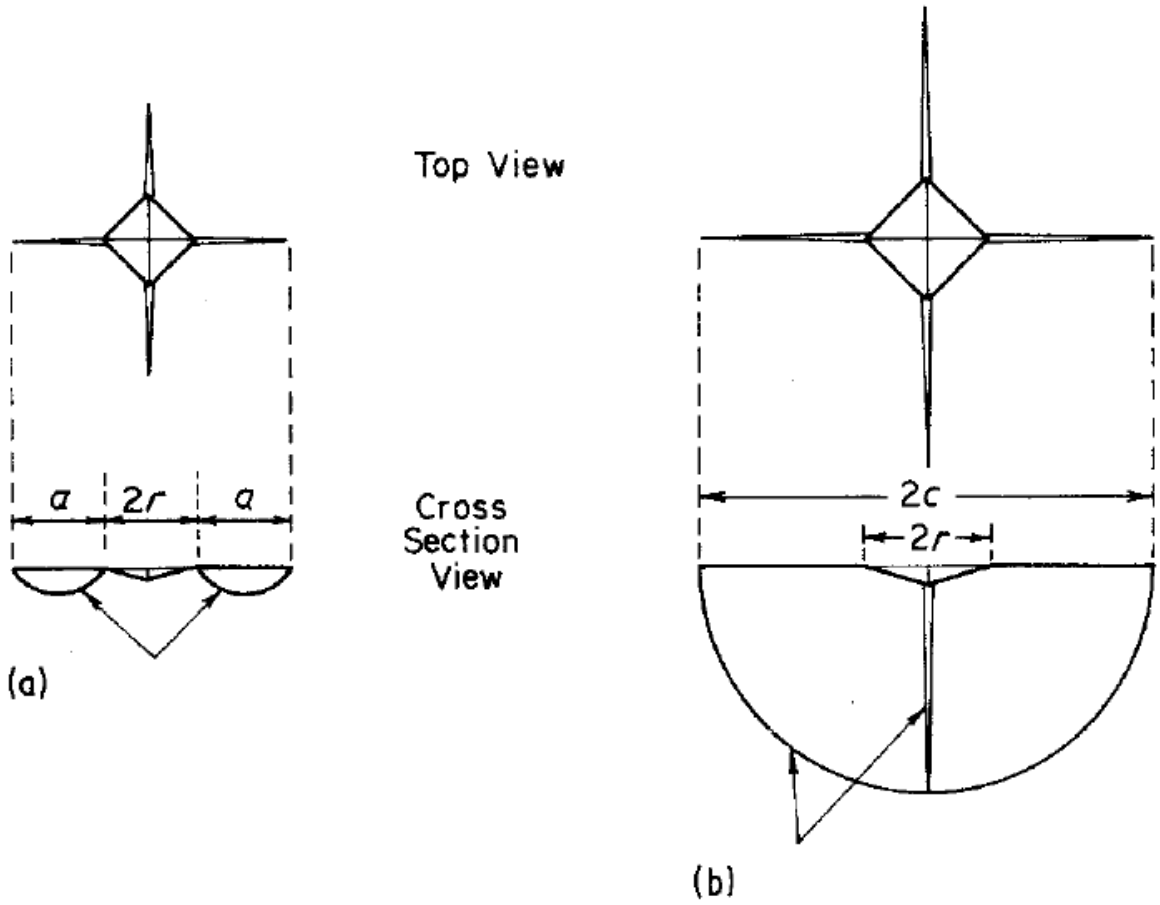

Figure 13. The radial palmqvist (a) and half penny (b) geometries for determining indentation fracture resistance.[58,61]

There are two different crack geometries shown in Figure 13, namely the radial and the half penny shapes. In the half penny geometry, the fracture pattern shown is represented by the peak load "P" and the dimensions of the plastic impression "r", with the radial/median crack length "c". The indentation fracture resistance (IFR), which is often termed 'toughness', of the material can be measured by analysis of the cracks generated through Vickers indentation. With the aid of an optical or electron microscope, the cracks that form at the corners of the diamond indenter can be measured. Taking into account the measured crack lengths, elastic modulus, peak load, a constant § (equal to

5.44 x 10^{-3}) and the Vickers Hardness, a value for the indentation fracture resistance of the material can be calculated using the following equation:[61,63]

$$Kc = \S \cdot \left(\frac{E}{H}\right)^{\frac{1}{2}} \cdot \left(\frac{P}{co^{\frac{3}{2}}}\right) \qquad \text{Eqn 14}$$

It can be seen that as the crack length gets larger, the fracture toughness decreases. Consequently, for good indentation fracture resistance values, cracks that are small in length are required, thus maximizing the toughness parameter. Although the half penny crack geometry works well with more brittle materials, such as pure ceramics, it was found that the Palmqvist or radial crack pattern better describes the geometry that more ductile materials, such as cermets, experience.[58] Therefore, a more accurate model to quantify the indentation fracture resistance of cermets is:[64]

$$K_c = \beta(HW)^{0.5} \qquad \text{Eqn 15}$$

Where "β" is a constant equal to (8.89 x 10^{-2}), "H" is the Vickers hardness value and "W" is defined in the following equation:[58]

$$W = (P - P_o)/(4\bar{a}) \qquad \text{Eqn 16}$$

Where "ā" is the average measured crack length produced by an indentation and "P_o" is extrapolated from a plot of crack length vs indentation load, which is ultimately defined as the indentation load at which cracks begin to form in a particular material.

As mentioned previously, half penny cracks invariably form in more brittle materials, while Palmqvist cracks form in ductile systems.[58,61,63,65] Niihara et al have studied the crack formation for various ceramic based materials and determined a method for predicting whether a material will have half penny or Palmqvist type cracks, by examining the ratio of crack length to indentation size. In this instance, if the ratio is below 2.5 the material is believed to be more ductile in nature, and if the ratio is above 2.5 it is considered brittle.[66]

2.7.3 Wear Behavior

Tribology is the science of friction, lubrication and wear. The wear of materials can occur either during the interaction of two surfaces, or during the interaction of an exposed surface with abrasive particles, fluids, chemicals or heat.[67] In general the varying mechanisms of wear can be divided into two main categories, either mechanical, or all other incidences that involve an additional level of active chemistry, like oxidization or corrosion. The various modes of mechanical wear can further be divided into four main categories, which include: adhesion, abrasion, erosion and surface fatigue. In addition to these wear modes, the mechanism of fretting also exists, which is a combination of adhesive, abrasive and sometimes corrosive wear. From an industrial standpoint all of the modes mentioned lead to a loss of dimensional tolerances, higher operating costs and extra expenses such as part replacement.[67,68] Table 1 shows the various types of wear mechanism that may occur, along with the typical wear debris produced through each process.

Table 1. Types of mechanical wear mechanisms.[67,69]

Type of Wear	Wear particles/debris	Wear scar/surface topography
Abrasion	Particles Flat splinters	Grooves or furrows running parallel to surface Discontinuous if hard phases are present in wear track Comet tails in low stress (surface scratching)
Adhesion	Flake splinters	Sliding tongue wedge
Erosion	Thin flakes Fine particles	Pits & cavities Wave fronts Lamellar pattern
Surface fatigue	Pitting Flaky wear	Delamination of particles Ratchetting

Adhesive wear is one of the most common types of wear, and involves the strong adhesive forces between adjacent surfaces and the loss of material due to it.[68] The sliding surfaces under load adhere to one another through solid phase welding, and any detachment from either of the surfaces involved results in a loss of material.[67] This loss of material is caused by the fact that when surfaces are brought into contact with each other they do so through very small asperities.[70,71] This area of true contact is so small that after elastic deformation the stress level quickly reaches the yield stress of one of the materials, resulting in material loss. This material loss can be thought of as a cleaning action, because the surface contaminants are forced out. Cold welding can then occur at the junction points, which make it so a shear action is required to move one surface relative to the other. It is these welded junctions, along with the cross sectional contact areas of the two surfaces, that determines the amount of force required for

material loss of one surface. These shear strengths at the interface of the two materials can be easily influenced by that of surface contaminants, like oxide films, or liquids such as lubricants, which can reduce the amount of welding and ultimately the wear that a surface experiences.[68]

Abrasive wear has two distinct forms, either two- or three-body, and the classification is determined by the number of bodies involved in a particular instance. In two-body abrasion the material from a softer surface is removed or displaced by that of a harder one. While in three-body abrasion, a discrete third free body, usually a contaminant, is allowed to roll or slide between two opposing faces; the third body is often material removed from one of the two primary sliding faces.[69] Open three-body wear refers to the situation when the two opposing surfaces are sufficiently far enough apart to be considered completely independent of one another. The classification of whether the mechanism of wear is two- or three-body abrasion may in fact change over time, an example of such an instance would be when the third free body becomes either temporarily or permanently lodged in one of the surfaces, thus changing the type of wear from three- to that of two-body wear. In dry, unlubricated, two-body wear of two dissimilar loaded surfaces, the rate of material loss is determined by several factors including: applied load, sliding speed, surface topography, initial temperature, environment, time they are in contact, and the mechanical/chemical properties of the materials involved (e.g. hardness of the softer surface and coefficient of friction).[69]

Erosion damage is considered to be the gradual removal of material caused by the repeated deformation and cutting actions of relatively small particles impinging upon the surface of a substrate.[72] The rate at which wear erosion occurs depends on several key factors including:[73]

- The size, hardness, concentration and shape of the eroding particles.
- The properties of the substrate, such as its composition, elastic properties, hardness and morphology.

- The operating conditions that the process is occurring under, such as the velocity at which the erosive particles are traveling, and the impingement angle at which they are impacting the substrate.

In ductile materials it has been shown that the peak erosion rate occurs when the impinging particles are hitting a substrate's surface at an angle of approximately 30°, since the cutting nature is most effective at that condition.[74,75] While in more brittle materials, such as glasses and ceramics, damage from erosion is mainly caused by mechanisms like micro-cracking or plastic deformation from the impact of a particle. Consequently, damage increases as the amount of kinetic energy transferred is increased; therefore it is at a maximum when the impinging angle is 90°.[76] Some of the more common applications where one might encounter erosive wear behavior would be in the movement of slurries through pipes and pumping equipment.

Surface fatigue is when damage to a substrate's surface takes place by local pitting or flaking, caused by cyclic loading. The rate at which the removal of material occurs is a function of the number of stress cycles over a given volume, and the force at which the cycles are applied.[68] The contact stress is by far the most important factor in determining the fatigue life because, in parts such as bearings, it is inversely proportional to the ninth or tenth power of contact stress. Since the stress plays such a huge role, the application of lubricants can greatly increase the fatigue life by modifying the contact stress pattern that occurs on a given surface.[68]

2.8 Wear of Cermets

As discussed previously, wear can be classified in two distinct groups depending on the wear mechanisms involved. The first group is mechanical wear, which originates from the mechanical interaction between counterfaces. The second group involves chemical interaction, such as oxidation or tribochemical reactions between the counterfaces.[77] The two predominant forms of mechanical wear that occur in cermet systems are abrasive and adhesive wear. Abrasive wear can further be divided into either two- or three-body, where two-body wear is caused by the displacement of material from a solid surface due to hard particles sliding along that surface.[78]

Wear rates are determined in such a way that both the applied load and sliding distance are normalized, this is to make the comparison of different materials under differing conditions easier. The specific wear rate (k) is determined following:

$$k = \frac{V}{Fn \cdot s} \qquad \text{Eqn 17}$$

where the volumetric wear loss (V) is divided by the product of the normal applied load (Fn) and total sliding distance (s). Typically the specific wear rate is presented with units of $mm^3/(N \bullet m)$

In general, for cermets the volume lost due to wear increases in a nominally linear fashion with applied load. This linear relationship appears to agree with previous studies, which state the total volume lost during sliding depends upon both the duration of contact and the forces exhibited upon the material(s) during contact.[79,80] It can also be noted that the volumetric wear loss generally increases as the amount of binder is increased, which may be anticipated to happen due to the reduced amounts of the harder, more wear resistant ceramic phase.

One of the most common factors that cause damage to the microstructure of cermets is attributed to the preferential wearing away of the binder material, thus causing carbide grain pullout and fracture by removing the framework they were previously embedded in. The sequence of events that is believed to occur, leading to the carbide pullout, is as follows: removal of the binder phase from the surface, plastic deformation and grooving of the binder phase below the surface, accumulation of strain in the carbide grains, fracture and damage to the grains, intergranular cracking, and finally grain pullout.[81] This is due to the low hardness of the binder phase compared to the carbide, which on its own has very good wear resistance. The carbide grains can also exhibit fracture due to the high external forces exerted upon them during the wear test.

For the most part cermets are much more wear resistant when compared to pure metals or other wear resistant materials. Archard et al tested the wear response of various materials under unlubricated conditions using tool hardened steel as the counterface, at an applied

load of 3.92N. They reported 70/30 brass having a wear rate of around 2,500x10^{-7} mm^3/Nm, and WC using mild steel as the counterface at 30x10^{-7} mm^3/Nm.[82] These numbers are in contrast to the specific wear rate values obtained by others for cermet systems, where Pirso et al reported specific wear rates of 6 to 9x10^{-7} mm^3/Nm for volume percentages of binder from 18 to 30.6vol.% on WC-Co cemented carbides against a steel (0.45wt.% C), at loads of 40 and 180N using a block-on-ring test geometry.[83] In another study based upon TiC based cermets, coupled with a 304L stainless steel binder, it was found that the materials had wear rates of between ~5x10^{-7} mm^3/Nm to ~20x10^{-7} mm^3/Nm, over a range of binder volume percentages of 10 to 30 vol%.[84] The wear response of Ti(C,N)-Ni_3Al cermets have also been tested, and were found to have wear rates of between ~1x10^{-7} mm^3/Nm and ~12x10^{-7} mm^3/Nm for binder percentages of 20 to 40 vol%.[85] In both of these previous studies the cermets were produced through melt infiltration and used WC-Co as the counterface material.

2.9 Thermal Spray Coatings

A material's surface is exposed to many detrimental factors over its service life that will, over time, effect the material's mechanical properties. These factors include mechanisms such as wear and corrosion. In many cases the only way to ensure a material maintains its mechanical properties is to apply a protective coating to the surface that may have a considerable amount of compositional and property differences to that of the substrate.[3,86] Areas in which a coating may prove to be beneficial to a substrate include improving the wear properties, toughness, strength, hardness, or oxidation and/or corrosion resistance. There are three main categories that separate the various forms of coating processes, which include chemical-vapor deposition (CVD), physical-vapor deposition (PVD) and thermal spray.

Thermal spraying is a well-established family of low cost industrial surface treatments in which different types of materials such as metals, ceramics, composites or even plastics are coated evenly on many different substrates. The coating feed stock is fed into a heat source, in either a powder or wire form, where it is heated to a molten or semi-molten state and is systematically sprayed on to the desired surface, previously prepared by sand blasting.[87] Thermal spraying is important in the various groups of surface modification

technologies because it can deposit layers of material that range from several μm to several mm in thickness, over large surface areas at a relatively high rate, when compared to other coating processes such as electroplating, PVD and CVD.[88] There are three major categories of thermal spraying, including flame spray, electric arc spray, and plasma arc spray. Within those categories there are several techniques used to heat the feed stock to melting temperature, including plasma spraying, detonation spraying, wire flame spraying, high velocity oxy-fuel coating spraying (HVOF), warm spraying and cold spraying. Figure 14 shows a comparison of the various techniques, including the temperature ranges that are used while applying the feedstock materials, and the velocities that are reached for the material deposited onto the substrates. The technique chosen for a particular application typically depends on several key factors, including the desired coating material, coating performance requirements, economics and the size of the part itself.

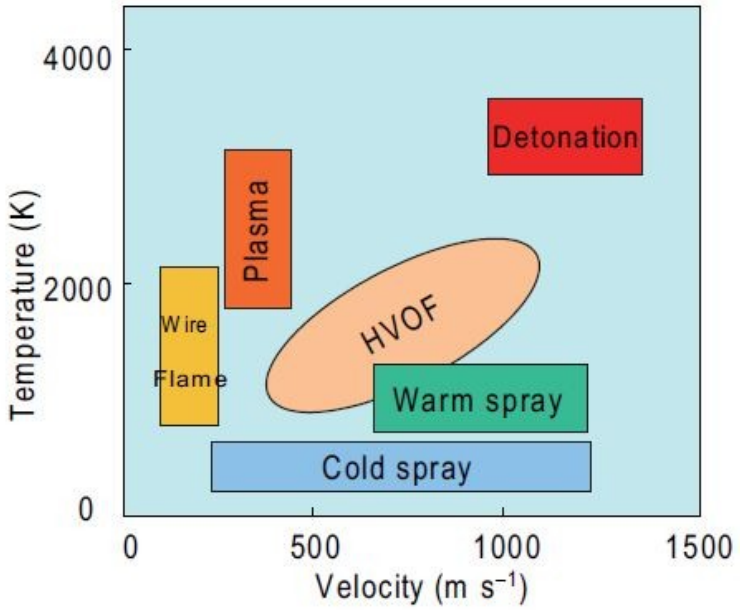

Figure 14. Comparison of various thermal spray techniques.[88]

2.9.1 HVOF Thermal Spray Process

In the 1980s, the technique of HVOF was developed, which is a form of flame spraying. HVOF uses a mixture of fuel and oxygen that is fed into a combustion chamber, where

the mixture is continuously ignited, which in turn releases a hot pressurized gas at pressures of around 1MPa. The gas exits the chamber and passes through a converging-diverging nozzle, reaching velocities exceeding 1000 ms^{-1}. The fuels used can be several different gases or liquids such as hydrogen, methane, propane, propylene, acetylene or kerosene. The powder material is fed into the jet at designated feed ports, either radially or axially, at rates around 20 to 120 g/min. The carrier gas is either nitrogen or argon, and the hot gases heat the particles and then accelerate them towards a substrate, at which point they impinge on the surface forming a uniform coating.[88,89] A typical spraying "stand-off" distance used in HVOF is in the range of 150 to 300 mm, achieving coatings with bond strengths as high as 90 MPa, with lower than 1% porosity.[89] During the process the combustion chamber, nozzle, and barrel are all continuously cooled by water. HVOF has been most successfully used with cermet systems, such as cemented carbides, and other corrosion resistant materials like stainless steels and nickel based alloys. Thicker deposits can be obtained in HVOF because of the reduced residual stresses, as well as higher deposition rates. Both of these advantages result in HVOF being a cheaper process when compared to plasma spraying.[90] Figure 15 shows a schematic diagram of the general mechanisms used in HVOF,[88] while Figure 16 shows a modern HVOF torch in operation.[89]

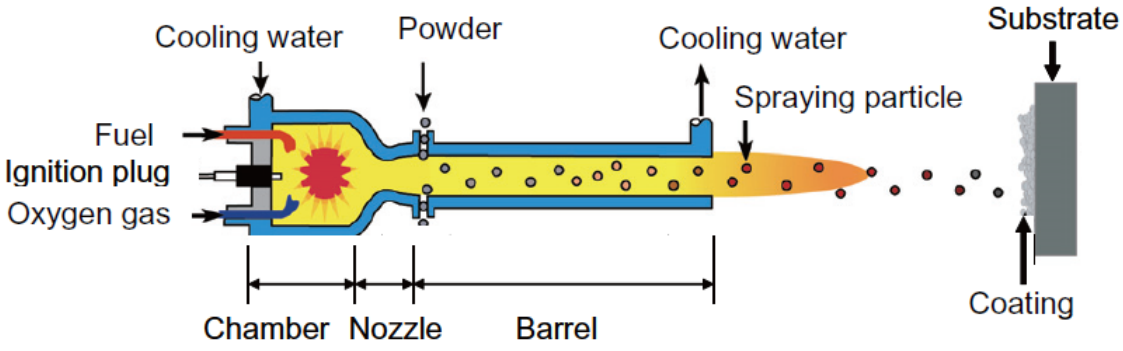

Figure 15. Schematic diagram of the HVOF process.[88]

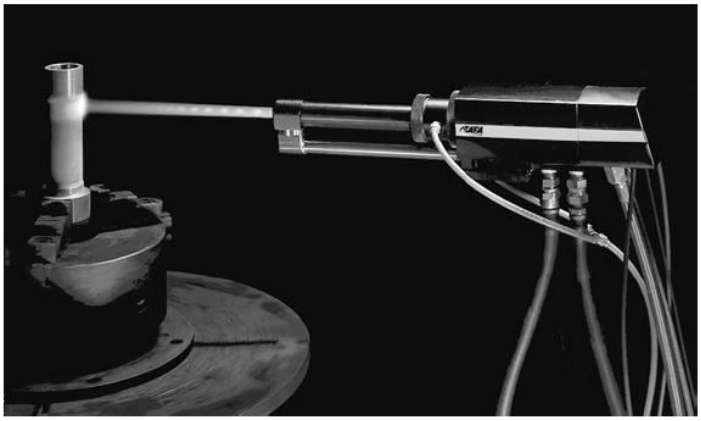

Figure 16. HVOF in operation.[96]

2.9.2 Materials Used for Thermal Spray Coatings

Cermet thermal spray coatings are invariably beneficial due to their high wear resistance, including abrasion and erosion, along with their resistance to extremely high temperature and corrosive environments.[91] In order to maximize the potential of the cermet coatings it is important to have a coating that has hard particles (e.g. carbides), spread evenly and consistently throughout the layer to provide good wear properties. The hardness and bond strengths of the applied cermet coatings are largely dependent on the impact velocity of the particles, therefore these properties are usually higher when a converging-diverging Laval type nozzle is used, which increases particle velocity (e.g. during HVOF deposition).[92] The coating should also have a large enough ratio between the carbide particles to that of the matrix, in order to provide adequate levels of toughness within the layer, without having any major defects or voids.[93] For the best resistance to abrasive wear the hardness and the cohesion of the carbide particles within the metallic matrix are very important, as are the residual stresses in the coating.[94] To obtain these optimized characteristics, one of the most commonly used thermal spray techniques is HVOF, although it is possible to get similar coating morphologies using other spray technologies.[95]

The reason for the wide spread use of HVOF for spraying cermets is due to its ability to consistently produce carbide based coatings with minimal amounts of porosity or decarburization, which reduces the volume fraction of the carbides present in the

coatings.[92] With HVOF, cermet coatings are able to obtain an overall porosity level of <2%, with no interconnected pores.[96] Recent studies have also shown that while using the rubber wheel abrasive test, coatings applied by HVOF have a higher abrasive resistance when compared to coatings applied by other methods such as plasma spraying, while also maintaining higher hardness and toughness.[96] The higher abrasive resistance directly corresponds with less decarburization occurring within the carbide phase.

2.10 Summary

This chapter has provided an introduction to cermets and their applications, along with the general physical properties of the materials that form Ti(C,N)-Ni_3Al based cermets, which are the emphasis of the present study. The typical methods used to characterize these materials have also been reviewed, including the Vickers hardness, IFR and the wear behavior, with emphasis on the modes of wear that generally occur in cermet systems. A comparison of the wear rates usually observed in cermets to less wear resistant pure metals was also made, where the typical wear rates obtained for a variety of materials were shown. Finally, since the ultimate goal of this thesis was to produce a bulk material to be subsequently used as a thermal spray coating, some general features of the thermal spray process were also discussed.

3 Materials and Methods

The materials and methods employed in this study are shown in detail throughout the following section. The cermet samples manufactured were processed by using a mixture of powdered ceramic (TiC, $Ti(C_{0.7},N_{0.3})$, $Ti(C_{0.5},N_{0.5})$, $Ti(C_{0.3},N_{0.7})$ and Mo_2C) and metallic (Ni and Ni/Al materials. The powders were sequentially mixed, pressed, and sintered. The densified samples were then polished and tested for various parameters in order to quantify the effects of the different compositions studied.

3.1 Materials

The powdered materials used in this study will be discussed in this section, properties such as density, average particle size and representative micrographs will be displayed.

3.1.1 Characteristics of Carbide Starting Powders

Varying amounts of C and N in the Ti(C,N) powders along with Mo_2C were the carbide phases used throughout the study. The average size of the powders used were Mo_2C (lot no. PL71887718; 1.0-2.0µm; ρ=8.9g/cm^3), TiC (lot no. PL20125339; D_{50}=1.25µm; ρ=4.93g/cm^3) both from Pacific Particulate Materials; $TiC_{0.7}N_{0.3}$ (lot no. L25809; D_{50}=2.10µm; ρ=5.02g/cm^3), $TiC_{0.5}N_{0.5}$ (lot no. L29865; D_{50}=1.74µm; ρ=5.01g/cm^3), $TiC_{0.3}N_{0.7}$ lot no. L25747; D_{50}=1.72µm; ρ=5.13g/cm^3) all from Treibacher Industrie AG. Figure 17 displays typical SEM images of these powders.

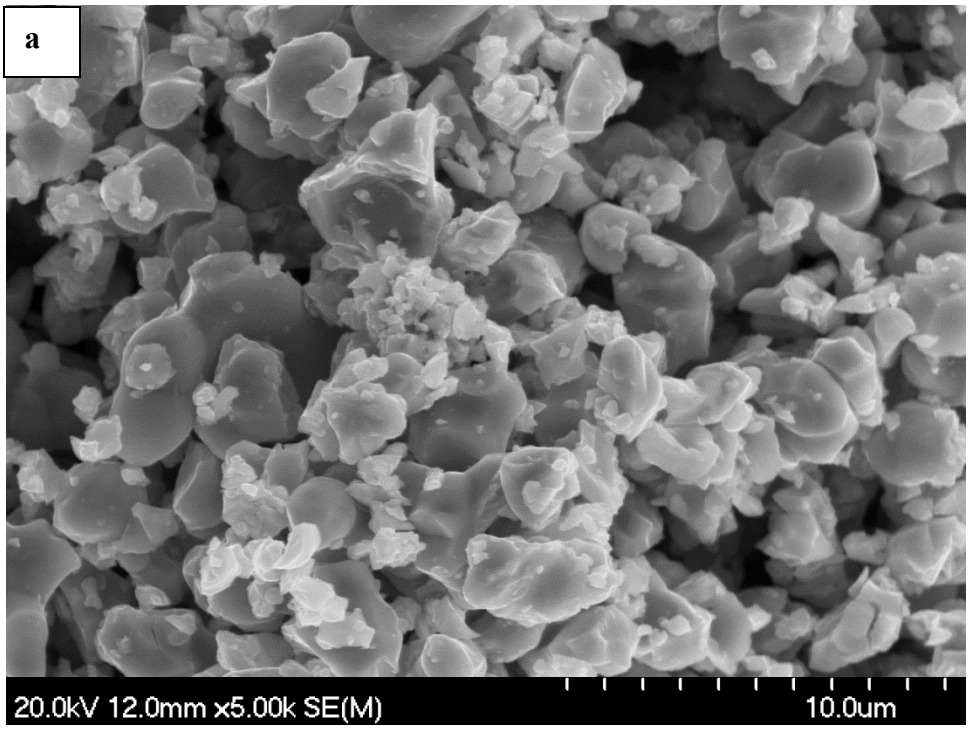
a
20.0kV 12.0mm x5.00k SE(M)
10.0um

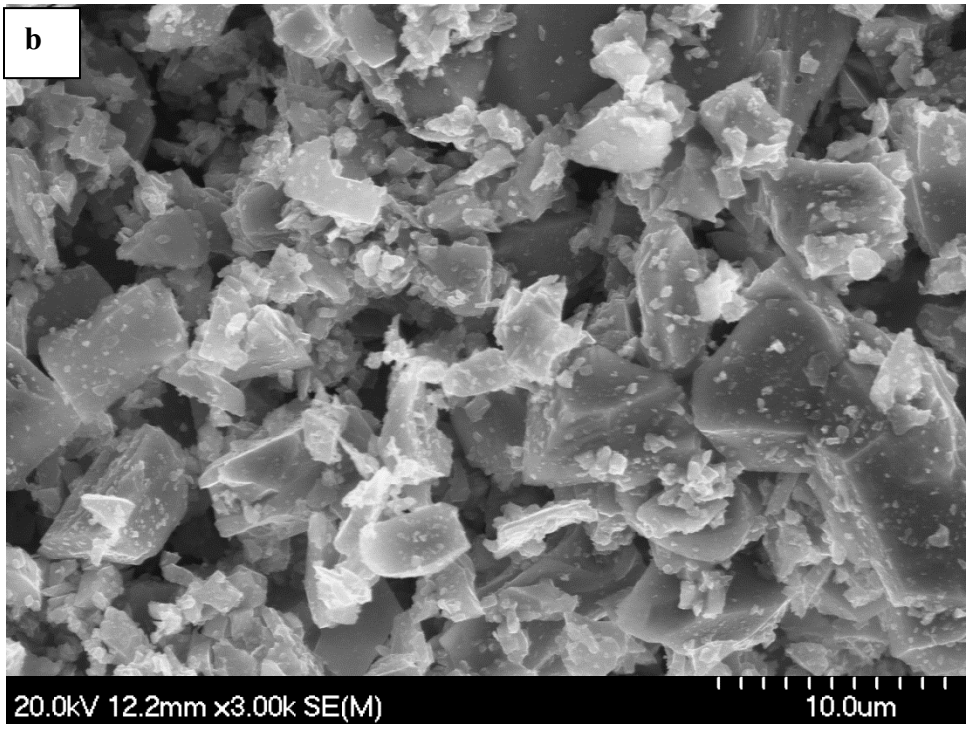
b
20.0kV 12.2mm x3.00k SE(M)
10.0um

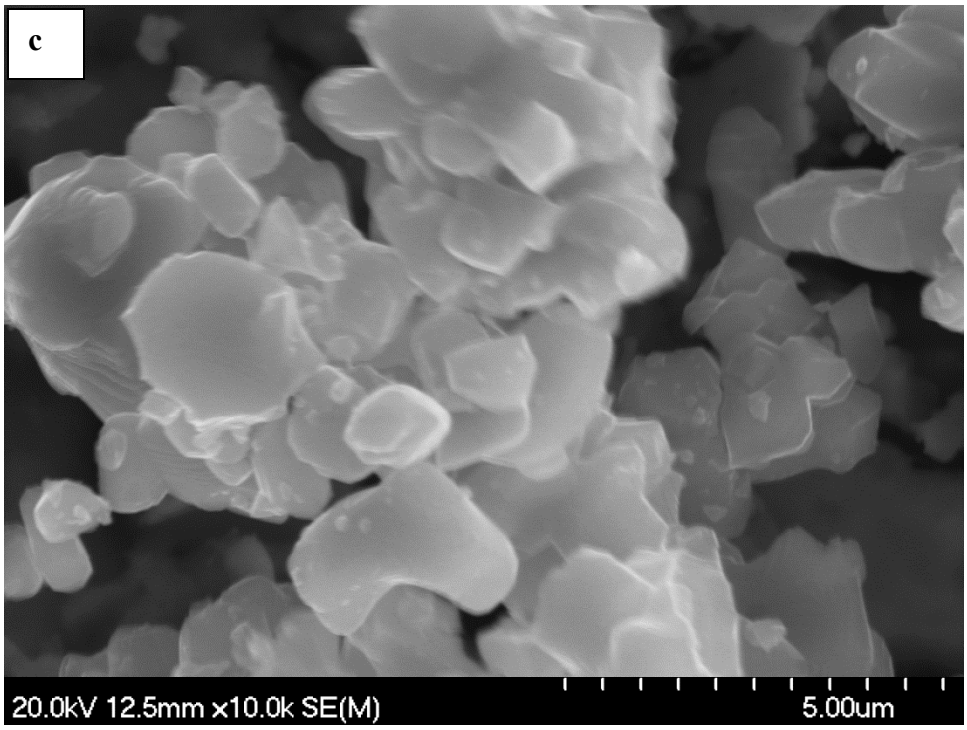
c
20.0kV 12.5mm x10.0k SE(M)
5.00um

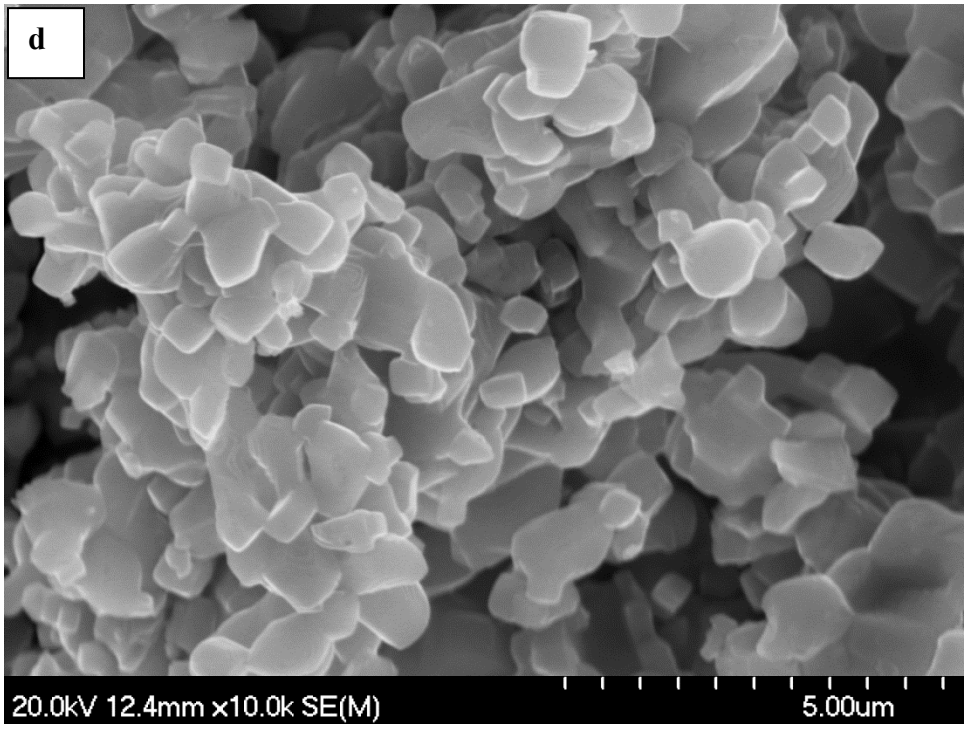
d
20.0kV 12.4mm x10.0k SE(M)
5.00um

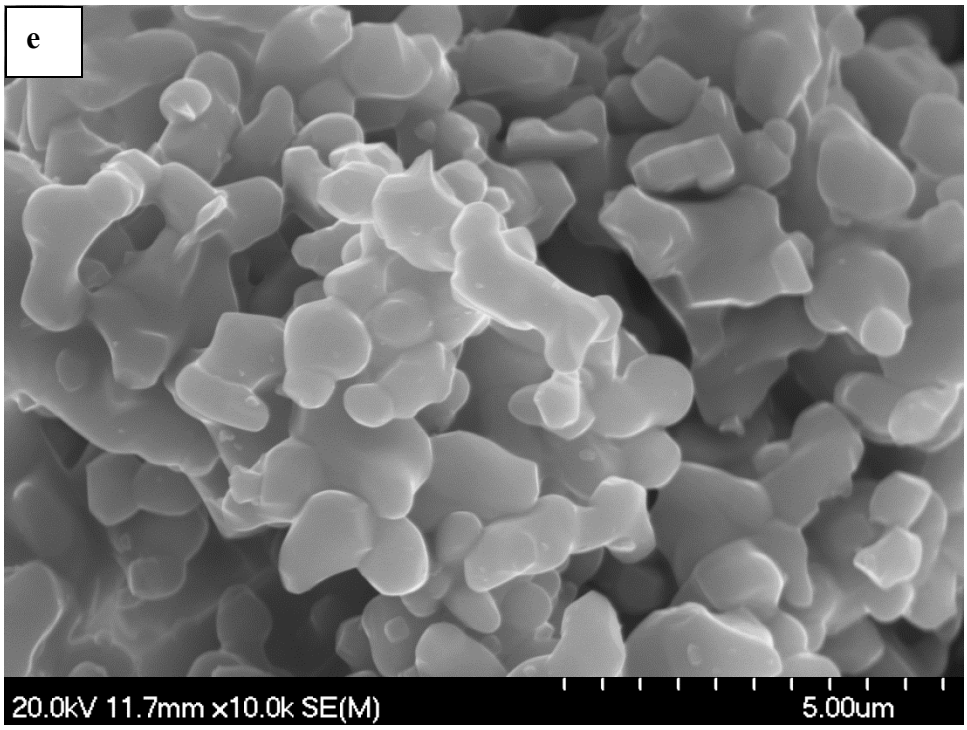

Figure 17. Representative SEM images of the carbide and carbonitride powders used in the present study: (a) Mo_2C, (b) TiC, (c) $Ti(C_{0.7},N_{0.3})$, (d) $Ti(C_{0.5},N_{0.5})$, and (e) $Ti(C_{0.3},N_{0.7})$.

3.1.2 Characteristics of the Starting Metallic Powders

The metallic powders used in this study were combined together to form the stoichiometrically correct Ni_3Al intermetallic. Ni (lot no. L10W013; 2.2-3.0 μm; ρ=8.91 g/cm^3), and Ni/Al 50/50 wt.% (lot no. D28X029; D_{50}=38μm; ρ=4.14g/cm^3), both from Alfa Aesar, were the powders used to generate Ni_3Al. Figure 18 shows typical SEM images of these powders.

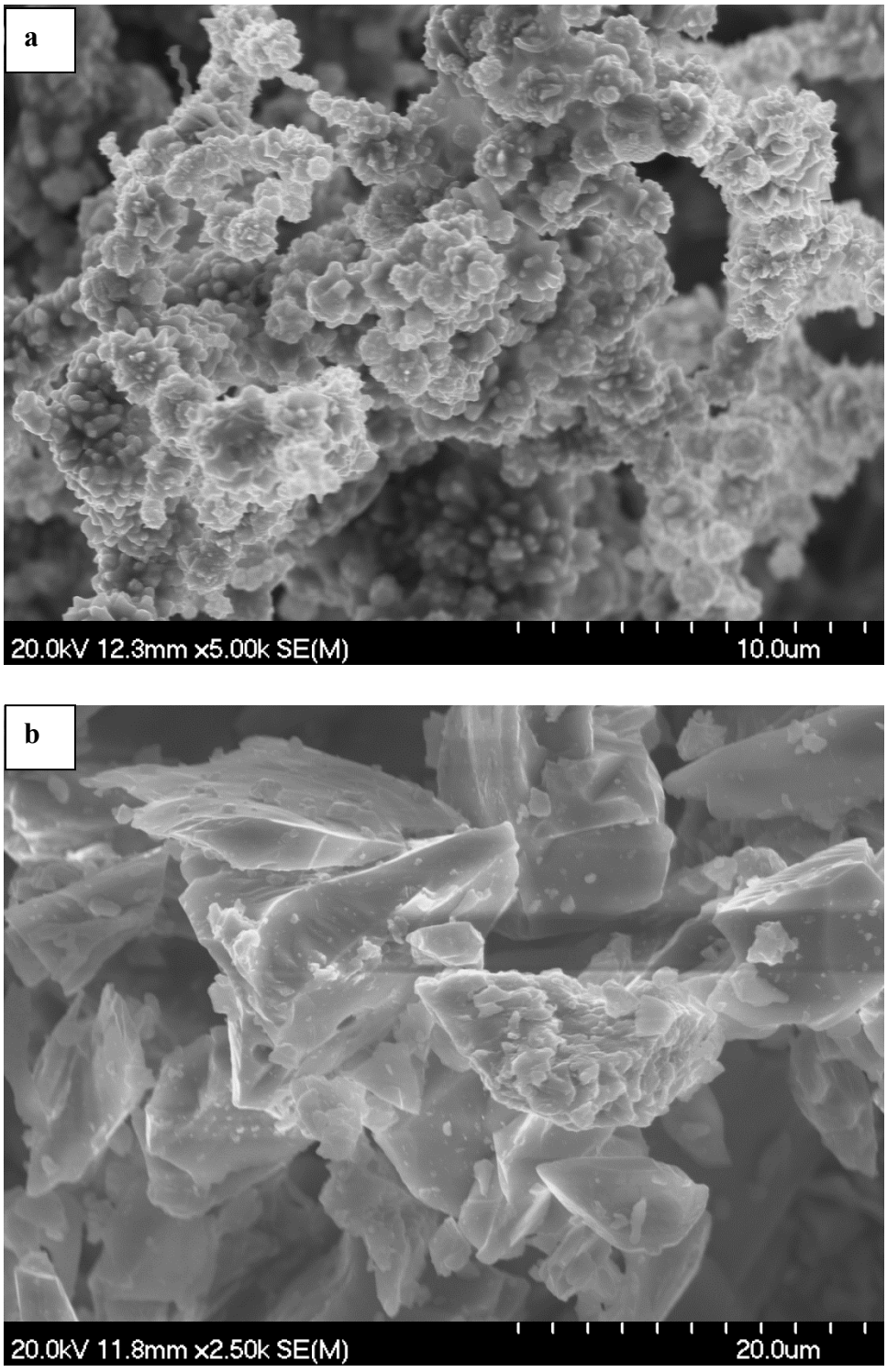

Figure 18. Representative SEM images of the metallic powders used in the present study: (a) Ni and (b) Ni/Al.

3.2 Experimental Procedures

The methods used to prepare and quantitatively examine the cermet samples studied in this report are outlined in detail in this section.

3.2.1 Sample Preparation

In order to manufacture the samples, individual powders were first weighed to their appropriate amounts to make a batch that was approximately 50 g in mass, including 0.5 wt.% of polyvinyl butyral (PVB) binder. The batch was then mixed with 200 mL acetone and 500 g of yttria stabilized zirconia milling media, and was placed on a ball milling machine at 50 rpm for a period of 24 hours to ensure full homogenization of the powders. The mixture was then left to dry in a fume hood for 24 to 48 hours in order to evaporate the acetone, before sieving through a 75 μm mesh. Approximately 0.6 mL of hexane was added to the uniformly mixed powders before being uniaxially pressed at 45 MPa into disks that were approximately 7 g in mass. The disks were then placed in sealed bags and compressed at 207 MPa using a cold isostatic press (CIP). The CIPed samples were then placed in alumina crucibles, on top of bubble alumina, and sintered at 1550°C for one hour inside a vacuum furnace, at approximately 20 mTorr. A heating ramp rate of 10°C/min was used, along with a nominal cooling rate of 25°C/min to room temperature.

The measurement of the sintered density of the cermets was conducted using Archimedes' principle in water at room temperature. This was followed by sequential polishing starting on a 125 μm diamond pad down to a 0.25μm diamond paste achieving a mirror like finish for further analysis.

3.2.2 Microscopic Observations

Scanning electron microscopy (SEM) (Model S-4700, Hitachi High Technologies) analysis was conducted in order to confirm the sintering response by examining various aspects of the cermets, such as the homogeneity of the ceramic phase throughout the microstructures and the presence of any defects present in the samples. The average grain size was calculated by using the linear intercept method, measuring at least 350 grains per composition, and multiplying the result by a factor of 1.56.[97] The contiguity was also measured for each composition by imposing a series of horizontal lines over the micrographs and counting the number of binder/binder and binder/carbide intercepts for

each corresponding line. With both the average grain size and contiguity values calculated for each composition the binder mean free path was able to be determined while using Equations 11 and 12.

3.2.3 Hardness and Indentation Fracture Resistance

The hardness was measured by calculating the average of five Vickers pyramid indentations (V-100A, Leco) per sample, at an applied load of 5 kgf, held for 10 seconds. While the indentation fracture resistance (IFR) was calculated by measuring the length of the cracks formed after a series of loads (5, 10, 20 and 30 kgf) were applied to each sample. This was performed in order to use linear extrapolation to calculate P_0, which is the lowest 'virtual' load where no cracking would occur in the system. Equations 15 and 16 were used, which relate to the model that predicts a Palmqvist type cracking system in more ductile ceramics in order to obtain a value for the IFR.

3.2.4 Reciprocating Wear Tests

All of the various combinations of the different cermets manufactured were analyzed in order to determine their reciprocating wear response by using a universal micro tribometer (UMT; Model UMT-1, Bruker Corp.). A spherical WC-Co (6.35 mm diameter, Grade 25 with 6 wt.% Co, McMaster-Carr) counterface was used, with a stroke length of 5.03 mm and an oscillation frequency of 20 Hz. The wear tests were conducted for a duration of two hours, perpendicular to the polished, flat cermet surface at room temperature (21 ± 2°C) and a relative humidity of 40-55%. Through a load censor the testing equipment was able to monitor and record features such as the dynamic normal loads, frictional forces and the depth of the wear tracks for the duration of the tests. Sliding wear evaluation was conducted at the applied loads of 20, 40 and 60 N.

In order to measure the amount of material lost during the wear tests an optical profilometer, with an 1 mm optical pen, was used to scan the wear surfaces. The scanning procedure was completed at a resolution of 5μm steps, in both the x and y directions, to examine both the wear tracks and the surrounding surface region. The profilometry data collected used an average of three area scans for the wear volumes calculated.

In addition to the wear resistance the tests outlined which included the Vickers hardness, IFR, microstructural analysis (ceramic grain size, contiguity and binder mean free path) and sintering response provided a clear overview of the present set of materials. From this general overview it becomes easier to compare this cermet system manufactured through a simple reaction sinter based method with other, more common systems currently in use within industry today.

4 Results and Discussion

In the following sections, topics such as the characterization of the powders through XRD examination, post sintered carbide grain sizes, typical microstructures, sintered densities and EDS analysis of the cermets are presented and discussed.

4.1 X-Ray Diffraction of Samples with Mo_2C

The XRD traces for the samples with Mo_2C present are presented in Figure 19, where the effects of varying amounts of Mo_2C on the phases in the samples are shown. From examining the traces it can be seen that for the lower volume fractions of Mo_2C present, no new phases are noticeable. However as the amount of Mo_2C is increased up to 5 and 10 vol%, a new phase that corresponds with a Mo_2C peak starts to form in the samples.

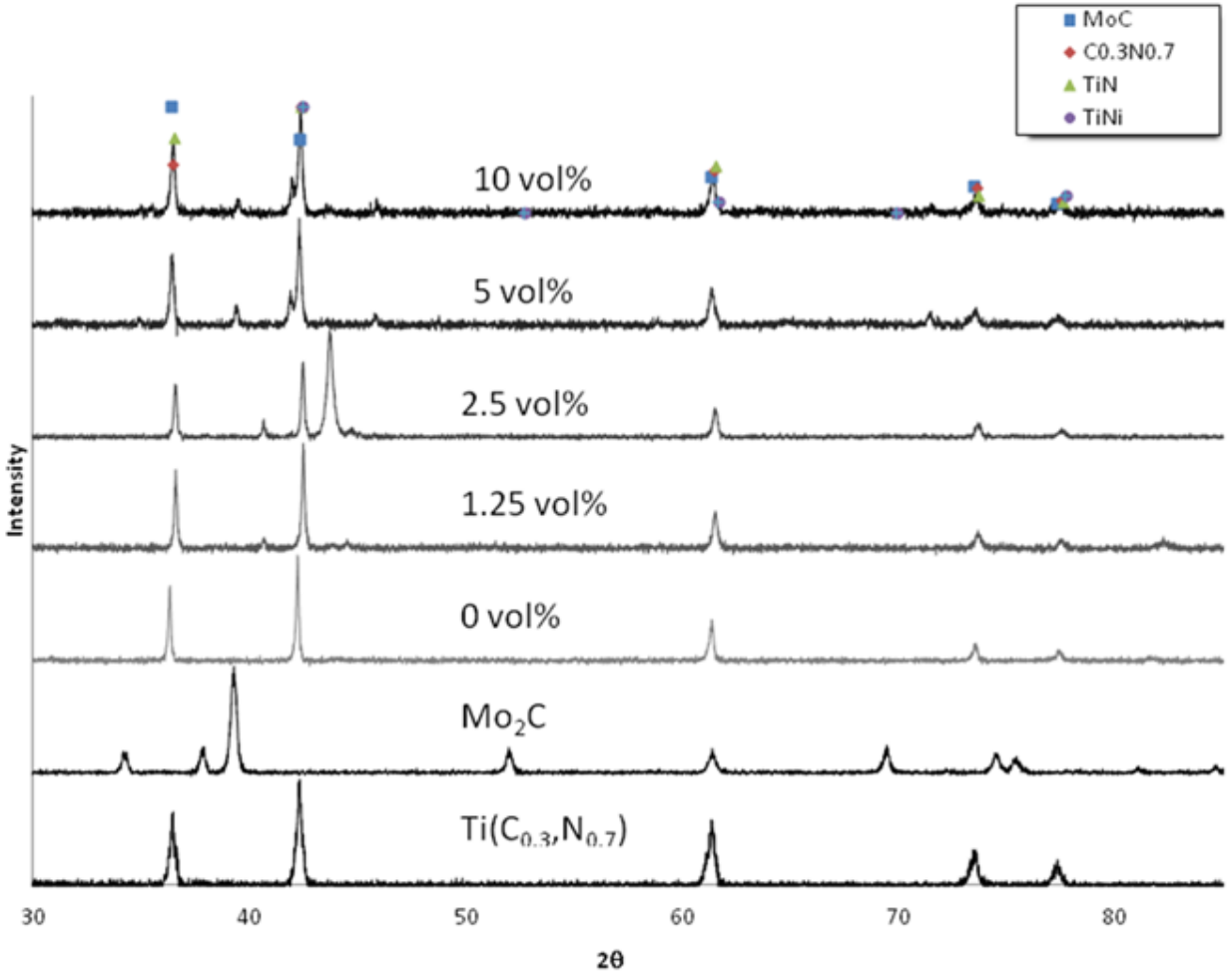

Figure 19. XRD spectra obtained for $Ti(C_{0.3},N_{0.7})$-Ni_3Al with varying amounts of Mo_2C.

4.2 Energy-dispersive X-ray Spectroscopy Characterization of Samples with Mo_2C

In order to determine the chemical composition of the various phases present in the two extremes of the cermets with Mo_2C (i.e. 1.25 and 10 wt.%), energy dispersive X-ray spectroscopy (EDS) analysis was performed in the SEM. Figure 20 displays micrographs of the samples, with three phases clearly present in the microstructure. The lightest shade is believed to be rich in Mo, while the darkest phase is the carbonitride grains, with the grey phase being the binder. Table 2 displays the chemical composition of the various phases, in atomic percent, obtained by averaging analyses in six separate locations in each distinct corresponding region of the microstructure. It can be seen that as the volume percentage of Mo_2C is increased the regions rich in Mo become more clearly defined, with higher amounts of Mo present throughout the sample. The Mo-rich phase appears to be a solution of Mo, C, N and Ni with relatively low amounts of Ti and Al present. The EDS results also indicate the presence of Mo in both the carbide and binder phases in the cermets, although its quantity is somewhat low compared to the Mo rich phase.

(a)

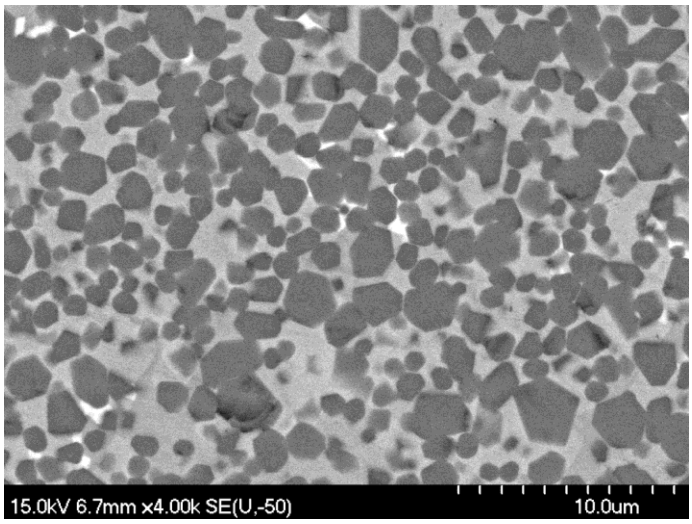
15.0kV 6.7mm x4.00k SE(U,-50)
10.0um

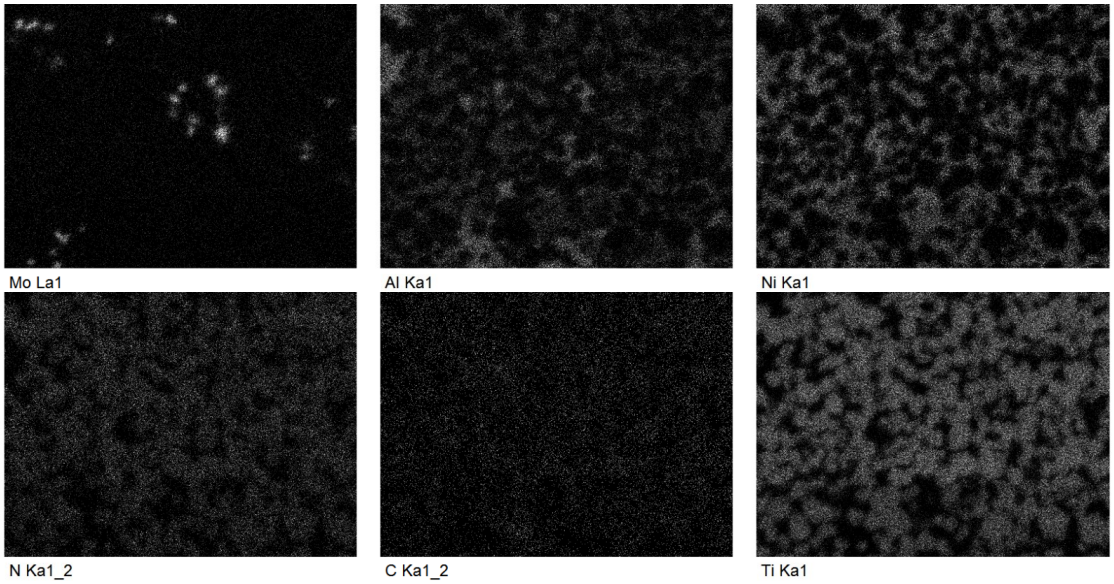
Mo La1
Al Ka1
Ni Ka1
N Ka1_2
C Ka1_2
Ti Ka1

(b)

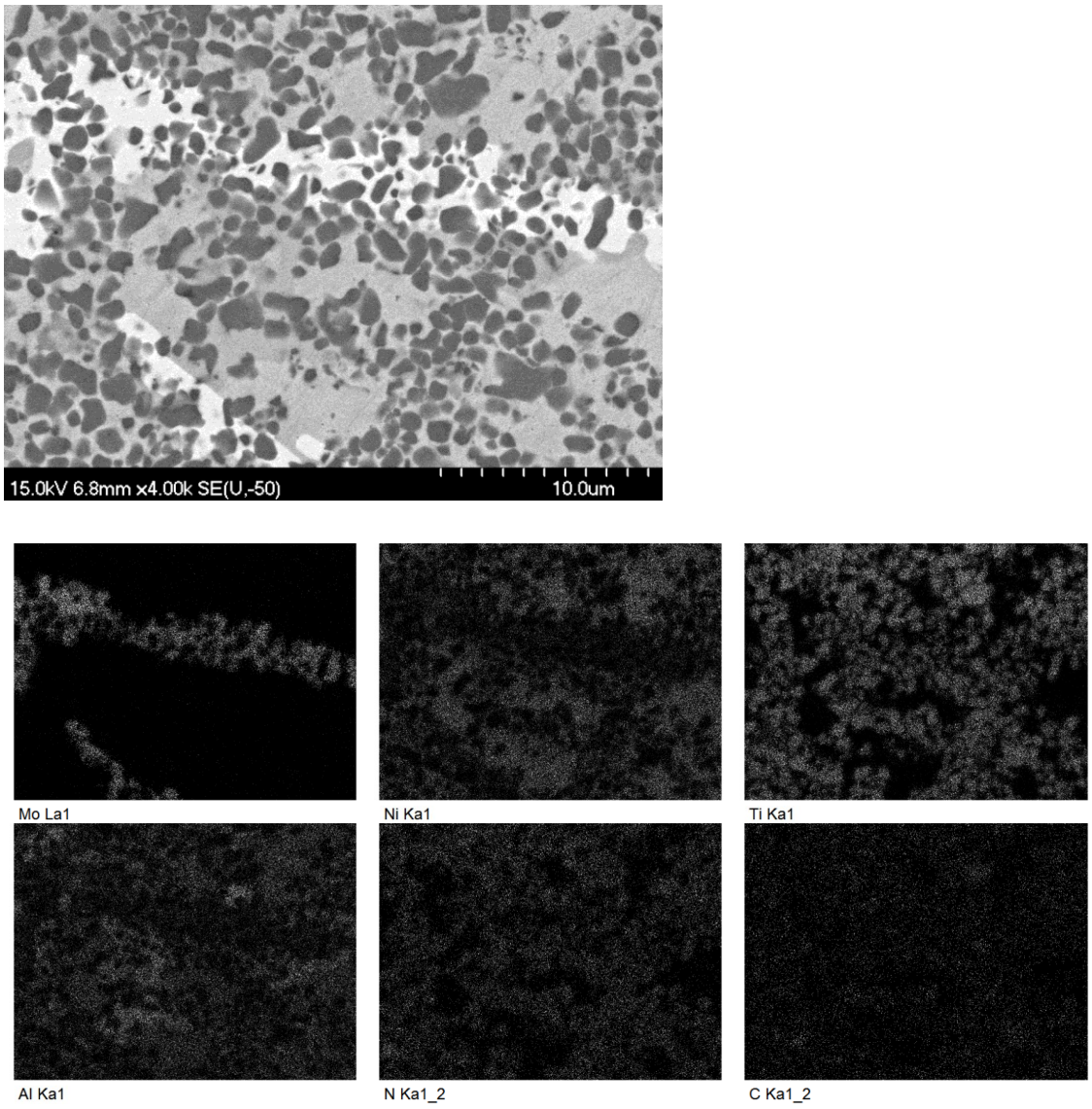

Figure 20. SEM micrographs and EDS analyses of $Ti(C_{0.3},N_{0.7})$-40 vol% Ni_3Al, prepared with: (a) 1.25 vol% Mo_2C, and (b) 10 vol% Mo_2C.

Table 2. EDS analysis of the chemical composition of phases present in the $Ti(C_{0.3},N_{0.7})$-40 vol% Ni_3Al-Mo_2C samples.

	1.25 vol%			10 vol%		
Element (at%)	Carbide	Binder	Mo Phase	Carbide	Binder	Mo Phase
C	18.5	15.1	21.0	25.4	11.9	24.9
N	35.2	8.8	28.1	24.1	2.8	16.1
Al	1.0	12.8	1.9	1.1	18.0	6.9
Ti	40.9	10.1	26.0	41.0	5.2	3.2
Ni	4.0	52.3	16.5	7.8	60.4	21.2
Mo	0.3	0.9	6.6	0.5	1.8	27.8

It is clear from both the XRD and EDS results that, as the amount of Mo_2C is increased in the microstructure, the corresponding phases present and chemical compositions in the cermets change. At the lower volume percentages the effect of Mo_2C is relatively small, as noted from the XRD spectra. However, when the amount is increased up to 5 and 10 vol%, a new phase becomes apparent, along with higher amounts of Mo present in the binder phase of the materials. These changes in the microstructure ultimately change the physical response of the samples, including the hardness, IFR and wear resistance as seen in subsequent chapters.

5 The Sliding Wear of TiC and Ti(C,N) Cermets Prepared with a Stoichiometric Ni_3Al Binder

Tyler L. Stewart and Kevin P. Plucknett

Materials Engineering Programme, Department of Process Engineering and Applied Science, Dalhousie University, 1360 Barrington Street, Halifax, Nova Scotia, CANADA

Abstract

TiC and Ti(C,N) based cermets offer several improved characteristics relative to conventional WC-based 'hardmetals', such as lower mass and improved oxidation resistance, which are combined with high toughness, hardness and wear resistance. In the present work the tribological behaviour of TiC and Ti(C,N) cermets has been evaluated under reciprocating sliding conditions. The cermets were produced using an *in-situ*, reaction sintering procedure to form the stoichiometric Ni_3Al binder, with the binder contents varied from 20 to 40 vol%. Wear tests were conducted using a ball-on-flat geometry, with a WC-6 wt% Co sphere as the counter-face material, for loads from 20 to 60 N. The wear response was characterised using a combination of optical profilometry, scanning electron microscopy, energy dispersive X-ray spectroscopy, and focused ion beam microscopy. Initially, two-body abrasive wear was observed to occur, which transitions to three-body abrasion through generation of debris from the cermet and counter-face materials. Ultimately, this wear debris is incorporated into a thin tribolayer within the wear track, which indicates a further transition to an adhesive wear mechanism. It was found that specific wear rates of the cermets increased with both applied load. The highest wear resistance was found for intermediate Ni_3Al contents.

Keywords: Abrasive wear; Adhesive wear; Tribolayer; Scanning electron microscopy; Focused ion beam microscopy

*email contact: kevin.plucknett@dal.ca

5.1 Introduction

Traditionally, tungsten carbide-cobalt (WC-Co) cemented carbides have been widely applied in demanding wear environments [1]. However, WC-Co has a number of performance limitations, such as poor oxidation and corrosion resistance, together with a high density [1]. As a consequence, titanium carbide and carbonitride (TiC and Ti(C,N), respectively) based cermets have received considerable recent attention due to a combination of favourable properties [2-5]. These include: high hardness, wear resistance, corrosion/erosion resistance, and fracture toughness [2-5]. TiC and Ti(C,N) cermets also have a good strength to weight ratio due to their low densities [2-5]. These cermets have been used in applications that utilise such properties, such as cutting tools and wear resistant coatings [6,7]. Ti(C,N) based cermets incorporate the benefits of both TiC and TiN, in the sense that in general the hardness increases proportionally with the percentage of TiC, while the wear properties improves with the amount of TiN [4]. TiN also has a superior thermal conductivity than TiC, which makes Ti(C,N) based cermets more thermal shock resistant than those based solely on TiC [4]. Typical metallic binders that have been used in the TiC and Ti(C,N) based cermets include nickel and cobalt [8], while more recently nickel aluminides and stainless steels have also been examined [9-11]. In particular, nickel aluminides based on the nominal stoichiometry Ni_3Al have many attractive properties, including a high oxidation resistance up to ~1100°C, due to the aluminium oxide (Al_2O_3) layer that forms [12,13]. Ni_3Al alloys also exhibit the ability to retain their strength and stiffness to elevated temperatures [14], which is a characteristic that is also transferred to related cermets [15].

In cermet systems the bulk mechanical properties, such as the fracture toughness and hardness, are invariably determined by the binder volume fraction and composition, as well as related microstructural parameters (e.g. the ceramic grain size and contiguity, as well as the metallic binder mean free path). For a constant grain size, the bulk hardness typically increases while the fracture resistance decreases, with both decreasing binder volume fraction and binder mean free path [16,17]. These parameters also influence the wear response, such that typically an increased binder content results in a reduction in the wear resistance [18,19]. Similarly, reducing the grain size also often increases the wear

resistance, as there is a reduced tendency towards cracking and fragmentation of the ceramic phase [20].

In the present work, TiC and Ti(C,N)-based cermets have been prepared with a nominally stoichiometric Ni_3Al binder through a simple *in-situ* reaction sintering process [21,22]. Ni_3Al contents have been varied from 20 to 40 vol%, while various Ti(C,N) compositions have also been assessed. The influence of composition upon the sintering response has been assessed, paying particular attention to microstructural development. The cermet properties have been evaluated using both Vickers indentation and reciprocating wear testing.

5.2 Experimental Procedure

The TiC (lot no. PL20125339; D_{50}=1.25 μm) powder was obtained from Pacific Particulate Materials (Vancouver, BC, Canada). The $Ti(C_{0.7},C_{0.3})$ (lot no. L25809; D_{50}=2.10 μm), $Ti(C_{0.5},N_{0.5})$ (lot no. L29865; D_{50}=1.74 μm), and $Ti(C_{0.3},N_{0.7})$ (lot no. L25747; D_{50}=1.72 μm) powders were all obtained from Treibacher Industrie AG (Althofen, Austria). The Ni_3Al binder constituents, in the form of Ni (lot no. L10W013; 2.2-3.0 μm) and Ni/Al 50/50 wt% (lot no. D28X029; D_{50}=38 μm) powders, were obtained from Alfa Aesar (Ward Hill, MA, USA). Powder mixtures were ball milled with 0.5 wt% polyvinyl butyral resin in acetone, using yttria stabilized zirconia media, at a media:powder ratio of 10:1 by mass. The mixture was then left to evaporate in a fume hood for a period of 24 hours before being sieved through a 75 μm mesh. The mixed powders were uniaxially pressed at 45 MPa (with ~0.6 ml hexane to act as a volatile binding aid during compaction) into disks (~31.75 mm diameter x ~4 mm thick). The disks were then sealed in plastic bags and cold isostatically pressed (CIPed) at 207 MPa. For sintering, the CIPed samples were placed on top of bubble alumina in an alumina crucible, with sintering performed at 1550°C for 1 hour under dynamic vacuum (~20 mTorr). A heating rate of 10°C/min was used, while the nominal cooling rate was 25°C/min (below ~800°C a slower, natural furnace cool was maintained).

The density of the sintered cermets was determined using Archimedes' principle, in water, at room temperature. Materialographic preparation for microscopy and subsequent

testing involved sequential grinding and polishing, starting with a 125 μm diamond impregnated resin pad and finishing with 0.25 μm diamond paste. Microstructural characterization was performed using scanning electron microscopy (SEM; Model S-4700, Hitachi High Technologies, Toyko, Japan), with associated compositional analysis performed in the SEM using energy dispersive X-ray spectroscopy (EDS; Inca X-max^N, Oxford Instruments, Concord, MA, USA). The grain size distributions and average grain sizes were determined using the mean lineal intercept method [23], from digital SEM images, using a commercial digital image-processing package (Image Pro, Media Cybernetics, Rockville, MD, USA). The contiguity and binder mean free path were determined in a similar manner, following the approach of Gurland [24,25]. The contiguity, C, relates the ratio of ceramic-ceramic to ceramic-binder interfaces intercepted per unit line length, and is determined following [24]:

$$C = \frac{2N_{c/c}}{2N_{c/c}+N_{c/b}} \qquad \text{Eqn 18}$$

where $N_{c/c}$ and $N_{c/b}$ are the number of ceramic-ceramic (e.g. TiC-TiC) and ceramic-binder (e.g. TiC-Ni_3Al) interfaces, respectively. The mean free path, d_b, is a measure of the Ni_3Al ligament dimensions between the ceramic grains, and is given by [24]:

$$d_b = \frac{1}{1-C}\left(\frac{V_b}{V_c}\right) d_c \qquad \text{Eqn 19}$$

where d_c is the mean ceramic grain size, and V_b and V_c are the volume fractions of the Ni_3Al binder and ceramic phases, respectively (it is assumed that $V_b + V_c = 1$).

The Vickers hardnesses (Model V-100A, Leco, St. Joseph, MI, USA) of the samples were determined at a load of 5 kgf to prevent indentation crack formation. Conversely, the indentation fracture resistance (IFR) was determined from the indentation crack lengths formed by Vickers indentations conducted at a higher load of 30 kgf. The IFR values were then determined using the approach of Niihara, assuming Palmqvist-type sub-surface cracking [26]

The reciprocating wear response of the cermets was determined following the same procedure as outlined for previous studies [10,11], using a ball-on-flat testing geometry on a universal micro-tribometer testing platform (UMT; Model UMT-1, Bruker Corp.,

Campbell, CA, USA). An applied normal load range of 20 to 60 N was examined, using a 6.35 mm diameter WC-Co counter-face sphere with 6 wt% Co. Wear tests involved 2 hours of reciprocating, dry sliding at a frequency of 20 Hz, with a track length of 5.03 mm; this gives a total sliding distance of ~1.45 km. The wear tests were performed at room temperature (21 ± 2ºC), with a relative humidity of 40-55%. The UMT system allows dynamic measurement of the coefficient of friction (COF) during wear testing. Optical profilometry examination was used to determine the volume of material removed during each test performed (Model PS50 Optical Profilometer, Nanovea, Irvine, CA). The specific wear rate, *k*, for each material was then calculated from the wear volume using the Lancaster approach [27], following:

$$k = \frac{V}{Pd} \qquad \text{Eqn 20}$$

where V is the volume of material removed (in mm^3), P is the applied load (in N), and d is the total sliding distance (in m). In addition to the microstructural characterisation methods outlined previously, the wear tracks were also examined using a focused ion beam microscope (FIB; Model F-2000A, Hitachi High Technologies, Tokyo, Japan). The FIB allows excision of small volumes of material through ion milling with Ga^+ ions [28]. In the present work this has been applied to section through any tribolayer that has been formed, to determine both the approximate tribolayer thickness and to assess any sub-surface damage generated immediately below the tribo-pair contact region.

5.3 Results and Discussion

5.3.1 Cermet Characterisation

The sintered cermets all achieved density values in excess of 98% of theoretical (Figure 21), with the exception of $Ti(C_{0.3},N_{0.7})$ prepared with the lowest binder content (i.e. 20 vol%). The reduced sintered density is due to the detrimental effect increasing N:C ratio has on the solubility of the Ti(C,N) in a molten metal [5]. This also is believed to affect wettability, as reported for previous studies of $Ti(C,N)/Ni_3Al$ cermets processed using a melt-infiltration method, and using the sub-stoichiometric Ni_3Al alloy IC-50, which includes both Zr and B additions [10].

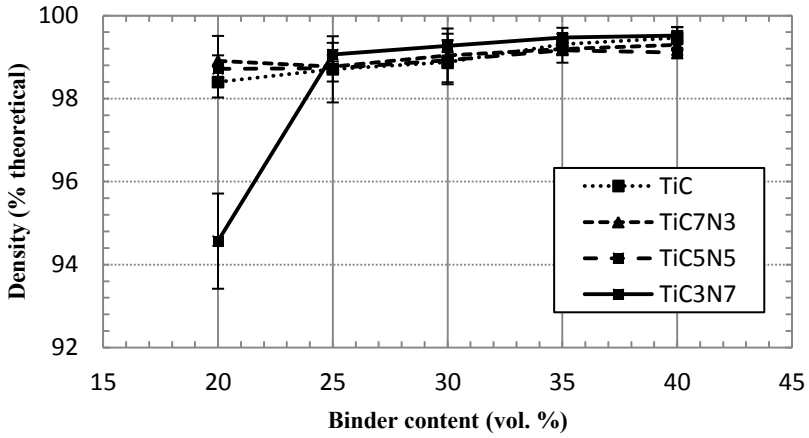

Figure 21. The effects of Ni_3Al binder content on the final sintered densities of the TiC and Ti(C,N) cermets.

The generally good densification characteristics for the TiC-Ni_3Al and Ti(C,N)-Ni_3Al systems are confirmed from examining the microstructures of representative examples of the processed materials, as shown in Figure 22. The cermets are generally homogeneous, with occasional isolated Ni_3Al-rich regions. The TiC grains were for the most part angular, while the Ti(C,N) based materials were more rounded, suggesting that the Ti(C,N) grains have a higher relative associated surface energy [29]. Qualitatively, it can also be seen from the SEM micrographs that the average grain size is significantly reduced for samples with N present in the ceramic phase, as compared to only TiC. A core/rim structure is apparent in the TiC samples when using back-scattered electron (BSE) imaging in the SEM, which is more sensitive to minor variations in average atomic number than conventional mixed secondary electron/BSE imaging. Through EDS analysis it was determined that the core is comprised of (undissolved) TiC, while the rim was mainly Ti and C, with relatively small amounts of W in solid solution. This W is believed to arise from an attrition step during the commercial preparation of the TiC powders. Figure 23 shows an EDS compositional profile across a TiC grain, highlighting the transition through the core-rim structure. In this case small amounts of W are clearly detected in the outer rim. There also appears to be a contrast in the grey levels seen in the binder phase, which is thought to be small amounts of W incorporation.

(a)

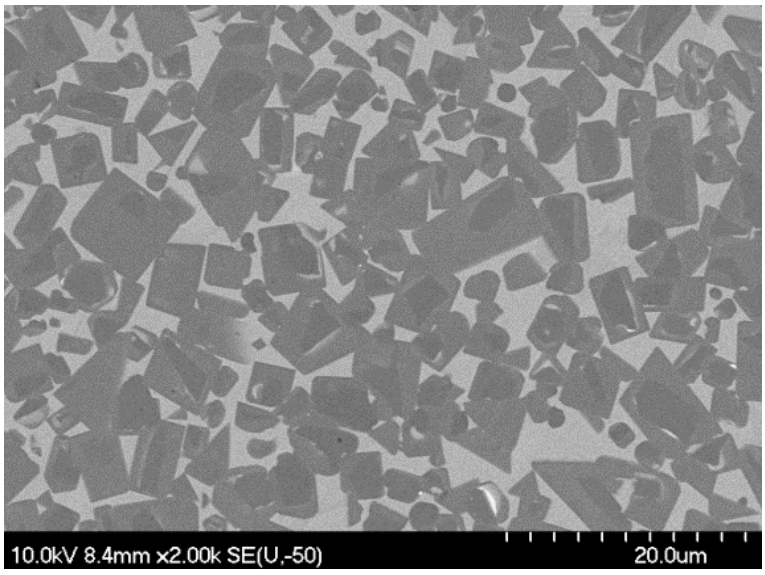

(b)

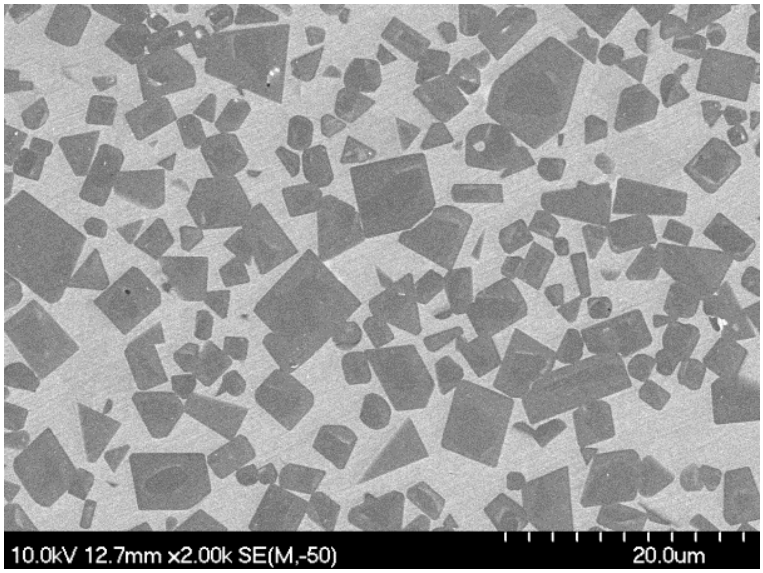

(c)

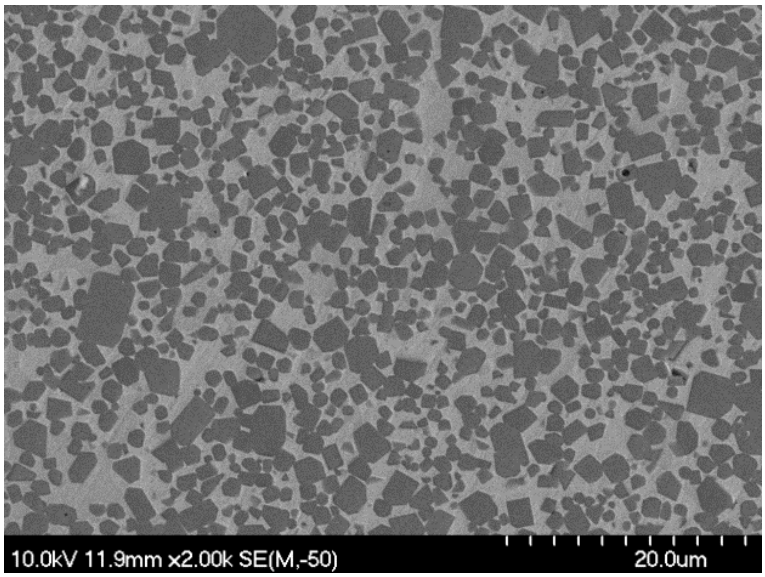

Figure 22. Representative SEM images of selected cermet samples: (a) TiC/20vol% Ni_3Al, (b) TiC/40vol% Ni_3Al, and (c) $TiC_{0.5}N_{0.5}$/40vol% Ni_3Al.

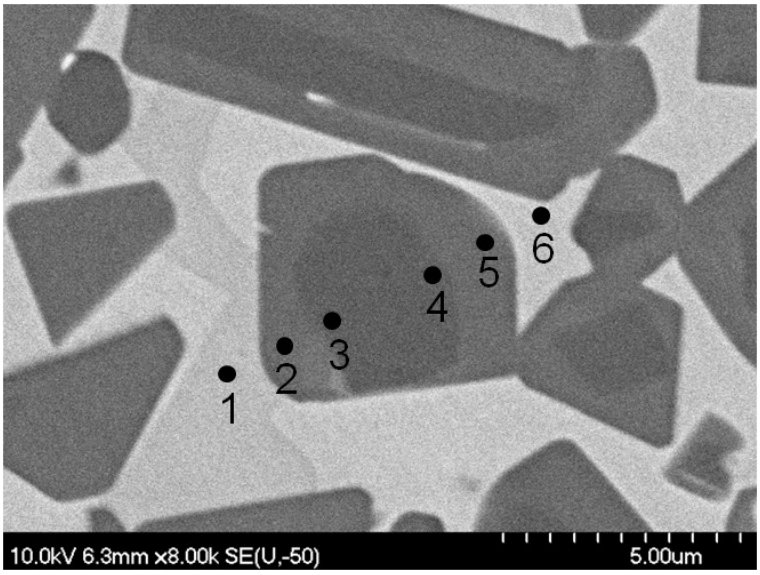

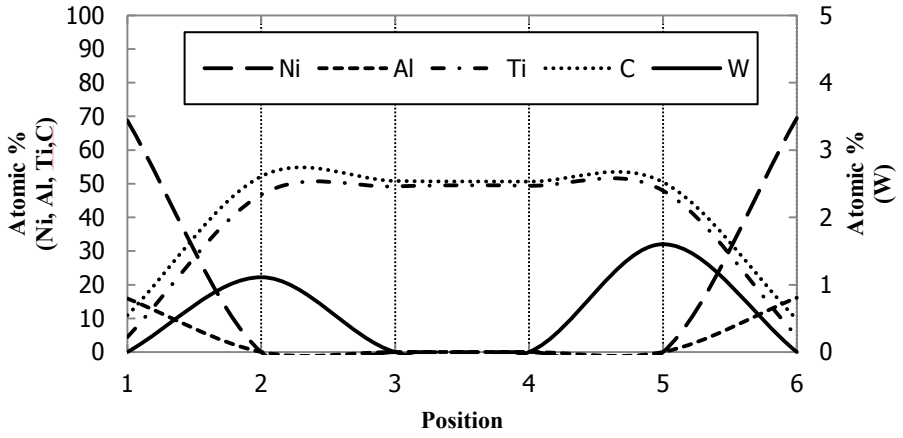

Figure 23. EDS point analyses demonstrating the composition of core-rim structure observed for the TiC-Ni_3Al cermets.

Figure 24 presents data for the mean grain size as a function of both the Ni_3Al volume fraction and the TiC/Ti(C,N) composition. It is clear that there is a considerable refinement of the grain size through incorporation of N into the ceramic. As noted previously, increasing N content in Ti(C,N) is reported to reduce the solubility in molten metals, which can be anticipated to have an effect on grain growth. However, there is little impact of binder volume fraction on the mean grain size. This observation is broadly similar to prior studies on both TiC-Ni_3Al and TiC-stainless steel cermets prepared by melt-infiltration [11,12], and indicates an interface controlled grain growth mechanism. In the present case, the resulting grain size is predominantly related to whether N is present, or not.

An important microstructural parameter in relation to the overall toughness and wear response of a cermet is the binder mean free path [30], which is effectively a measure of the average dimension of the ductile metal ligaments. This parameter takes both the grain size and the contiguity of the ceramic grains (e.g. TiC) into account, and is therefore also a good indication of whether the ceramic phase becomes more or less aggregated as the composition is varied from a low to high binder content. In general, it can be expected that as the amount of binder is increased, the mean free path should also increase, while the contiguity decreases. Figure 25 presents a measure of both the ceramic phase contiguity (Figure 25 (a)) and Ni_3Al binder mean free path (Figure 25 (b)) as a function of both the binder volume fraction and the ceramic phase composition. With increasing

binder content the contiguity can be seen to decrease, as can be expected from simply diluting the ceramic phase volume. It is also broadly apparent that decreasing the C:N ratio (i.e. increasing the N content) increases the contiguity, which can be expected if wetting is also adversely affected by such a change; in this case there is now effectively more aggregation of the ceramic particles. The mean free path broadly increases with binder content, as anticipated from prior studies [12]. In terms of the effect of C:N ratio, this is more subtle, and there is little effect for the Ti(C,N) powders. However, the N-free TiC cermets show significantly increased ligament dimensions, in line with their coarser microstructure, as highlighted previously in the grain size data presented in Figure 24 and the micrographs in Figure 22.

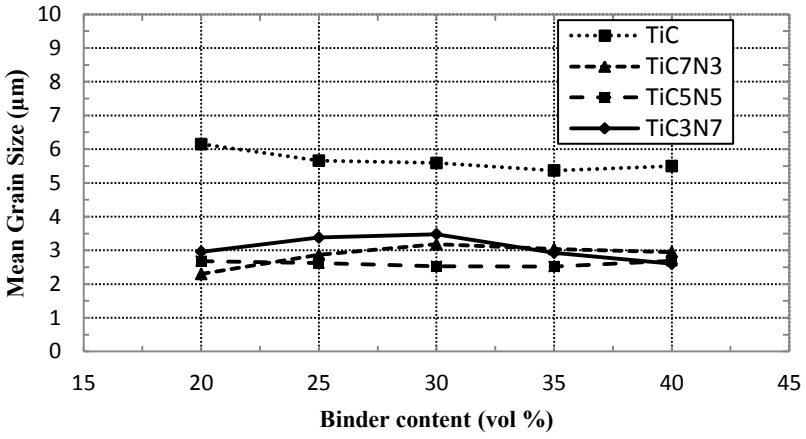

Figure 24. The mean ceramic-phase grain sizes as a function of Ni_3Al content and TiC or Ti(C,N) composition.

(a)

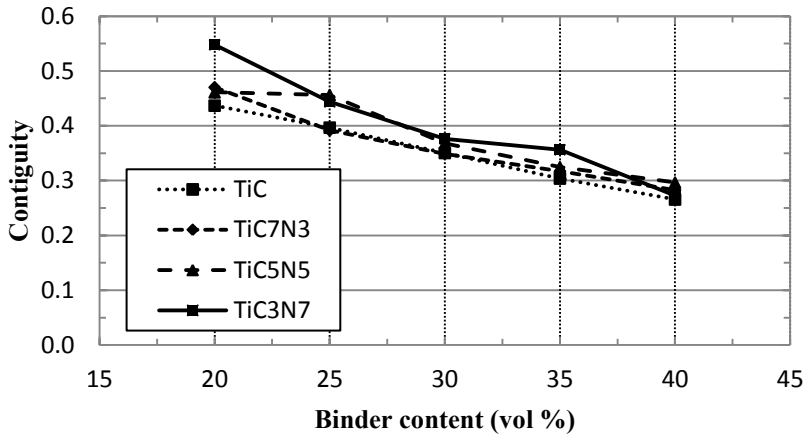

(b)

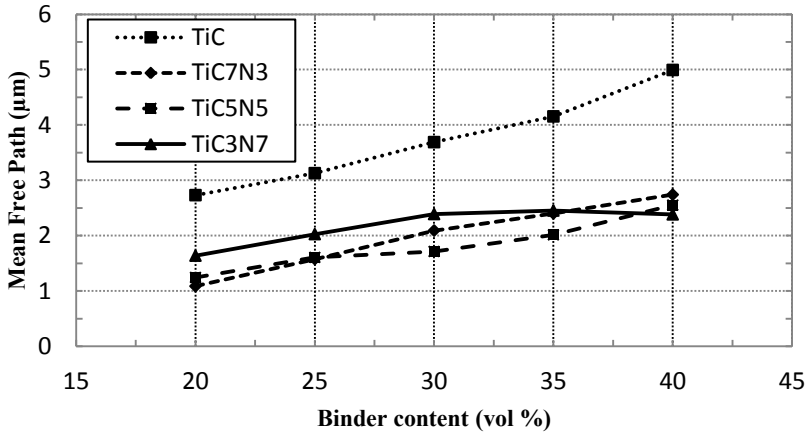

Figure 25. (a) The effects of Ni_3Al binder content and Ti(C,N) composition on: (a) the ceramic-ceramic contiguity, and (b) the binder mean free path.

5.3.2 Hardness and Indentation Fracture Resistance

In a cermet system the volume fraction of each component typically plays a key role in deciding the mechanical properties that it will exhibit. As the volume of the high elastic modulus ceramic phase is increased so too is the hardness. Conversely, the fracture toughness invariably decreases with increasing amounts of the harder phase. The mean hardness values achieved for the reaction sintered TiC- and Ti(C,N)-Ni_3Al cermets developed in the current work are presented in Figure 26. It is apparent that the TiC-based cermets exhibit the highest hardness, while the higher N content Ti(C,N)-based

materials exhibit the lowest hardness values. This general trend is comparable to previous studies of Ti(C,N)-based materials [31]. In general, the hardness of the cermets follows an approximately linear trend of decreasing with an increase in binder volume fraction. For the highest N content samples, with 20 vol% Ni_3Al binder, there is a sharp decrease in hardness that reflects the lower sintered densities achieved for that composition, as noted previously in Figure 21.

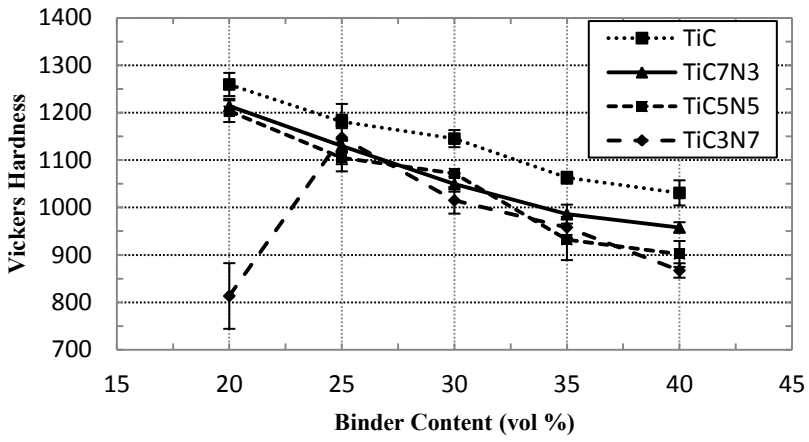

Figure 26. The effects of Ni_3Al binder content and Ti(C,N) composition on the Vickers indentation hardness. Each data point is the average of 5 measurements.

It is generally observed that the fracture toughness of cermets increases as the volume percentage of the binder phase is increased [17,32]. This is due to the fact that the fracture plane will contain more of the tougher metallic phase and less of the brittle ceramic. The ductile metal ligaments then bridge across the crack(s), impeding crack opening and growth [33,34]. For the case of Vickers indentation, the equation that is preferably used for calculation of the IFR depends upon the type of sub-surface cracking that occurs, either radial-median or Palmqvist [26]. To determine this, the ratio of the crack length, *c*, to the indentation size, *a*, can be assessed. If it is below 2.5 then the sample is believed to exhibit a more ductile behavior in the sense that Palmqvist-type cracks can be expected, instead of the half penny cracks, which are common for more brittle materials[26]. For the present case, by lowering the cermet binder content, the material should become more brittle, and therefore a transition point from Palmqvist to median-radial half penny cracks should ultimately arise. This transition point for the current materials is projected to arise below ~10 vol% binder, based on assessment of the

c:*a* ratio, and consequently it is assumed that all the materials in this study exhibit Palmqvist-type cracking behavior. Figure 27 displays the IFR of the samples that were examined in this study. It is apparent that as the binder content was increased the IFR increased proportionally. Generally, the samples experienced approximately the same increase in IFR, except for the highest binder content TiC sample, where there was a noticeable sharp increase from one composition to another. For this particular composition there is also a noticeably greater standard deviation, which may highlight some inhomogeneity in the structure, resulting in a greater spread of IFR values.

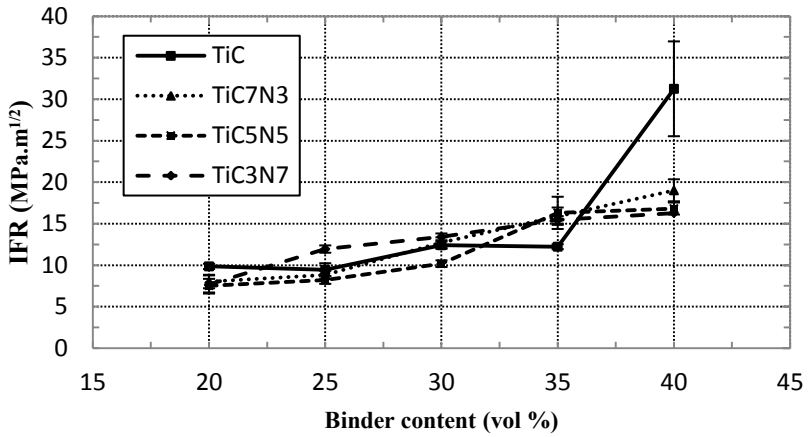

Figure 27. The effects of binder content and TiC or Ti(C,N) composition on the measured IFR, calculated assuming Palmqvist cracking [26]. Values are the mean of 5 measurements.

5.3.3 Reciprocating Wear Behaviour

The dynamic COF curves obtained for selected compositions, at applied loads from 20 to 60 N, are presented in Figure 28. It is apparent that for the lowest load (20 N) there is a greater amount of variation in the recorded COF curves over the duration of the wear tests, and these tests also invariably take longer to reach a steady state. At the higher loads of 40 and 60N, the variation is lower and steady state conditions are obtained at a relatively faster rate. This trend is more readily observed while examining the COF curves for the higher volume percentage of binder, which suggests that the metal binder content plays a key role in the frictional response of these materials. The steady state response is an indication that sufficient material has been removed to create a coupled

surface in which the tribo-pairing can slide without interference from any asperities that may be present on either face.

(a)

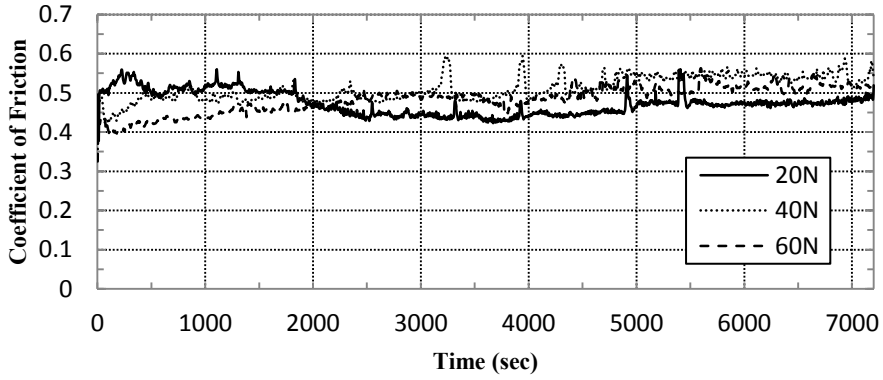

(b)

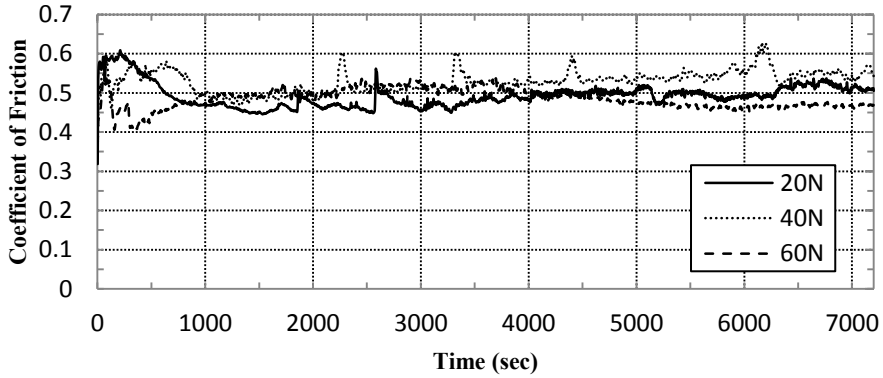

(c)

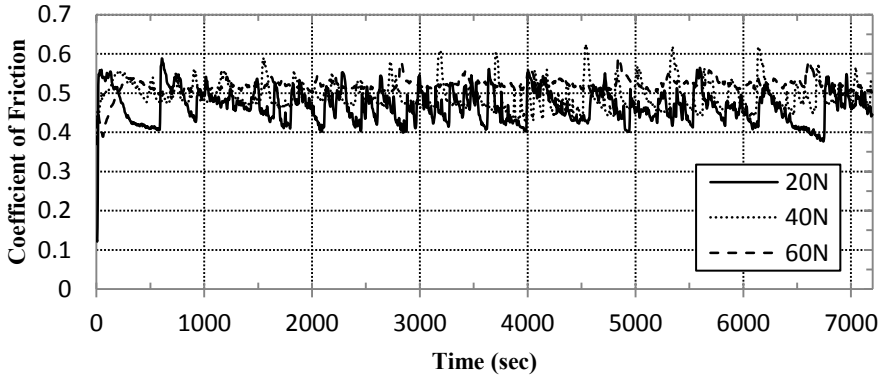

Figure 28. The instantaneous COF obtained with 20 to 60 N applied loads for: (a) $Ti(C_{0.7},N_{0.3})$ with 20 vol% Ni_3Al, (b) $Ti(C_{0.5},N_{0.5})$ with 20 vol% Ni_3Al, and (c) $Ti(C_{0.5},N_{0.5})$ with 40 vol% Ni_3Al.

From Figure 29 it can invariably be seen that as the binder content is increased, the steady state COF decreases slightly. This trend may be due to the increasing formation of a tribolayer during reciprocating sliding, discussed in more detail in section 3.4, which is likely to be more prevalent for the higher binder content samples. The COF values observed for the present materials are consistently within the range of 0.45 to 0.52, which are broadly comparable to those observed with generally similar cermet materials. For example, Ti(C,N)/Ni based cermets, with various carbide additions, exhibited steady state COF values between 0.46 and 0.52 with applied loads of 20 and 50 N, using a 100Cr6 steel counterface [35]. In a related study to the present one, examining TiC and Ti(C,N) cermets processed by melt-infiltration with a sub-stoichiometric Ni_3Al alloy (IC-50), Buchholz and colleagues reported steady state COF values between 0.3 and 0.45 [10]. Similarly, TiC-stainless steel cermets, with a 304L grade binder, exhibited steady state values of the COF between 0.18 and 0.38. Bonny and colleagues reported both static and dynamic COF values between 0.39 and 0.76 for various WC-Co tribo-pairs [36].

(a)

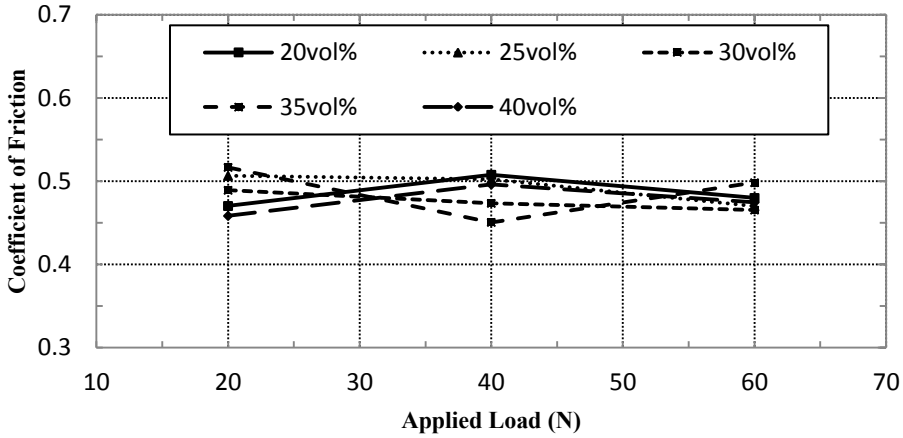

(b)

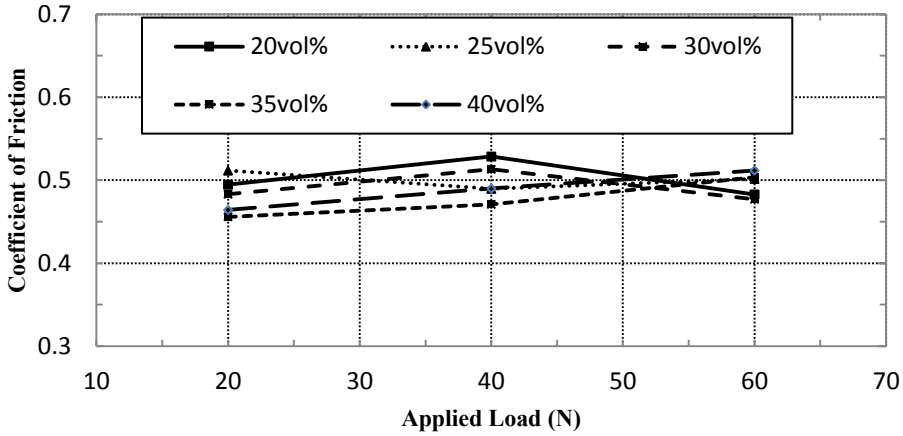

Figure 29. The effects of Ni_3Al binder content on measured, steady state COF obtained under applied loads between 20 and 60 N, for: (a) $Ti(C_{0.7},N_{0.3})$, and (b) $Ti(C_{0.5},N_{0.5})$.

The measured volume loss that arises during the reciprocating wear tests is presented in Figure 30. In general, the volume loss increases in a nominally linear manner with applied load. This response corresponds with previous studies that demonstrate that the total volume lost during sliding depends upon both the duration of contact and the forces exhibited upon the material during contact [27,37]. It can also be noted from Figure 30 that the highest volumetric wear loss is generally observed with the highest binder content, which can be anticipated due to the decreasing amounts of the harder, more wear resistant ceramic phase. However, it is often apparent that the lowest wear volumes

correspond with intermediate levels of binder, highlighting a compromise in response between high toughness and high hardness. As the amount of Ni_3Al binder is increased the contiguity of the ceramic grains decreases, as shown previously in Figure 25(a). There is consequently a decrease in the rigid ceramic/ceramic contact area throughout the microstructure. Conversely, the binder mean free path is increased with the amount of binder present (Figure 25 (b)), and the material effectively becomes tougher and more damage tolerant. These parameters therefore provide a good indication as to how the material will likely respond during wear tests, since the influence of the ceramic phase can be determined from these observations. It should be noted that the significantly higher wear volume noted for $Ti(C_{0.3},N_{0.7})$ with 20 vol% Ni_3Al arises due to the high residual porosity (Figure 21), and hence lower hardness and IFR (Figures 6 and 7).

(a)

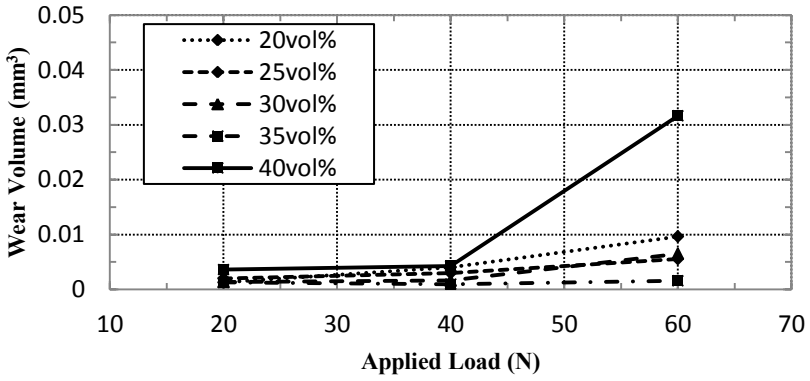

(b)

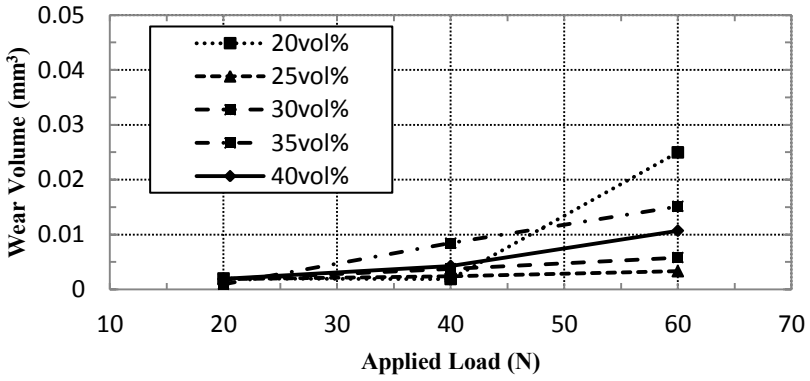

(c)

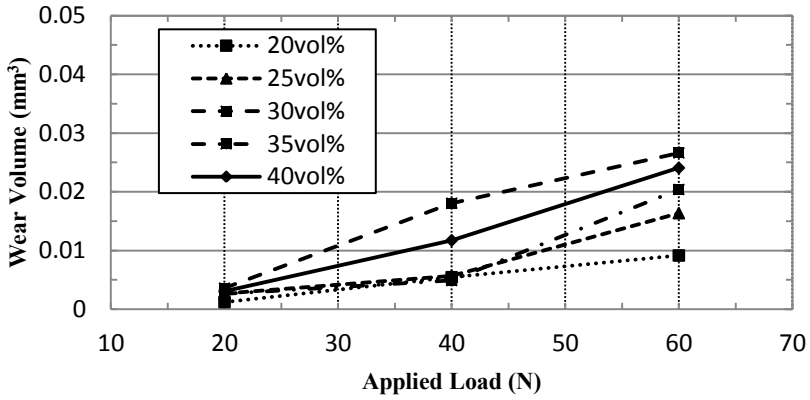

(d)

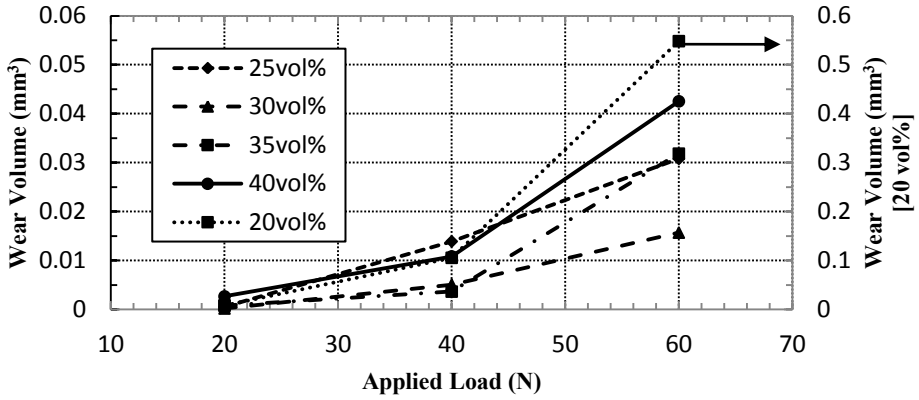

Figure 30. The measured wear volumes as a function of applied load and Ni_3Al binder content, for: (a) TiC, (b) $Ti(C_{0.7},N_{0.3})$, (c) $Ti(C_{0.5},N_{0.5})$, and (d) $Ti(C_{0.3},N_{0.7})$.

The specific wear rates were subsequently calculated from the volumetric wear loss values, as shown in Figure 31, following Eqn. 20. As would be expected, the specific wear rate data follow a similar trend to that of the volumetric loss values. As the specific wear rate is normalised by the load in the Lancaster equation, it could be argued that the applied load should not be a factor in the specific wear rates measured. However, it is clear that this assumption is somewhat contradicted by the calculated values shown in Figure 31, and a similar response has been noted by other researchers for comparable cermet systems [10,11,35]. A probable explanation for such observations is that the wear mode is transitioning with increasing load, such that material loss increases; this is discussed in greater detail in Section 3.4.

The actual measured specific wear rates, typically between 0.5 and 5 x 10^{-7} mm^3/Nm, compare favourably with a variety of other cermet systems measured using similar approaches. Notably, this range is approaching an order of magnitude better than those made for similar TiC-Ni_3Al cermets prepared through the melt infiltration process. Those prior materials exhibited occasional processing flaws, in the form of large voids (up to ~200 μm in length), which will result in localized stress concentration during wear tests, resulting in an increased rate of material loss. Pirso and colleagues reported specific wear rates between 6 and 9 x 10^{-7} mm^3/Nm, for similar volume percentages of binder (18 to 30.6 vol.%), when testing WC-Co cemented carbides against a carbon steel (0.45 wt.% C) at loads of 40 to 180 N [38]. In another study on fine grained (0.07 and 1.2 μm) WC-Co cemented carbides, with between 11.7 and 30.5 vol% binder, Jia and Fischer determined specific wear rates between 3 and 7 x 10^{-7} mm^3/Nm at an applied normal load of 9.8 N [33].

(a)

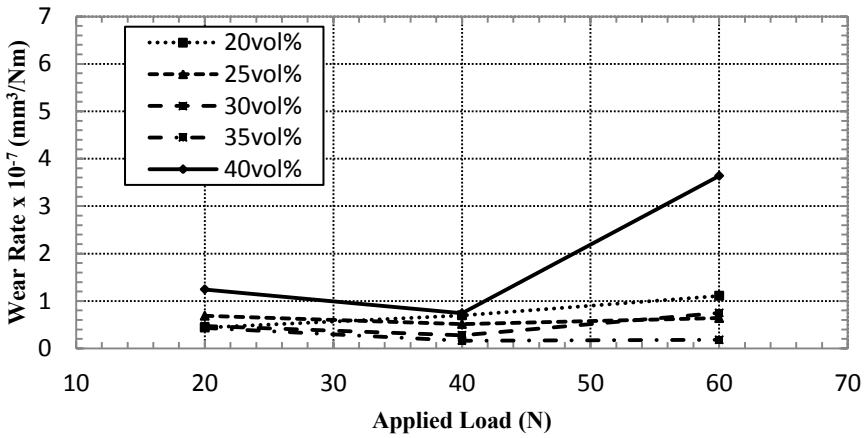

(b)

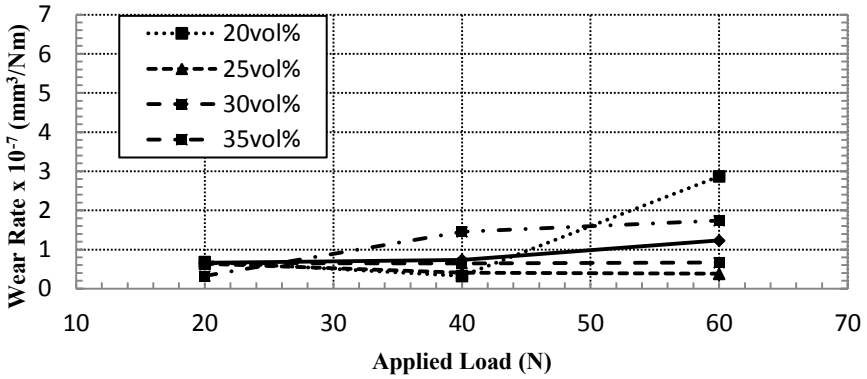

(c)

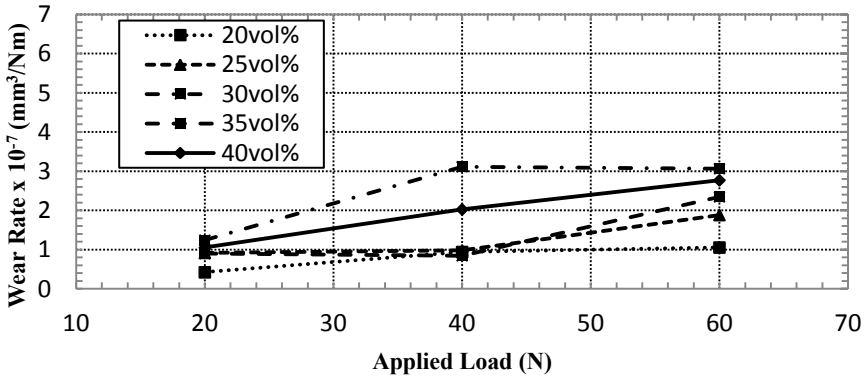

(d)

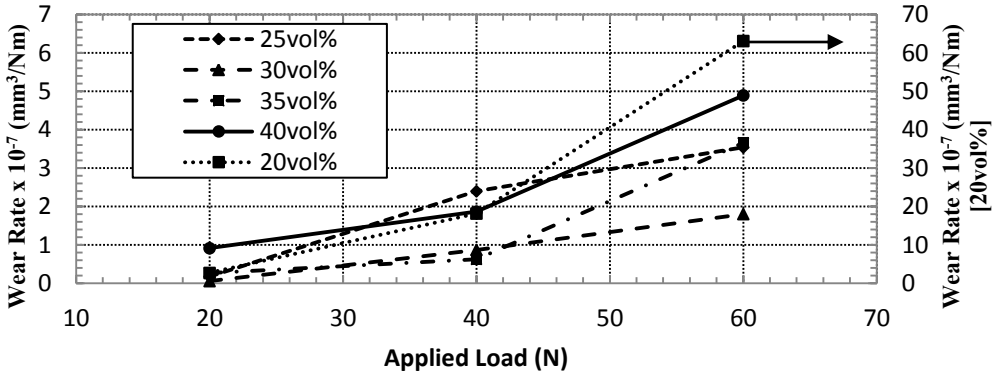

Figure 31. The specific wear rates for the TiC and Ti(C,N) cermets as a function of binder content and applied test load: (a) TiC, (b) $Ti(C_{0.7},N_{0.3})$, (c) $Ti(C_{0.5},N_{0.5})$, and (d)

$Ti(C_{0.3},N_{0.7})$. Note the scale change (right hand axis) for samples prepared with $Ti(C_{0.3},N_{0.7})$ and 20 vol% Ni_3Al.

5.3.4 Microstructural Analysis of Wear Tracks

During the wear process features can be observed in the wear track that indicate not only the type of wear mechanism(s), but also the severity. Factors such as the damage accumulation in the vicinity of the wear track, damage to the ceramic grains, and the formation/amount of tribolayer that is generated during the sliding process. As seen in Figure 32, there is no evidence of microstructural damage in the region adjacent to the wear track (e.g. plastic deformation evident in the form of surface uplift or ceramic particle cracking). Evidence for the formation of a tribolayer is readily apparent, although again it does not appear to have advanced beyond the limits of the wear track itself. One potential cause of damage to the microstructure adjacent to the wear track would be a rapid rise in temperature generated from the frictional forces arising during the reciprocating tests. However, through use of a thermal imaging camera it has been determined that the temperatures achieved are not sufficient to cause substantial damage to the structure. For the lowest applied load of 20 N the sample temperature rose to ~68°C in the wear track region, at 40 N to ~89°C, while at the highest load of 60 N the temperature rose to ~100°C. These values agree for the most part with previous studies that investigated the influence of temperature on the wear of similar cermets [38].

(a)

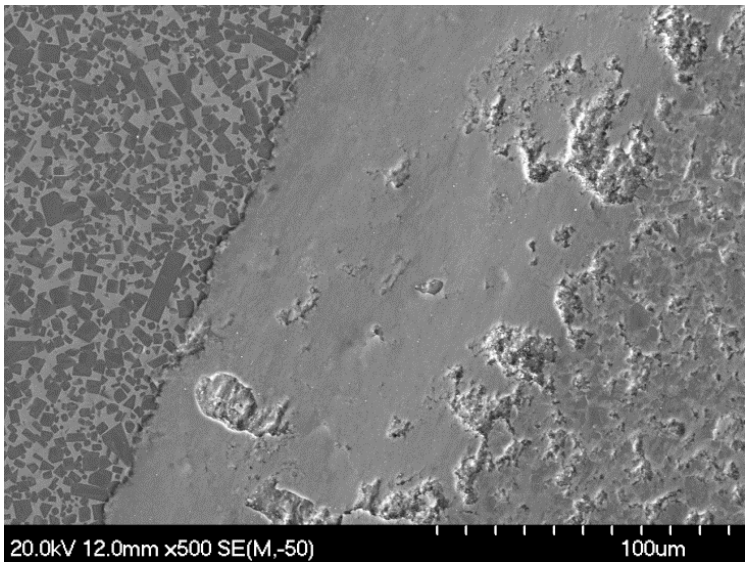

(b)

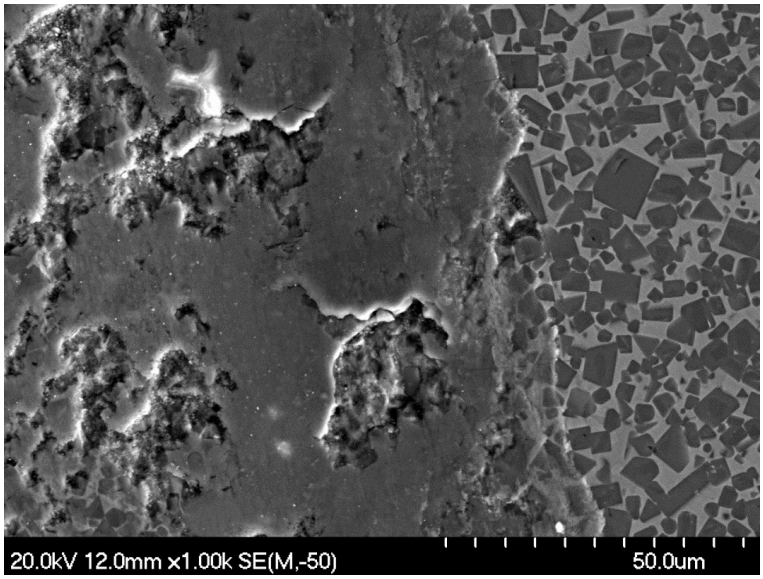

Figure 32. Typical examples of the wear track microstructures, showing minimal damage or microstructural change in the region immediately adjacent to the wear tracks: (a) $Ti(C_{0.7},N_{0.3})$ with 20 vol% Ni_3Al, (b) TiC with 35 vol% Ni_3Al. Both samples were tested using a 60 N applied load.

The extent of tribolayer formation on the samples during sliding increases with the applied load, as shown in Figure 33. At the lowest load (20 N) there is limited evidence of the binder phase being removed, while the ceramic grains are still apparent. Binder removal results from extrusion under the moderately high Hertzian loading. In this instance there seems to be little tribolayer formed. As the load is increased to 40 N, the damage becomes more noticeable, and the formation of a tribolayer starts to become apparent. There is also evidence of the ceramic grains being pulled out of the cermet structure. Upon further increase of the load to 60 N, the appearance of a tribolayer becomes significantly more obvious. The tribolayer forms when the third-body wear debris is sufficiently reduced in size to form a homogenous mass that is essentially forced into the wear track under the high contact loading. In prior studies it has been shown that the tribolayer contains a high oxygen content [39], which is confirmed in the present work in Section 3.5 of this study. It can act as a form of a lubricant to a certain extent, which can influence the COF values observed during the wear tests. Since the layer invariably has a high oxide content, it is inherently brittle in nature. In confirmation of

this, cracking is apparent in the tribolayer of the samples in Figure 33 under the highest applied load.

(a)

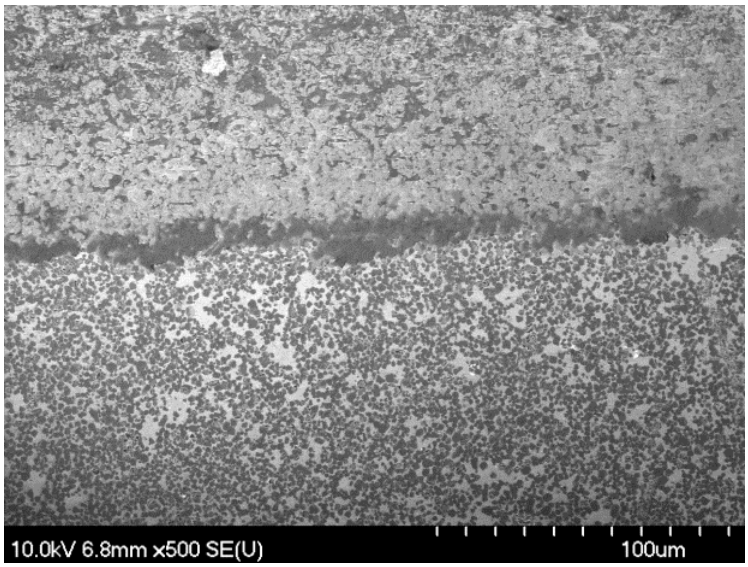

(b)

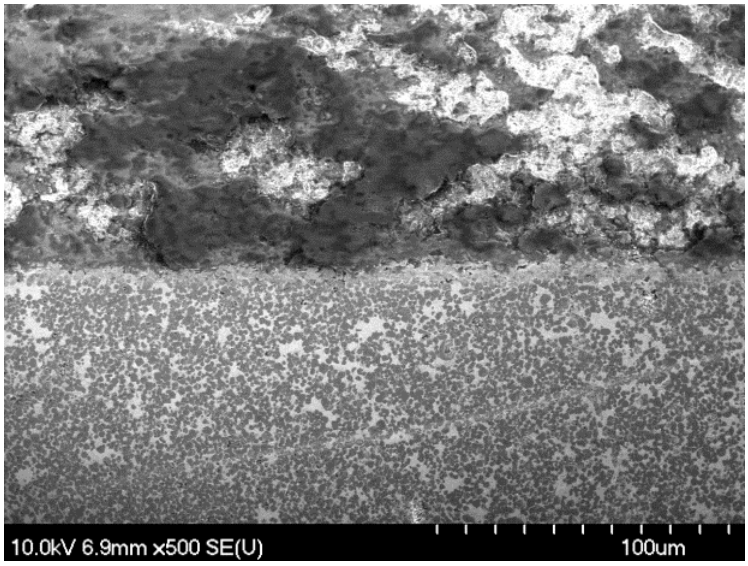

(c)

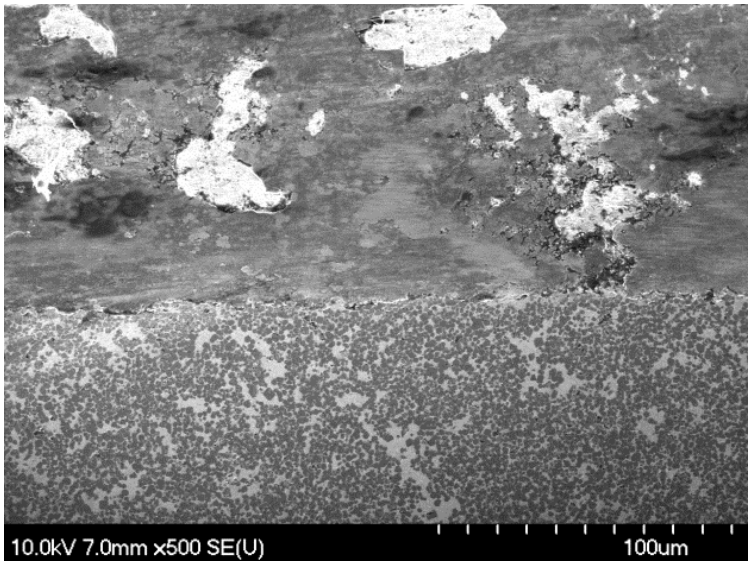

Figure 33. Typical examples of the formation of tribolayers within the wear track of $Ti(C_{0.3},N_{0.7})$ with 40 vol% Ni_3Al, under applied loads of: (a) 20 N, (b) 40 N, and (c) 60 N.

During the early stages of cermet wear, damage to the microstructure can be attributed to preferential removal of the binder material, through extrusion, which leads to fragmentation of the ceramic grains and their removal from the framework they were previously embedded in. The sequence of events that is believed to occur that leads to the ceramic damage is as follows: removal of the binder phase from the surface, plastic deformation of the binder phase below the surface, accumulation of strain in the ceramic grains, their fracture and fragmentation, and finally grain fragment pullout and removal [40]. This sequence arises due to the low hardness of the binder phase when compared to the ceramic (i.e. TiC or Ti(C,N)), which on its own has very good wear resistance. The ceramic grains can also exhibit direct fracture due to the high contact forces exerted upon them during the test. Evidence for grain fragmentation within the wear track can be seen in Figure 34(a). Here there are individual grains that remain *in-situ*, but are showing early evidence of damage accumulation in the form of cracks and partial material removal. Figure 34(b) shows a broadly similar region, where initial evidence of tribolayer build-up is apparent within the wear track (to the left hand side), with material being smeared across the surface of the ceramic grains. At the edge of the wear track there is a greater

amount of tribolayer build-up, and some evidence of spalling of this layer is also now apparent.

(a)

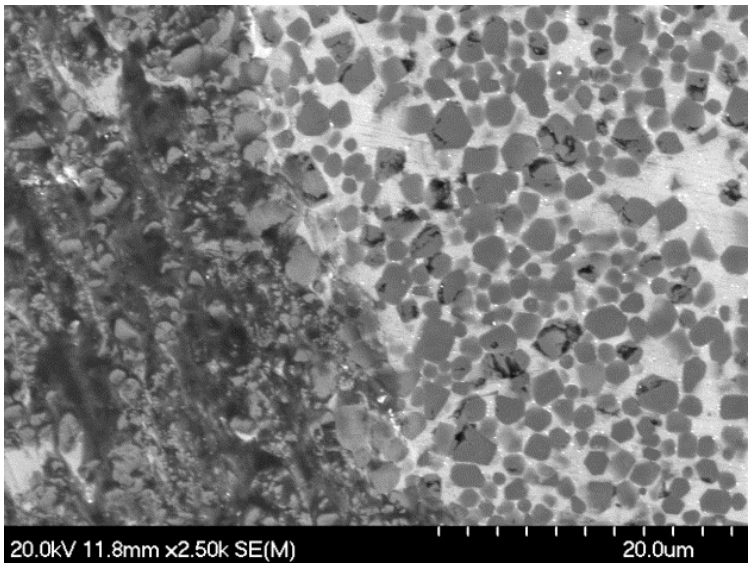

(b)

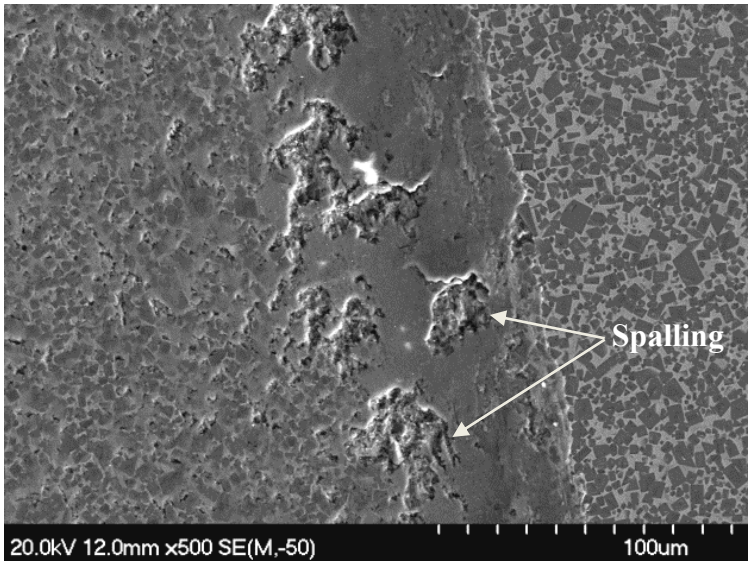

Figure 34. (a) SEM image showing wear of the binder phase and carbide fracture/removal in $Ti(C_{0.3},N_{0.7})$ with 40 vol% Ni_3Al, tested at an applied load of 40 N. (b) Spalling of the tribolayer in TiC with 30 vol% Ni_3Al, tested at an applied load of 60 N; the wear track is on the left hand side of the image. In this instance some initial smearing of the binder material also appears to be occurring.

In order to assess both the thickness of the tribolayer and whether sub-surface damage was occurring, FIB microscopy was used to section through the tribolayer of selected compositions. Figure 35 demonstrates a FIB machined section through the tribolayer formed at 80 N load in Ti($C_{0.3}$,$N_{0.7}$)-25 vol%. BSE imaging shows the remaining protective tungsten layer (bright contrast) deposited on the surface of the tribolayer (dark contrast), as highlighted in Figure 35(a). The tribolayer itself is approximately 1.5 to 2.5 μm thick in this region, and it can be seen that the sub-surface cermet region is worn somewhat irregularly, such that the tribolayer thickness and cermet surface profile varies quite significantly. In terms of the external tribolayer surface, this is actually relatively flat, and presumably corresponds closely to the surface profile of the WC-Co counter face sphere. The tribolayer appears to exhibit discrete laminae, from repeated deposition of fine, third-body material during the wear tests, as well as evidence of cracking (Figure 35 (b)). The fine, light contrast material that is clearly present both on the surface of the tribolayer and through its thickness is debris from the WC-Co ball. Examining the cermet region below the tribolayer, two further features can be noted. There is no evidence of any cavitation within the ductile metal binder, or any sub-surface cracking or ceramic grain fracture. In order to determine the approximate location of the maximum shear stress under Hertzian loading a simplified model which assumes an elastic material was applied, where the contact radius *a* is given by [41,42]:

$$a^3 = \frac{4kPr}{3E} \qquad \text{Eqn 21}$$

where *E* is the Young's modulus, *r* is the radius of the counterface material, *P* is the applied normal load and the constant *k* is equal to:

$$k = \frac{9}{16}\left[(1-\nu^2)\frac{(1-\nu\prime^2)E}{E\prime}\right] \qquad \text{Eqn 22}$$

where the prime notation denotes the counter face material. To determine both the elastic moduli and the Poisson's ratio of the cermet and counterface materials the effective bulk modulus *K* and shear modulus μ of the composites need to be determined (where the r and m denotes the reinforcement and matrix respectively). An upper and lower estimate of the moduli are then determined following [43]:

$$K^{upper} = K\mathrm{r} + (1 - \mathrm{f})\left[\frac{1}{K\mathrm{m} - K\mathrm{r}} + \frac{3\mathrm{f}}{3K\mathrm{r} + 4\mu\mathrm{r}}\right]^{-1} \quad \text{Eqn 23}$$

$$K^{\mathrm{lower}} = K\mathrm{m} + \mathrm{f}\left[\frac{1}{K\mathrm{r} - K\mathrm{m}} + \frac{3(1-\mathrm{f})}{3K\mathrm{m} + 4\mu\mathrm{m}}\right]^{-1} \quad \text{Eqn 24}$$

$$\mu^{\mathrm{upper}} = \mu\mathrm{r} + (1 - \mathrm{f})\left[\frac{1}{\mu\mathrm{m} - \mu\mathrm{r}} + \frac{6\mathrm{f}(K\mathrm{r} - 2\mu\mathrm{r})}{5\mu\mathrm{r}(3K\mathrm{r} + 4\mu\mathrm{r})}\right]^{-1} \quad \text{Eqn 25}$$

$$\mu^{\mathrm{lower}} = \mu\mathrm{m} + \mathrm{f}\left[\frac{1}{\mu\mathrm{r} - \mu\mathrm{m}} + \frac{6(1-\mathrm{f})(K\mathrm{m} - 2\mu\mathrm{m})}{5\mu\mathrm{m}(3K\mathrm{m} + 4\mu\mathrm{m})}\right]^{-1} \quad \text{Eqn 26}$$

After taking the average of the upper and lower estimates of both the bulk and shear moduli the effective elastic modulus and Poisson's ratio of the composites can be calculated by [44]:

$$E = \frac{9K}{1 + \frac{3K}{\mu}} \quad \text{Eqn 27}$$

$$\nu = \frac{3K - 2\mu}{2(\mu + 3K)} \quad \text{Eqn 28}$$

The approximate location of the maximum shear stress is then equal to ~0.5a. Thus for the TiC-Ni_3Al [45-47] cermet, under an applied normal load of 60 N and with WC-Co [48-50] as the counterface, the approximate location of the maximum shear stress is around 44 μm beneath the surface of the material.

(a)

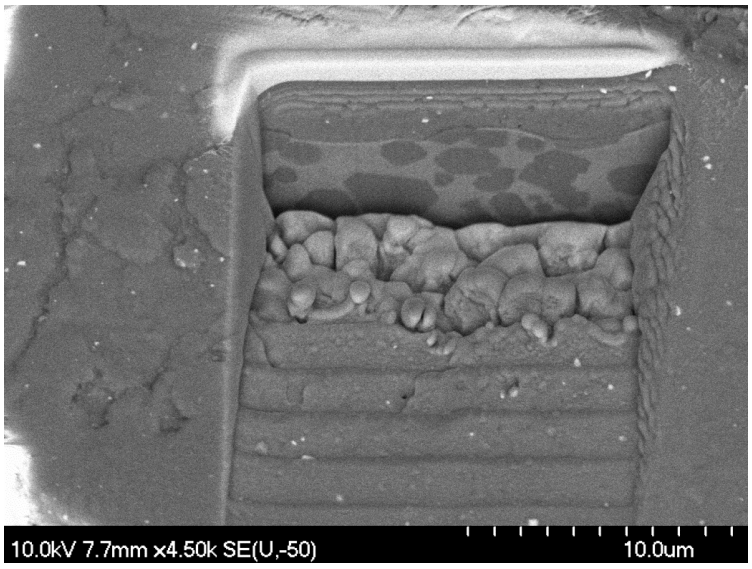

(b)

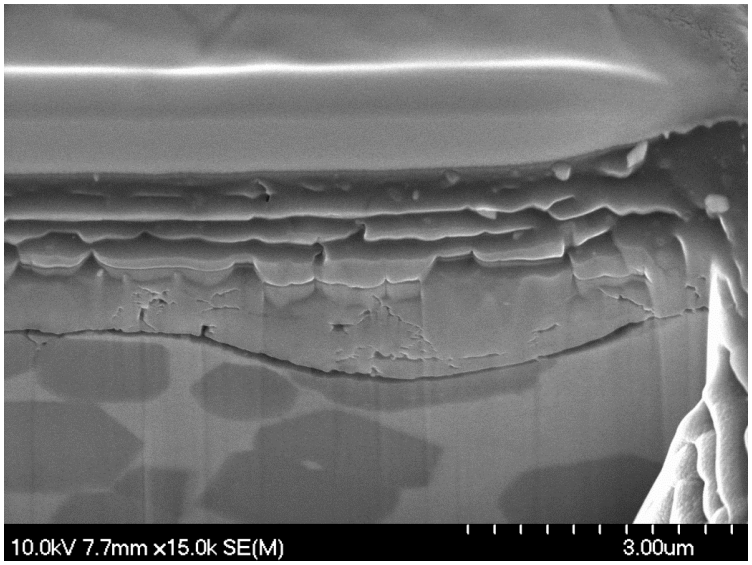

Figure 35. FIB generated section through the tribolayer in $Ti(C_{0.3},N_{0.7})$ with 25 vol% Ni_3Al after wear testing under a load of 80 N for 120 minutes: (a) Low magnification BSE image showing the staircase cut and remnant W protective layer. (b) Higher magnification, mixed SE/BSE image of the end of the cut showing the tribolayer thickness, wear track profile and cracking in the tribolayer.

5.3.5 Chemical Composition of the Tribolayer

The tribolayers that were formed during the reciprocating wear tests were analysed to characterise their respective compositions, and to assess the influence of both the applied load and ceramic phase composition. Tables 3 and 4 highlight data obtained from area EDS analyses of the nominal tribolayer compositions of selected samples. It is clear that there is a relatively high O incorporation into the tribolayer; initially the materials are prepared with starting components having low levels of O. This arises due to the two- to three-body wear transition, and the subsequent severe attrition of the third-body material during the reciprocating sliding motion. Ultimately this material is deposited as a homogeneous tribolayer, with little evidence of the original discrete ceramic and metallic phases. This process involves the repeated fracture and refinement of the ceramic particle debris, which will become intimately mixed with the intermetallic binder. Oxygen incorporation then occurs continuously due to the formation of new, clean surfaces, which subsequently rapidly oxidise to form a passive surface layer.

It is notable that the cermets with higher initial N contents also typically exhibit somewhat higher oxygen levels following testing, for both the low and high applied loads. This suggests that the tribolayer for these samples exhibits a higher degree of oxidation, in relation to the C-rich compositions, and correlates with the formation of the tribolayer at a higher rate. This broadly agrees with the observed specific wear rates, shown previously in Figure 31, where the higher N content samples invariably exhibited the highest wear rates. Comparing Tables 3 and 4, it is apparent that increasing the testing load (from 20 to 60 N) does not result in any significant increase in the O content. Similarly, binder content does not appear to have a great influence on the extent of O incorporation into the tribolayer. The presence of tungsten in the tribolayer suggests the transfer of material from the counter face sphere, which is a typical feature of adhesive wear.

A series of EDS mapping images, obtained in the SEM, are shown in Figure 36. This region shows the end of a wear track (for $Ti(C_{0.7},N_{0.3})$ with 30 vol% Ni_3Al), following testing at an applied load of 60 N for 120 minutes. There is a clear boundary between the unworn microstructure and the tribolayer, which is particularly evident from examining the oxygen levels. This further confirms the lack of thermal oxidation of the sample due to wear, and supports the third-body attrition process outlined earlier. Spalled regions within the tribolayer can also be seen, which are identified as dark areas within the tribolayer when assessing the O EDS map, and as lighter areas for the Ti, Ni and Al maps.

Table 3. The nominal tribolayer compositions (in at%) for TiC and Ti(C,N) samples, prepared with 25 vol% Ni3Al. All samples were tested at an applied load of 20 N for 120 minutes.

Element (KLM Line)	**TiC**	**Ti($C_{0.7}$,$N_{0.3}$)**	**Ti($C_{0.5}$,$N_{0.5}$)**	**Ti($C_{0.3}$,$N_{0.7}$)**
O (K)	44.55	52.56	38.85	65.29
C (K)	21.13	17.08	18.25	4.69
Ti (K)	21.25	22.85	27.67	16.42
Ni (K)	9.39	8.88	11.69	6.41
Al (K)	2.21	2.17	2.96	1.26
W (M)	0.79	0.65	0.58	0.34

Table 4. The nominal tribolayer compositions (in at%) for TiC and Ti(C,N) samples, prepared with 30 vol% Ni_3Al. All samples were tested at an applied load of 60N for 120 minutes.

Element (KLM Line)	**TiC**	**Ti($C_{0.7}$,$N_{0.3}$)**	**Ti($C_{0.5}$,$N_{0.5}$)**	**Ti($C_{0.3}$,$N_{0.7}$)**
O (K)	50.94	44.51	41.24	62.50
C (K)	15.49	16.78	16.90	5.28
Ti (K)	18.66	23.51	25.45	19.00
Ni (K)	10.58	11.26	12.60	9.55
Al (K)	2.61	3.07	3.16	2.85
W (M)	1.16	0.70	0.66	0.68

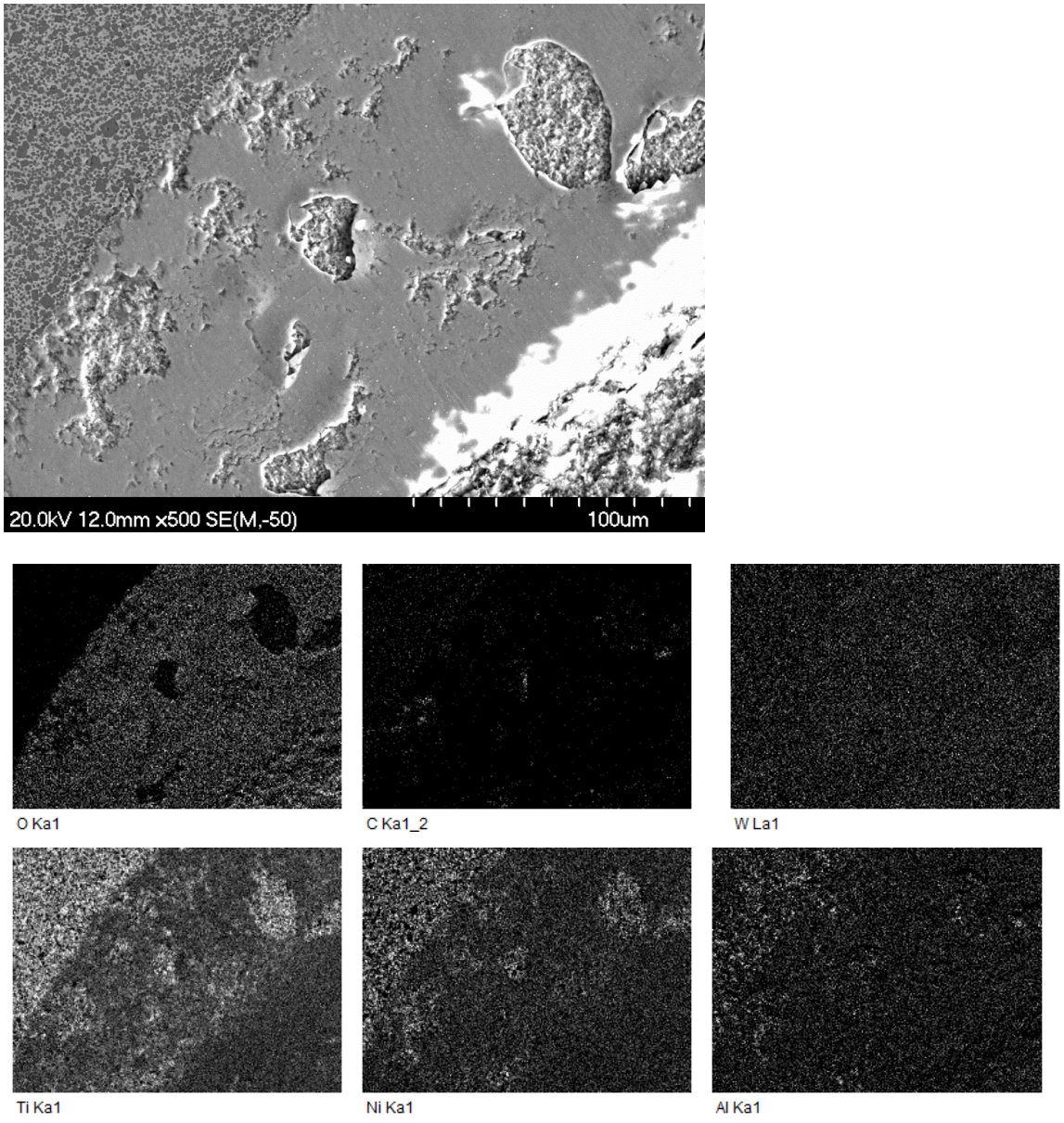

Figure 36. A series of elemental EDS maps of the edge of the wear track in $Ti(C_{0.7},N_{0.3})$, with 30 vol% Ni_3Al, tested at 60 N for 120 minutes.

The WC-Co counter face materials were also examined using EDS, and typical examples are shown in Tables 5 and 6. As with the test samples, a tribolayer is present on the counter face spheres following testing (Figure 37). The amount of oxygen present on the surface within this tribolayer broadly increases with the applied load. In addition, the presence of elements transferred from the test samples is also observed. At the lowest applied load (i.e. 20 N), the amount of oxygen transferred was significantly lower than at the higher loads of 40 and 60 N. This indicates that there was lower tribolayer generation

under these less severe wear conditions. At the lowest load there was also far less evidence of elemental material transferred over from the test samples, although this does increase at the higher loads. These lower material transfer levels infer that the extent of adhesive wear was reduced significantly under the lower load. The early stages of tribolayer development can also be seen through the EDS mapping, with regions high in oxygen and titanium present on the surface of the WC-Co sphere (Figure 37). Combining all of the information gathered through analysis of the compositions of both the cermets and WC-Co counter face materials, two primary conclusions can be drawn. Firstly, at the lowest applied load (i.e. 20 N), two-body abrasion is the predominant mechanism. A limited amount of three-body abrasive wear also occurs, leading to preliminary tribolayer formation through an adhesive wear mechanism. At the higher loads (i.e. 40 and 60 N), there is a more clear transition from two- to three-body abrasive wear, with the ultimate generation of a significant tribolayer on both the cermet and WC-Co surfaces. This again confirms an overall mechanism ultimately transitioning to adhesive wear.

Table 5. The nominal WC-Co counter face compositions (in at %) following sliding wear tests against $Ti(C_{0.7},N_{0.3})$ with 25 vol% Ni_3Al.

Element (KLM Line)	**20 N**	**40 N**	**60 N**
C (K)	42.60	31.92	36.44
O (K)	27.23	36.50	37.53
W (M)	20.21	19.44	15.09
Ti (K)	1.74	2.99	2.95
Co (K)	3.52	2.87	2.24
Ni (L)	1.77	3.23	2.90
Al (K)	0.00	0.00	0.34

Table 6. The nominal WC-Co counter face compositions (in at %) following sliding wear tests against $Ti(C_{0.7},N_{0.3})$ with 40 vol% Ni_3Al.

Element (KLM Line)	20N	40N	60N
C (K)	49.08	45.93	44.02
O (K)	16.35	30.23	30.69
W (M)	26.26	12.42	13.51
Ti (K)	0.66	2.73	2.70
Co (K)	4.19	1.77	2.08
Ni (L)	0.00	4.38	3.84
Al (K)	0.00	0.66	0.73

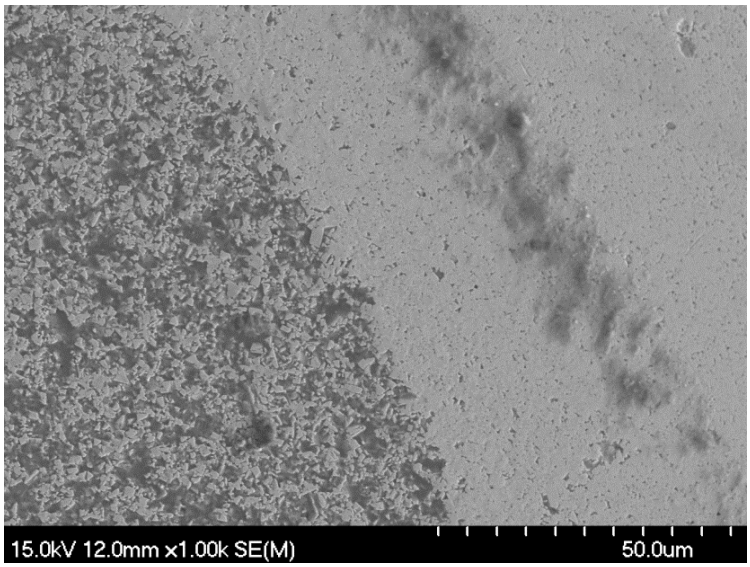

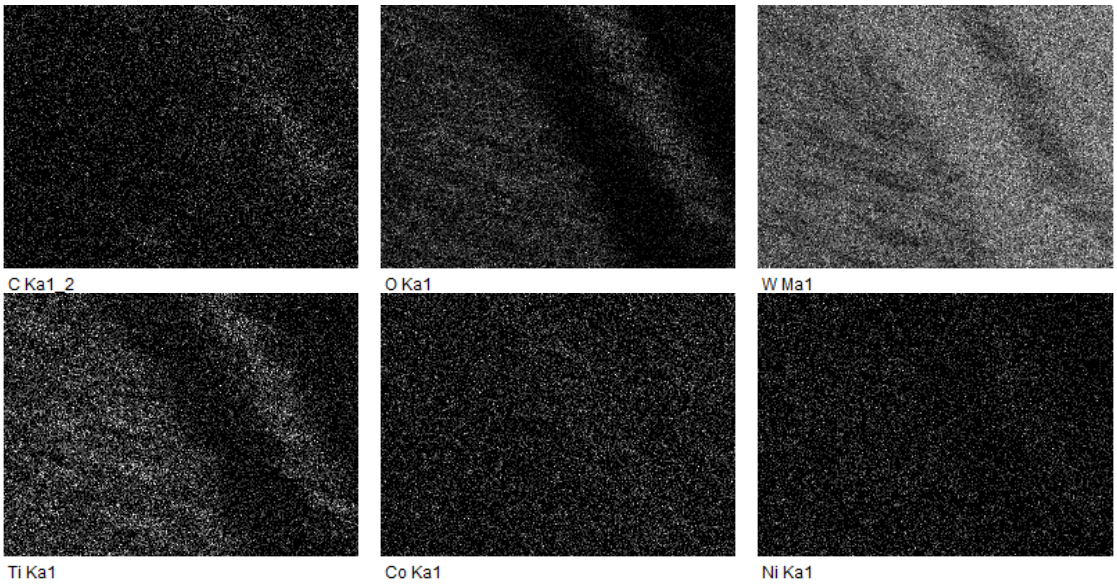

Figure 37. A series of elemental EDS maps of the edge of the wear track on a WC-Co counter face sphere, tested at 40 N for 120 minutes against a $Ti(C_{0.7},N_{0.3})$ sample with 25 vol% Ni_3Al.

5.4 Conclusions

Ti(C,N)-Ni_3Al based cermets were successfully manufactured through a simple reaction sintering process. All of the compositions achieved density values in excess of 98.5 % of theoretical, except for the highest nitrogen content samples prepared with 20 vol% of Ni_3Al. This was proposed to be due to the relatively poorer wetting response of the molten Ni_3Al on $Ti(C_{0.3},N_{0.7})$. Microstructural analysis confirmed a generally homogenous mixture of the carbide grains throughout the binder phase, with the average grain size of the TiC-based samples being nearly twice that of those prepared with Ti(C,N). Cermets with the lowest binder phase content (i.e. 20 vol%) achieved the highest hardness values, and the hardness also increased with increasing C:N ratio. Increasing the Ni_3Al binder content resulted in increasing IFR for the cermets, up to ~20 $MPa \cdot m^{1/2}$ for those prepared with Ti(C,N) and ~30 $MPa \cdot m^{1/2}$ for those with TiC.

The wear response of the TiC and Ti(C,N) based cermets was assessed using a reciprocating test geometry, dry sliding against a WC-Co counter face. It was shown that the COF was typically between 0.45 and 0.52, which is comparable to a number of alternate cermet systems. The fluctuation in COF was largest under the lowest applied

loads and for the highest binder content samples. The wear track volumes and specific wear rates were observed to increase with the applied load and, to a lesser extent, with the Ni_3Al binder content. However, it was invariably noted that intermediate binder contents provided the lowest wear rates. Overall, cermets that were based on TiC typically showed the best wear resistance, which decreased with an increasing N content in the Ti(C,N) ceramic phase. The observed wear rates were found to be comparable, and even slightly lower than WC-Co and TiC-Ni cermets reported in other studies. Microstructural examination demonstrated the continuous accumulation of damage in the TiC or Ti(C,N) phase, leading to the release of fragments of the cermets into the tribo-pair coupling. This resulted in a transition from two- to three-body abrasive wear. Ultimately, the third-body debris is sufficiently refined through attrition to form a tribolayer, on both the cermet and the WC-Co counter face, highlighting a further transition to an adhesive wear mode. The extent of this attrition is confirmed by the high O content in the tribolayer.

5.5 References

[1] Humenik, M., & Parikh, N. (1956). Cermets, 1. Fundamental concepts related to microstructure and physical properties of cermet systems. *Journal of the American Ceramic Society, 39*(2), 60-63.

[2] Ettmayer, P., Kolaska, H., Lengauer, W., & Dreyer, K. (1995). Ti(C,N) Cermets - Metallurgy and properties. *International Journal of Refractory Metals and Hard Materials, 13*(6), 343-351.

[3] Cardinal, S., Malchère, A., Garnier, V., & Fantozzi, G. (2009). Microstructure and mechanical properties of TiC-TiN based cermets for tools application. *International Journal of Refractory Metals and Hard Materials 27*(3), 521-527.

[4] Zhang, S. (1993). Titanium carbonitride-based cermets - Processes and properties. *Materials Science and Engineering A 163*(1), 141-148.

[5] Zhang, H., Yan, J., Zhang, X., & Tang, S. (2006). Properties of titanium carbonitride matrix cermets. *International Journal of Refractory Metals and Hard Materials 24*(3), 236-239.

[6] Russias, J., Cardinal, S., Aguni, Y., Fantozzi, G., Bienvenu, K., & Fontaine, J. (2005). Influence of titanium nitride addition on the microstructure and mechanical properties of TiC-based cermets. *International Journal of Refractory Metals and Hard Materials 23*(4), 358-362.

[7] Bolognini, S., Feusier, G., Mari, D., Viatte, T., & Benoit, W. (1998). High temperature mechanical behaviour of Ti (C, N)-Mo-Co cermets. *International Journal of Refractory Metals and Hard Materials 16*(4), 257-268.

[8] Qi, F., & Kang, S. (1998). A study on microstructural changes in Ti(CN)–NbC–Ni cermets. *Materials Science and Engineering A 251*(1), 276-285.

[9] Stewart, T., Collier, R. B., Farhat, Z. N., Kipouros, G. J. and Plucknett, K. P. (2010). Melt-infiltration processing of titanium carbide-stainless steel cermets. *Ceramic Engineering and Science Proceedings 31*(8), 97-104.

[10] Buchholz, S., Farhat, Z. N., Kipouros, G. J., & Plucknett, K. P. (2013). Reciprocating wear response of Ti(C,N)-Ni_3Al cermets. *Canadian Metallurgical Quarterly 52*(1), 69-80.

[11] Onuoha, C. C., Kipouros, G. J., Farhat, Z. N., & Plucknett, K. P. (2013). The reciprocating wear behaviour of TiC-304L stainless steel composites prepared by melt infiltration. *Wear 303*(1-2), 321-333.

[12] Plucknett, K. P., & Becher, P. F. (2001). Processing and microstructure development of titanium carbide–nickel aluminide composites prepared by melt infiltration/sintering (MIS). *Journal of the American Ceramic Society*, *84*(1), 55-61.

[13] Stoloff, N. S. (1989). Physical and mechanical metallurgy of Ni_3Al and its alloys. *International Materials Reviews*, *34*(1), 153-184.

[14] Deevi, S. C., & Sikka, V. K. (1996). Nickel and iron aluminides: An overview on properties, processing, and applications. *Intermetallics. 4*(5), 357-375.

[15] Plucknett, K. P., Becher, P. F., & Waters, S. B. (1998). Flexure strength of melt-infiltration-processed titanium carbide/nickel aluminide composites. *Journal of the American Ceramic Society*, *81*(7), 1839-1844.

[16] Pickens, J. R., & Gurland, J. (1978). The fracture toughness of WC-Co alloys measured on single-edge notched beam specimens precracked by electron discharge machining. *Materials Science and Engineering*, *33*(1), 135-142.

[17] Shetty, D. K., Wright, I. G., Mincer, P. N., & Clauer, A. H. (1985). Indentation fracture of WC-Co cermets. *Journal of Materials Science. 20*(5), 1873-1882.

[18] Upadhyaya, G. S. (1998) Cemented tungsten carbides: Production, properties, and testing, Noves Publications.

[19] Larsen-Basse, J. (1983). Effect of composition, microstructure and service conditions on the wear of cemented carbides. *J. Met.*, *35*(11), 35-42.

[20] Engqvist, H., Axén, N., & Hogmark, S. (1998). Resistance of a binderless cemented carbide to abrasion and particle erosion. *Tribology Letters*, *4*(3-4), 251-258.

[21] Zhang, S. C., Hilmas, G., & Fahrenholtz, W. (2007). Zirconium carbide–tungsten cermets prepared by in situ reaction sintering. *Journal of the American Ceramic Society*, *90*(6), 1930-1933.

[22] Hong, F., & Lewis, M. H. (2009). Ceramic-matrix composites via in-situ reaction sintering. In *Proceedings of the 17th Annual Conference on Composites and Advanced Ceramic Materials, Part 2 of 2: Ceramic Engineering and Science Proceedings, Volume 14, Issue 9/10* (pp. 699-706). John Wiley & Sons, Inc..

[23] Mendelson, M. I. (1969). Average grain size in polycrystalline ceramics. *Journal of the American Ceramic Society, 52*(8), 443-446.

[24] Gurland, J., & Bardzil, P. (1955). Relation of strength, composition, and grain size of sintered WC-Co alloys. *J. Metals*, *7*.

[25] Nakamura, M., & Gurland, J. (1980). The fracture toughness of WC-Co two-phase alloys—A preliminary model. *Metallurgical and Materials Transactions A*, *11*(1), 141-146.

[26] Niihara, K., Morena, R., & Hasselman, D. P. H. (1982). Evaluation of K_{IC} of brittle solids by the indentation method with low crack-to-indent ratios. *Journal of Materials Science Letter. 1*(1), 13-16.

[27] Lancaster, J. K. (1967). The influence of substrate hardness on the formation and endurance of molybdenum disulphide films. *Wear. 10*(2), 103-117.

[28] Giannuzzi, L. A., & Stevie, F. A. (1999). A review of focused ion beam milling techniques for TEM specimen preparation. *Micron*, *30*(3), 197-204.

[29] German, R. M. (1985). Liquid phase sintering. *Plenum Publishing Corporation*. New York.

[30] Engqvist, H., Jacobson, S., & Axén, N. (2002). A model for the hardness of cemented carbides. *Wear*, *252*(5), 384-393.

[31] Yang, Q., Lengauer, W., Koch, T., Scheerer, M., & Smid, I. (2000). Hardness and elastic properties of $Ti(C_xN_{1-x})$, $Zr(C_xN_{1-x})$ and $Hf(C_xN_{1-x})$. *Journal of alloys and compounds*, *309*(1), L5-L9.

[32] Pickens, J. R., & Gurland, J. (1978). The fracture toughness of WC-Co alloys measured on single-edge notched beam specimens precracked by electron discharge machining. *Materials Science and Engineering*, *33*(1), 135-142.

[33] Jia, K., & Fischer, T. E. (1997). Sliding wear of conventional and nanostructured cemented carbides. *Wear*, *203*, 310-318.

[34] Sigl, L. S., Mataga, P., Dalgleish, B., McMeeking, R., & Evans, A. (1988). On the toughness of brittle materials reinforced with a ductile phase. *Acta Metallurgica, 36*(4), 945-953.

[35] Kumar, B. M., Basu, B., Vizintin, J., & Kalin, M. (2008). Tribochemistry in sliding wear of TiCN-Ni-based cermets. *Journal of Materials Research. 23*(5), 1214-1227.

[36] Bonny, K., De Baets, P., Ost, W., Vleugels, J., Huang, S., Lauwers, B., & Liu, W. (2009). Influence of electrical discharge machining on the reciprocating sliding wear response of WC-Co cemented carbides. *Wear*, *266*(1), 84-95.

[37] Archard, J. F. (1953). Contact and rubbing of flat surfaces. *Journal of Applied Physics*, *24*(8), 981-988.

[38] Pirso, J., Viljus, M., & Letunovits, S. (2004). Sliding wear of TiC–NiMo cermets. *Tribology International. 37*(10), 817-824.

[39] Campbell, P. Q., Celis, J. P., Roos, J. R., & Van der Biest, O. (1994). Fretting wear of selected ceramics and cermets. *Wear*, *174*(1), 47-56.

[40] Gee, M., Gant, A., & Roebuck, B. (2007). Wear mechanisms in abrasion and erosion of WC/Co and related hardmetals. *Wear. 263*(1), 137-148.

[41] Lawn, B., & Wilshaw, R. (1975). Indentation fracture: Principles and applications. *Journal of Materials Science, 10*(6), 1049-1081.

[42] Lawn, B. R. (1998). Indentation of ceramics with spheres: a century after Hertz. *Journal of the American Ceramic Society*, *81*(8), 1977-1994.

[43] Hashin, Z., & Shtrikman, S. (1963). A variational approach to the theory of the elastic behaviour of multiphase materials. *Journal of the Mechanics and Physics of Solids*, *11*(2), 127-140.

[44] Budiansky, B. (1965). On the elastic moduli of some heterogeneous materials. *Journal of the Mechanics and Physics of Solids*, *13*(4), 223-227.

[45] Hannink, R. H. J., & Murray, M. J. (1974). Elastic moduli measurements of some cubic transition metal carbides and alloyed carbides. *Journal of Materials Science*, *9*(2), 223-228.

[46] Fatmi, M., Ghebouli, M. A., Ghebouli, B., Chihi, T., Boucetta, S., & Heiba, Z. K. (2011). Study of structural, elastic, electronic, optical and thermal properties of Ni3Al. *Romanian Journal of Physics*, *56*(7-8), 935-951.

[47] Dey, G. (2003). Physical metallurgy of nickel aluminides. *Sadhana, 28*(1-2), 247-262.

[48] Ibrahim, I. A., Mohamed, F. A., & Lavernia, E. J. (1991). Particulate reinforced metal matrix composites—a review. *Journal of materials science*, *26*(5), 1137-1156.

[49] Sigl, L. S., & Schmauder, S. (1988). A finite element study of crack growth in WC-Co. *International Journal of Fracture*, *36*(4), 305-317.

[50] Doi, H., Fujiwara, Y., Miyake, K., & Oosawa, Y. (1970). A systematic investigation of elastic moduli of WC-Co alloys. *Metallurgical and Materials Transactions*, *1*(5), 1417-1425.

6 The Microstructure and Sliding Wear Behavior of $Ti(C_{0.3},N_{0.7})$ -Mo_2C-Ni_3Al Cermets

Tyler L. Stewart and Kevin P. Plucknett*

Materials Engineering Programme, Department of Process Engineering and Applied Science, Dalhousie University, 1360 Barrington Street, Halifax, Nova Scotia, CANADA

Abstract

Combining hard but brittle Ti(C,N) ceramic particles with the ductile Ni_3Al intermetallic produces a ceramic-metal composite, or cermet, with high wear resistance. However, for high N content Ti(C,N) cermets, the wettability of molten Ni_3Al is relatively poor, which leads to materials with residual porosity. Through a reaction sintering process, various amounts of Mo_2C (1.25, 2.5, 5 and 10 vol%) were incorporated into $Ti(C_{0.3},N_{0.7})$-Ni_3Al cermets, with the aim of improving the densification behaviour. Materials were prepared with Ni_3Al binder contents from 20 to 40 vol%, and were densified by vacuum sintering. Mo_2C was found to improve upon the wettability during sintering, thus enhancing the densification, especially at the lower binder contents. The sliding wear and Vickers indentation behavior of the cermets were assessed. It was found that Mo_2C additions had a positive effect on both the hardness and indentation fracture resistance of the samples, but had a detrimental effect on the sliding wear response of the cermets. This behaviour was attributed to increased microstructural inhomogeneity with Mo_2C additions.

Keywords: Three-body abrasion, Adhesive wear, Tribochemistry, Electron Microscopy, Hardness, Intermetallics

*Contact author: kevin.plucknett@dal.ca

6.1 Introduction

The properties of ceramic-metal composites, or cermets, are determined by several key factors of the ceramic phase that include grain size and shape, homogeneity, and connectivity. The metallic binder phase is also very important, with both the amount and composition playing a key role in determining the characteristics of the cermet [1]. In combination, these aspects play a crucial role in determining the physical properties of the cermet, such as hardness, toughness, strength, and wear resistance. As a consequence, the interactions between the ceramic and the metal binder phase must be taken into consideration in order to obtain a cermet with the desired properties. For example, there must ideally be a combination of both good wetting of the molten metal on the ceramic at the sintering temperature and some limited solubility of the ceramic phase in the metal [2]. If a system has poor wettability then the final structure will have a degraded densification response, with retained porosity that will likely act as stress raisers, resulting in a cermet with relatively poor physical properties [3]. For a given cermet system alloying additions can be made that alter the interaction between the ceramic and metallic phases, in such a fashion that a poor wetting system can be transformed into a system that densifies fully upon sintering.

There are several microstructural parameters that are readily measurable that help to control the properties of the cermets. One such feature is the contiguity of the ceramic phase, which is the ratio of the ceramic/ceramic interfacial area to the total interface surface area [4,5], and is a measure of the connectivity of the hard ceramic phase. Contiguity ranges from 0 (totally dispersed, with no contacting grains) to 1 (fully agglomerated). As the contiguity increases, the hardness also increases while the fracture toughness decreases. Another measurable parameter is the binder mean free path, which relates to the dimensions of the ductile binder phase between the brittle carbide particles. In general, as the mean free path increases so too does the fracture toughness.

With this in mind, titanium carbonitride Ti(C,N) based cermets are an attractive alternative to more conventional tungsten carbide-cobalt (WC-Co) cemented carbides for a variety of industrial applications. Their relatively low densities make them more practical for use in structural applications, particularly when mass is a design factor. The high toughness, hardness, and wear resistance of Ti(C,N)-based cermets also makes them

promising for use as protective coatings on parts that are susceptible to high amounts of wear. Ti(C,N) cermets combine the high hardness properties generally associated with TiC, with the beneficial toughness attributes of TiN [2]. However, they can suffer from poor wetting with some metallic binder systems as the fraction of TiN is increased [6,7]. This poor wettability can have a detrimental effect on sintering, leading to the retention of residual porosity. Ultimately, this has a negative impact on both the mechanical and tribological properties. One approach used to reduce the poor wettability of Ti(C,N) ceramics is through additions of Mo, in either its elemental or carbide form, as Mo_2C [7-9]. Improved wetting results in a reduction of microstructural defects such as voids and micro-cracks, an increase in the interphase bond strength, and also improved phase homogeneity [10].

In the present study the intermetallic nickel aluminide (Ni_3Al) is used as the binder phase for a high nitrogen content Ti(C,N) system [11]. Ni_3Al has excellent physical properties at elevated temperatures as well as a high oxidation resistance up to around 1100°C [12]. TiC-Ni_3Al cermets have been shown to exhibit high strength retention to ~1000°C [12], which is far in excess of WC-Co based materials [13]. However, while these materials show considerable promise, previous studies have shown that melt infiltration processed Ti(C,N)-Ni_3Al cermets with a high N:C ratio exhibit relatively poor sintering [14]. This response reduces the wear resistance, due to degraded wetting during processing and retained porosity. In order to alleviate this, the effects of Mo_2C additions are examined in the current study, in terms of microstructure development, Vickers indentation response and sliding wear behaviour.

6.2 Experimental Procedures

6.2.1 Cermet Raw Materials and Preparation

The raw powders used in the present study were Ti($C_{0.3}$,$N_{0.7}$) (lot no. L25747; D_{50}=1.72 μm) from Treibacher Industrie AG (Althofen, Austria); Mo_2C (lot no. PL71887718; 1.0-2.0 μm) from Pacific Particulate Materials (Vancouver, BC, Canada); Ni (lot no. L10W013; 2.2-3.0 μm), Ni/Al 50/50 wt.% (lot no. D28X029; D_{50}=38 μm) both obtained from Alfa Aesar (Ward Hill, MA, USA). The Ti(C,N)-Ni_3Al-Mo_2C cermets were manufactured using a simple *in-situ* reaction sintering process, based on the approach

developed in a prior study [15]. The cermet compositions were prepared with a fixed Ni_3Al binder content of 20, 30 or 40 vol%, with the Mo_2C additions made by substituting for $Ti(C_{0.3},N_{0.7})$ on a volume basis; all of the compositions are therefore subsequently referred to on volume percentage basis for the Ni_3Al and Mo_2C contents, with the balance being $Ti(C_{0.3},N_{0.7})$. Powders of each component were individually weighed with 0.5 wt% polyvinyl butyral resin binder and then ball milled in acetone for a period of 24 hours, using yttria stabilized zirconia milling media at a ratio of 10:1 by mass to the powders. The milled powder mixture was then left to evaporate in a fume hood for a period of 24 hours before being sieved through a 75 μm stainless steel mesh. The pressing, sintering, polishing and further characterization of the various samples were performed using the same procedure outlined in a prior study [15].

6.2.2 Cermet Characterisation

Following sintering the densities of the cermets were determined by immersion is water, following Archimedes principle. They were then surface ground and polished to a finish of 0.25 μm for further evaluation. The microstructure of the polished cermets was assessed using optical microscopy (OM; Model BX-51, Olympus Corp., Tokyo, Japan) and field emission scanning electron microscopy (SEM; Model S-4700, Hitachi High Technologies, Tokyo, Japan). SEM observation was performed primarily using a purely back scattered electron (BSE) imaging mode, through application of a -50 V bias to the Hitachi ExB in column detector, to highlight atomic number related compositional contrast. Chemical analysis was conducted in the SEM using energy dispersive X-ray spectroscopy (EDS; Model X-Max^N (80 mm^2), Oxford Instruments, Concord, MA, USA). Quantitative analysis of grain size, contiguity and binder MFP were conducted on digital SEM images using the ImagePro software package where the contiguity was measured by superimposing a series of lines upon a representative microstructure and counting the number of carbide/carbide and carbide/binder intercepts. In this instance grain size was determined using the lineal intercept method [16], while both contiguity and binder MFP were determined using the approach outlined by Gurland [17].

The Vickers hardness and indentation fracture resistance (IFR) were determined using applied loads of 5 and 30 kg, respectively. In this instance the IFR was calculated using

the equation of Niihara [18], with the assumption of Palmqvist cracking in the cermets. The sliding wear response was assessed against a WC-6Co counter face sphere (6.35 mm diameter), with a reciprocating sliding distance of 5.03 mm at a frequency of 20 Hz (Model Universal Micro Tribometer (UMT), Bruker, Madison, WI, USA). The reciprocating conditions used relate to a total sliding distance of ~1.45 km, over a two hour period. Wear tests were conducted under applied loads between 20 and 60 N. The UMT system monitors the dynamic sliding coefficient during the wear tests. Wear track volumes were subsequently determined using an optical profilometer (Model PS50 Optical Profilometer, Nanovea, CA, USA), and these data were then used to calculate specific wear rates following the Lancaster approach [19]. After wear tests the associated damage was assessed using OM, SEM and EDS. The tribolayers formed during wear tests were also examined using focused ion beam microscopy (FIB; Model F-2000A, Hitachi High Technologies, Tokyo, Japan). FIB involved deposition of a tungsten protective strip prior to site specific Ga^+ ion milling to reveal the tribolayer through thickness structure, which was then examined using SEM. Further details regarding the characterisation procedures used can be found in prior publications [15,20].

6.3 Results and Discussion

6.3.1 Densification Behaviour and Microstructure Development

In cermet systems the wettability of a carbide by a molten metal is determined in part by its stability, in the sense that the lower the negative heat of formation a carbide has, the smaller the wetting angle is between the two phases [2]. Amongst the carbides that are composed of elements from groups IV, V, and VI of the periodic table, Mo_2C has the lowest heat of formation and therefore the lowest contact angle with liquid metals. As a consequence, Mo_2C is generally an excellent addition to systems with poor melt wettability [2]. From Figure 38 it can be seen that, in the absence of Mo_2C additions, samples with the lowest amount of Ni_3Al binder show relatively poor densification, achieving less than 95% of theoretical density. However, with an addition of only 1.25 vol% Mo_2C the final sintered density increases to ~99% of theoretical, highlighting the positive effect the carbide has upon the sintering response of Ti(C,N) cermets with high N:C ratios. In general the sintered densities of the samples all increased as the amounts of

Mo_2C and percentage of Ni_3Al were increased, and essentially all Mo_2C containing cermets were sintered to in excess of 99% of theoretical density.

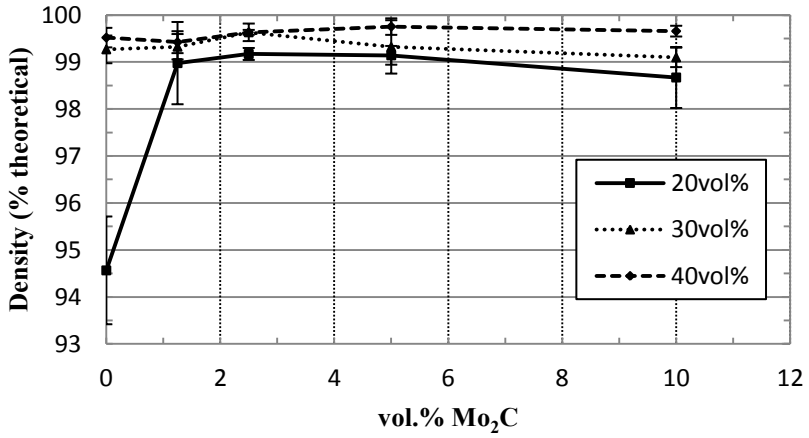

Figure 38. The effects of Mo_2C additions on the sintered densities of the $Ti(C_{0.3},N_{0.7})$-Ni_3Al cermets.

During liquid phase sintering carbide grain coarsening occurs, due to partial dissolution of the $Ti(C_{0.3},N_{0.7})$ into the binder phase, and subsequent re-precipitation. The reduction of surface energy of the solid particles is the primary driving force for small grains to dissolve and large grains to grow. It has been shown that the addition of Mo_2C acts as a grain refiner in the Ti(C,N) systems [2,9]. It has been suggested that the addition of Mo improves the wettability between the ceramic and metallic phases, which actually decreases the solubility of Ti(C,N) in the binder, and consequently limits grain growth by solution-precipitation [21]. The dissolution of the Ti(C,N) grains is then lowered by the presence of a shell that has high amounts of Mo, which is less soluble in the binder phase than Ti(C,N) alone. This shell formation creates more carbonitride grains with smaller Ti(C,N) cores and limits further growth under conventional sintering conditions [22,23]. However, it has also been suggested that Mo_2C acts as a grain refiner because of the retarding effect it has on the solid/solid boundary mobility of the Ti(C,N) grains, which is a common effect seen in ceramics [24]. The carbonitride grain size determines an important characteristic in the cermet system. Firstly, the *in-situ* hardness, which sets the upper limit of the hardness increases with decreasing grain size. Secondly, the binder MFP, which is proportional to the grain size, is reduced. Consequently, there is an increase the binder hardening effect by the reduction of the MFP [25]. Figure 39(a)

shows the mean $Ti(C_{0.3},N_{0.7})$ grain size as a function of the amount of Mo_2C present. It is clear that as the Mo_2C content is increased, the average grain size steadily decreases, from between 2.5 and 3.5 μm down to between 1.5 and 2.0 μm. It is worth noting that without the addition of Mo_2C the average grain sizes are substantially larger than that of the $Ti(C_{0.3},N_{0.7})$ starting powder, which has a D_{50} of ~1.7 μm. As the amount of Mo_2C increases the average particle size steadily decreases, approaching the average starting powder size.

Figure 39(b) highlights the effects of Mo_2C addition on the contiguity of the cermets, which is a measure of the contacts between $Ti(C_{0.3},N_{0.7})$ grains. It can be seen that the contiguity actually increases slightly with Mo_2C additions, for a constant Ni_3Al content, indicating greater aggregation of the carbonitride grains with increasing Mo_2C content. Typically, a uniformly dispersed microstructure is desired for optimum mechanical properties, with the hard ceramic phase homogeneously distributed throughout the metallic binder. In terms of crack propagation ceramic grain-grain contacts can be viewed as weak points within the structure, as a growing crack will more easily fracture such an interface than cut through a tough metallic ligament. As a consequence, this increasing contiguity may result in a reduced toughness and, potentially, wear resistance. In contrast to the contiguity, the binder MFP decreases with increasing Mo_2C addition, and therefore understandably scales with the $Ti(C_{0.3},N_{0.7})$ grain size. The volume percentage of the binder plays the largest role in determining this parameter, but other factors such as the contiguity and the average carbide grain size also have a relationship to the mean free path. From Figure 39 it can be seen that as the amount of Mo_2C is increased the binder MFP decreases by up to 50%, for the three Ni_3Al binder contents studied.

(a)

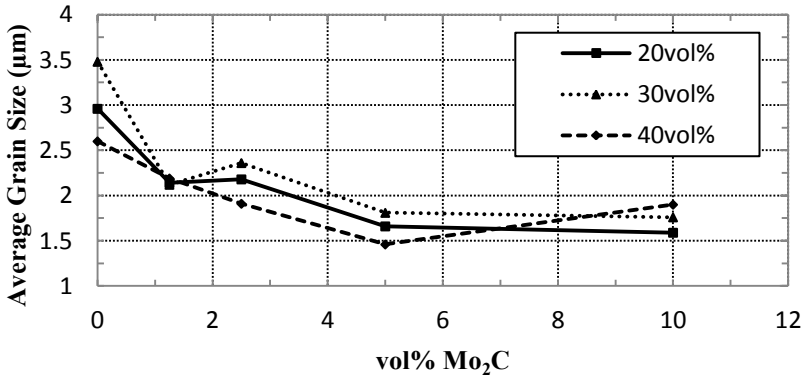

(b)

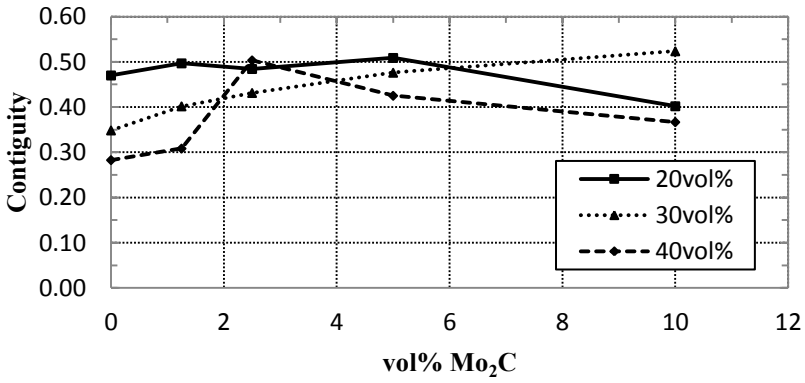

(c)

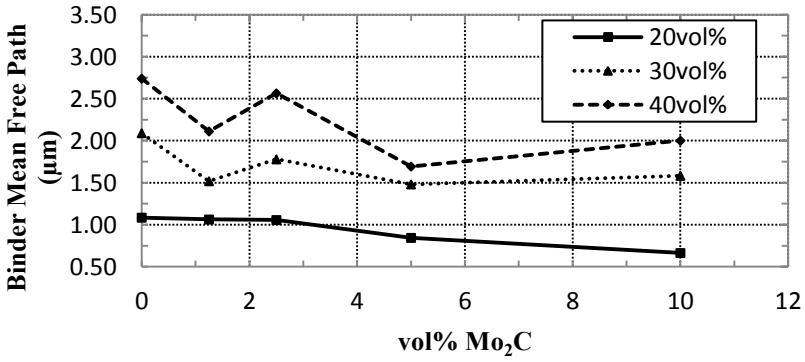

Figure 39. The effects of the Mo_2C and Ni_3Al contents on the microstructural parameters of the $TiC_{0.3}N_{0.7}$-Mo_2C-Ni_3Al cermets: (a) $Ti(C_{0.3},N_{0.7})$ grain size, (b) $Ti(C_{0.3},N_{0.7})$ contiguity, and (c) the Ni_3Al binder MFP.

The effects of Mo_2C additions on the microstructures of $Ti(C_{0.3},N_{0.7})$ samples with 30 vol% Ni_3Al, are shown in Figure 40. As the amount of Mo_2C is increased the agglomeration effects noted in terms of the binder MFP and contiguity can be seen, leaving regions of the microstructure depleted of the carbonitride phase. The grain refinement effects of the Mo_2C additions are also apparent. In addition, as the Mo_2C content is increased a third, brighter contrast phase becomes more apparent. EDS analysis demonstrates that these areas are rich in Mo. The typical core-rim structure, which often appears in Ti(C,N) cermets prepared with Mo_2C [23,26,27], was not visible in these particular samples, even when viewing the structure solely with BSE (Figure 41). The formation of the Mo phase in the binder and not in the usual core rim structure has been seen in a previous study where the thickness of the phase depended upon the quantity of Mo present in the samples [28]. Figure 42 highlights the microstructure at higher magnification, along with the associated EDS maps, confirming the presence of the Mo-rich secondary phase. It is clear that the Mo_2C regions are significantly larger than the initial powder size (~1-2 μm), and result from either an aggregation phenomena during the milling stage or through precipitation from a Mo-rich liquid phase during sintering. Examining the elemental maps in more detail, it is clear that there is no significant association of C with the Mo-rich regions, indicating that the precipitation/phase separation mechanism may be more probable.

(a) (b)

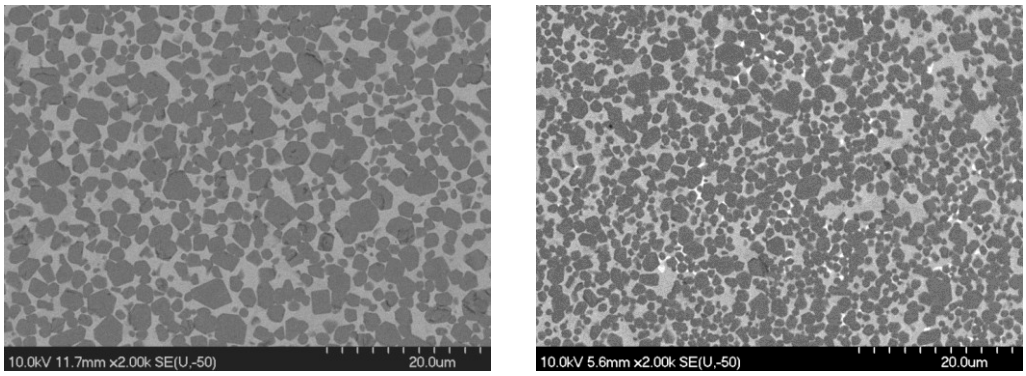

(c)

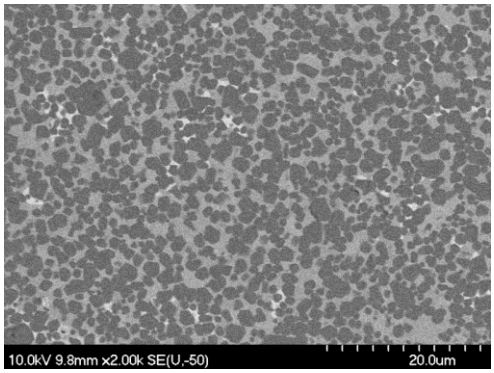

(d)

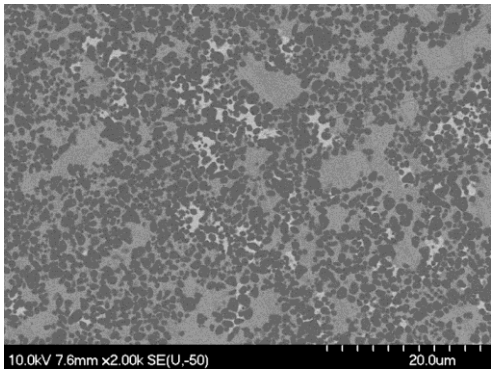

(e)

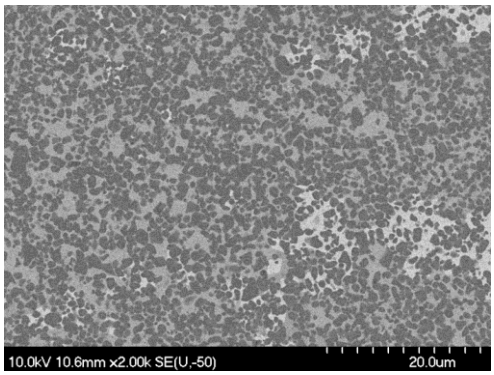

Figure 40. Typical SEM micrographs of the effects of varying levels of Mo_2C on the microstructure of $Ti(C_{0.3},N_{0.7})$ prepared with 30 vol % Ni_3Al: (a) 0 vol% Mo_2C, (b) 1.25 vol% Mo_2C, (c) 2.5 vol% Mo_2C, (d) 5 vol% Mo_2C, and (e) 10 vol% Mo_2C.

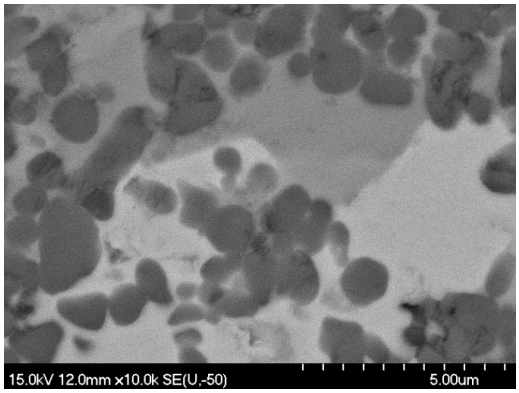

Figure 41. High magnification BSE image of 30 vol% Ni_3Al-10 vol% Mo_2C highlighting the $Ti(C_{0.3},N_{0.7})$ phase, demonstrating the absence of a core-rim structure in the present materials.

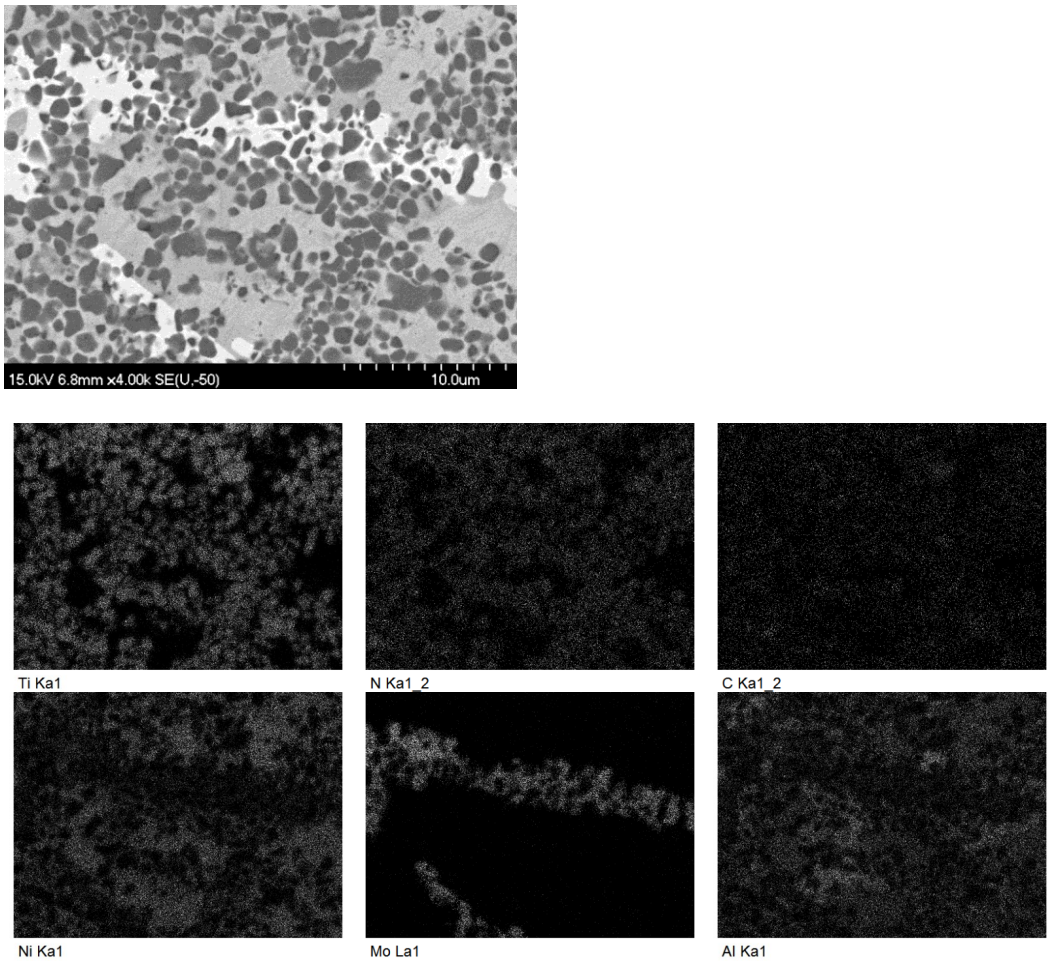

Figure 42. EDS elemental mapping of the microstructure of $Ti(C_{0.3},N_{0.7})$-40 vol. % Ni_3Al-10 vol. % Mo_2C cermets, highlighting the presence of sizeable Mo-rich regions.

6.3.2 Hardness and Indentation Fracture Resistance

Figure 43(a) demonstrates the effects of Mo_2C addition on the hardness of the $Ti(C_{0.3},N_{0.7})$-Ni_3Al cermets. Broadly speaking, the hardness increases with decreasing Ni_3Al binder content, as the lower modulus intermetallic is replaced by the significantly higher modulus ceramic phase. The response is more complex at the lowest Ni_3Al binder contents. As demonstrated previously in Figure 38, in the absence of Mo_2C, the cermet density is negatively impacted for 20 vol% Ni_3Al, which is also reflected in a significantly reduced hardness (Figure 43(a)). However, just 1.25 vol% Mo_2C addition results in a 40 % increase in the hardness for this composition, due to the significant improvement in densification. The hardness ultimately decreases slightly at the highest Mo_2C content, as a significant portion of the $Ti(C_{0.3},N_{0.7})$ phase is replaced by the lower

hardness Mo_2C [26]. The addition of Mo has also been reported to potentially result in some solid solution strengthening of the binder phase [2,23]. As the amount of Mo_2C is increased the quantity of Mo dissolved in the binder is also increased, eventually forming the discrete Mo-rich regions noted earlier.

The effects that Mo_2C have on the IFR of the cermets are presented in Figure 43(b), and the response is somewhat more complex than for the hardness. For the lowest Ni_3Al contents it is apparent that the IFR increases proportionally with the amount of Mo_2C added to the microstructure for a given volume percentage of binder, with a maximum increase of ~55% from the Mo_2C-free samples for cermets prepared with 10vol% Mo_2C. However, the effect that Mo_2C has on the samples varies greatly depending upon the volume percentage of binder present. At 30 vol% Ni_3Al binder the response is less significant, and the IFR is almost independent of the Mo_2C content, with a peak increase of ~30% noted for the lowest Mo_2C addition (1.25 vol%). For the samples with 40 vol% binder the increase was as much as 130%, which largely arises from the low density and IFR arising in the absence of Mo_2C. In this instance the peak in IFR is actually occurring at 2.5 vol% Mo_2C, and then decreases significantly for higher Mo_2C additions, in a manner similar to the hardness (Figure 43(a)). There is a general IFR trend for the 30 and 40 vol% Ni_3Al cermets, with a peak at relatively low Mo_2C contents, and then a reduction in IFR at higher levels Mo_2C. These transitions can be seen to follow the microstructural observations highlighted earlier (Figure 40), that with increasing Mo_2C content there is both a decreasing homogeneity in the microstructure and an increase in both the volume fraction and size of the Mo-rich regions. The reduction of the carbide grain sizes also play a key role in the reduction of the IFR for the higher amounts of Mo_2C, where larger grains are normally associated with higher IFR values [26,29,30]. Clearly, in the present case Mo_2C additions above 2.5 vol% result in a significant degradation of both microstructural homogeneity and mechanical properties.

(a)

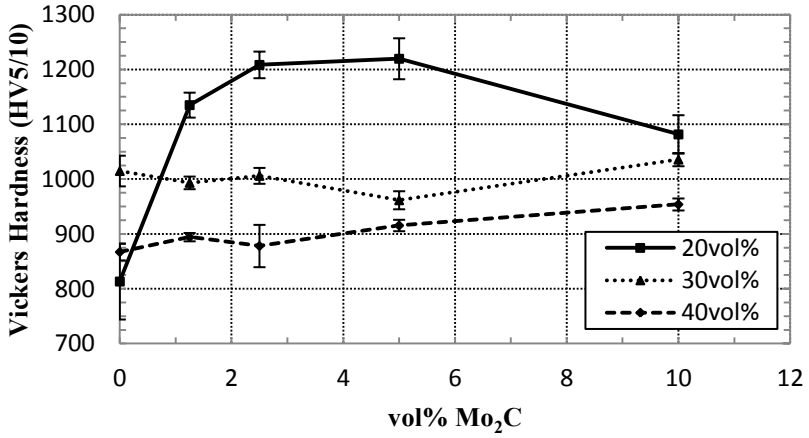

(b)

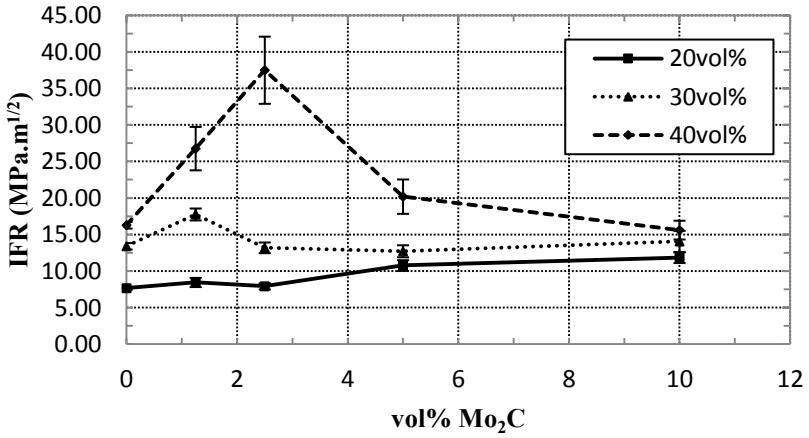

Figure 43. The effects of Mo_2C and Ni_3Al contents on: (a) the Vickers hardness, under a 5 kg load, and (b) the IFR, under a 30 kg load.

6.3.3 Reciprocating Wear Behaviour

Typical examples of the COF curves for samples with varying compositions are presented in Figure 44. There is no significant influence from the composition of the sample on the resulting curves, with steady state COF values typically within the range of 0.55 to 0.65. This is somewhat surprising given the significant differences observed within the microstructures that arise from varying the Mo_2C content in particular. It is apparent from Figure 44 that the most significant variation arises from the applied load during wear tests. At the lowest load (20 N) the COF curves invariably highlight a

'running in' period, where there are moderate fluctuations before the COF reaches a relatively steady state value. Typically this steady state response is reached within approximately 30 to 60 minutes, and highlights the probability of a transition in wear mechanism during this period. Conversely, at the higher loads of 40 and 60 N, a steady state COF response was achieved much more rapidly, typically within 5 to 10 minutes. This response indicates that any transition in wear mechanism occurs rapidly, and the materials quickly reach a condition where they are wearing in a nominally predictable manner.

(a)

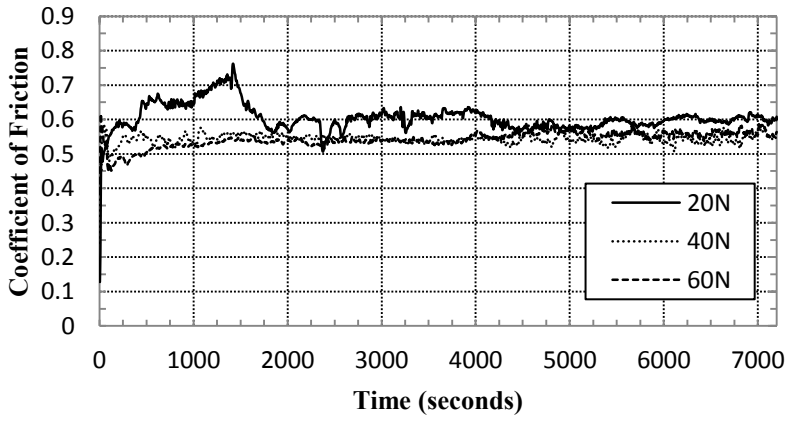

(b)

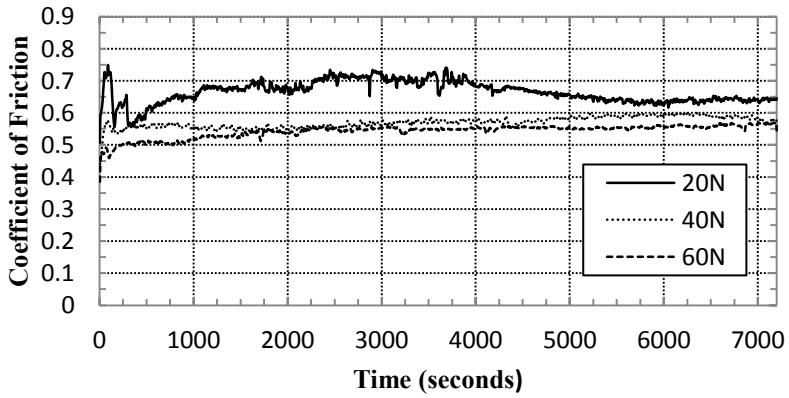

Figure 44. The effects of applied load on the typical COF curves obtained for: (a) 20 vol.% Ni_3Al and 1.25 vol.% Mo_2C, and (b) 40 vol.% Ni_3Al and 10 vol.% Mo_2C.

The mean COF values for the 20, 40 and 60 N applied loads, determined by calculating the average COF value for the complete duration of the reciprocating wear tests are shown in Figure 45. It is apparent that there is a greater variation in the COF values for the samples subjected to an applied load of 20 N. In this instance there appears to be a general increase in the COF values as the amount of Mo_2C was increased. The clear exception to this trend is the 20 vol% Ni_3Al samples, prepared without Mo_2C additions, which show the highest COF of all. This likely arises from the high residual porosity in these samples, resulting in a different wear response, which is discussed in greater detail in the subsequent paragraphs. In contrast to the response at the lowest load, at 60 N the COF is largely constant at ~0.55 for all the various compositions. Ozdemir and colleagues reported COF values between ~0.53 and ~0.76 for hot-press, reaction sintered Ni_3Al tested under relatively low loads (2 to 10 N) [31]. Broadly similar COF values to those determined for the current cermets were reported by Gong et al, for an Fe-containing Ni_3Al alloy, with a COF of 0.55 ± 0.02 [32]. This value was shown to increase to 0.68 ± 0.02 with a 6 vol% Cr_3C_2 addition in that work, but was lower to 0.45 ± 0.02 with a similar volume fraction addition of MnS.

(a)

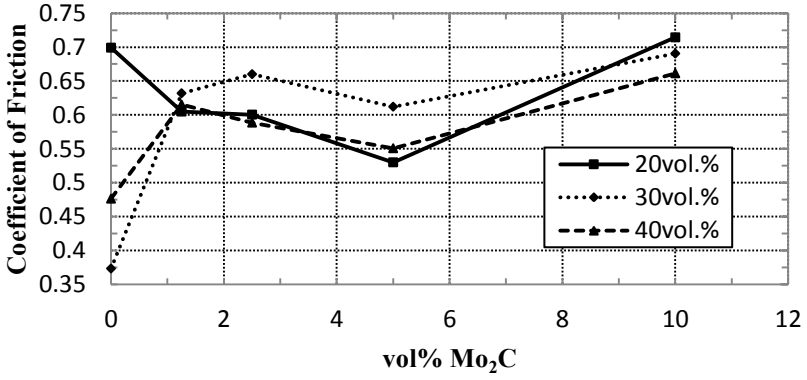

(b)

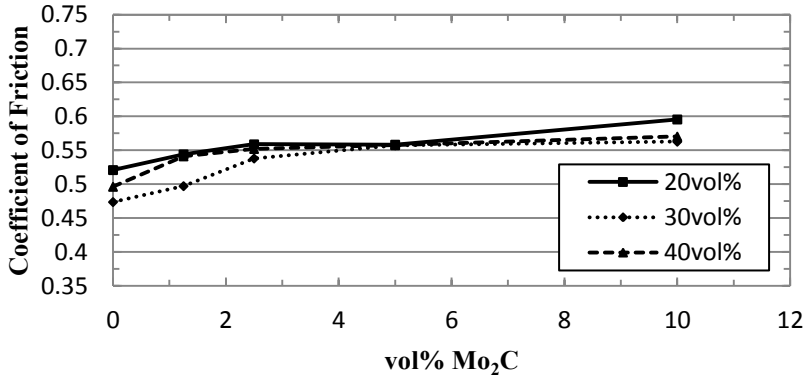

(c)

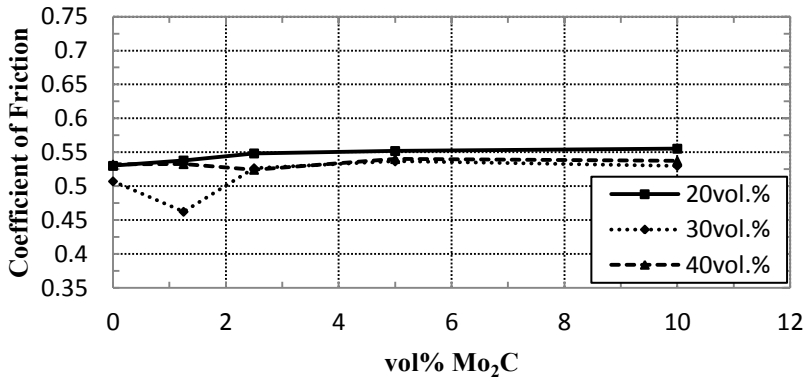

Figure 45. The effects of Ni_3Al and Mo_2C contents on the average COF at: (a) 20 N, (b) 40 N, and (c) 60 N.

Figure 46 presents the specific wear rate values for the various $Ti(C_{0.3},N_{0.7})$ cermet samples tested in the present study. Several features are apparent from examination of this data. It is generally apparent that as the applied load and binder content were increased so too did the wear rate, although there is some apparent scatter in the data. This increasing wear rate trend was also seen in broadly similar cermet systems using the same testing apparatus [14,33]. There was also a substantial decrease in the specific wear rate for the lowest binder content samples (20 vol% Ni_3Al) when the Mo_2C content was increased from 0 to 1.25 vol.%. As noted earlier, these samples suffered from retained porosity in the absence of Mo_2C additions, which results in significantly increased wear rates. This likely arises as both the hardness and toughness are negatively impacted by

the presence of the porosity, and the cermet will effectively have a lower modulus. As a consequence, greater damage is imparted into the microstructure under the Hertzian contact loads, and the measured wear rate increases. However, with the introduction of Mo_2C the wettability of the system was improved, thus resulting in significantly increased sintered densities and improved wear resistance.

In contrast, for the samples with 30 and 40 vol% binder there was an increase in the specific wear rate when the Mo_2C content was increased from 0 to 1.25 vol% Mo_2C. This is potentially due to the introduction of the third Mo phase making the microstructure inhomogeneous. Increasing the Mo_2C content even further can be anticipated to improve the wettability of the system, allowing the constituents to form a stronger bond with one another. There is also further refinement of the $Ti(C_{0.3},N_{0.7})$ grain size with increased Mo_2C addition. It is believed that these factors broadly contribute to an increasing wear resistance of the system relative to the lower Mo_2C contents (excluding the Mo_2C-free samples which generally exhibit the lowest specific wear rates), even though the microstructural inhomogeneity is greatest in the high Mo_2C containing cermets. It should be noted that the specific wear rates for the Mo_2C containing cermets examined in the present study are consistently higher than were observed for a range of TiC and Ti(C,N) prepared with a similar reaction sintered Ni_3Al binder, but without Mo_2C additions [15]. In that prior study, the measured wear rates were between 0.5 and $5x10^{-7}$ mm^3/Nm, compared to values between 2 to $35x10^{-7}$ mm^3/Nm for the materials examined in the current study. A further comparable study, for Ti(C,N)-based cermets prepared with the IC-50 Ni_3Al alloy (a sub-stoichiometric composition containing Zr and B [34,35]) using melt infiltration, also resulted in similarly low specific wear rates, between 0.5 and $10x10^{-7}$ mm^3/Nm [14].

(a)

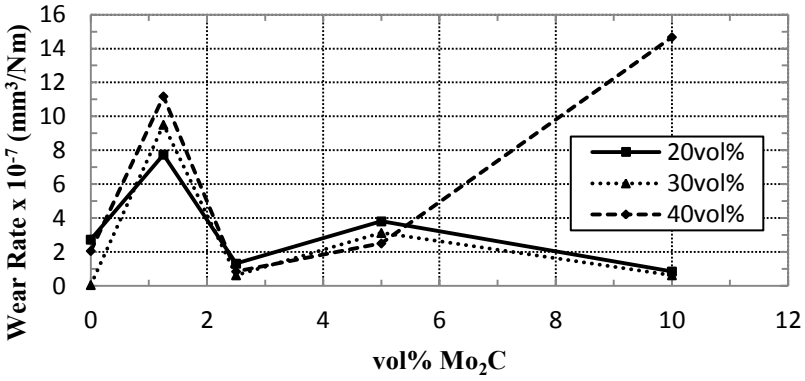
Wear Rate x 10-7 (mm3/Nm)
16
14
12
10
8
6
4
2
0
0
2
4
6
8
10
12
vol% Mo2C
20vol%
30vol%
40vol%

(b)

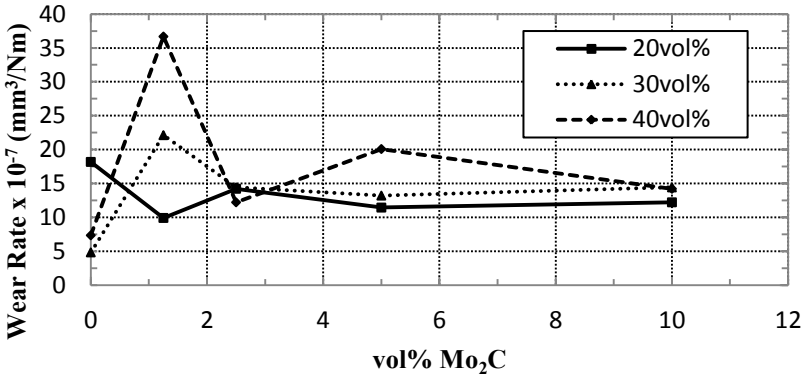
Wear Rate x 10-7 (mm3/Nm)
40
35
30
25
20
15
10
5
0
0
2
4
6
8
10
12
vol% Mo2C
20vol%
30vol%
40vol%

(c)

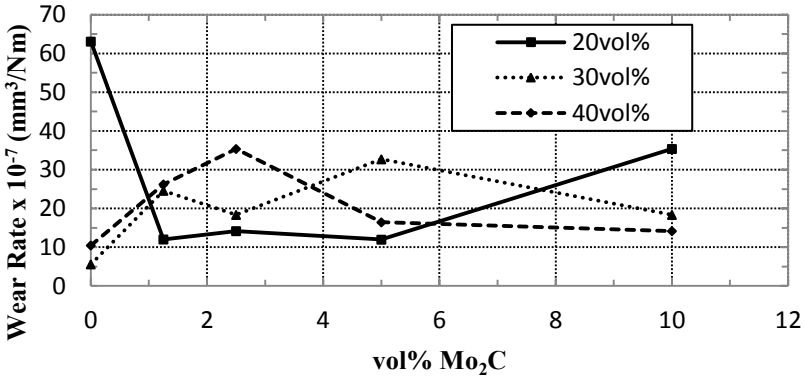

Figure 46. The effects of Ni_3Al and Mo_2C contents upon the specific wear rates of the $Ti(C_{0.3},N_{0.7})$ based cermets, at applied loads of: (a) 20 N, (b) 40 N, and (c) 60 N.

6.3.4 Microstructural Examination

The severity of wear the samples suffered during sliding varied as the amount of Mo_2C was increased. This was especially apparent in the samples with the lowest Ni_3Al binder content of 20 vol%. As demonstrated in Figure 46(c) the amount of Mo_2C present greatly influenced the specific wear rate of the 20 vol% Ni_3Al samples. In the absence of Mo_2C additions the wear rate was ~$60x10^{-7}$ mm^3/Nm, while for 1.25, 2.5, and 5 vol% the rate was ~$10x10^{-7}$ mm^3/Nm, before rising again to ~$35x10^{-7}$ mm^3/Nm. Representative SEM images of the ends of the wear tracks of these samples can be seen in Figure 47, where the damage to the microstructure becomes less obvious as the amount of Mo_2C is increased, before increasing again for the highest Mo_2C content.

(a) (b)

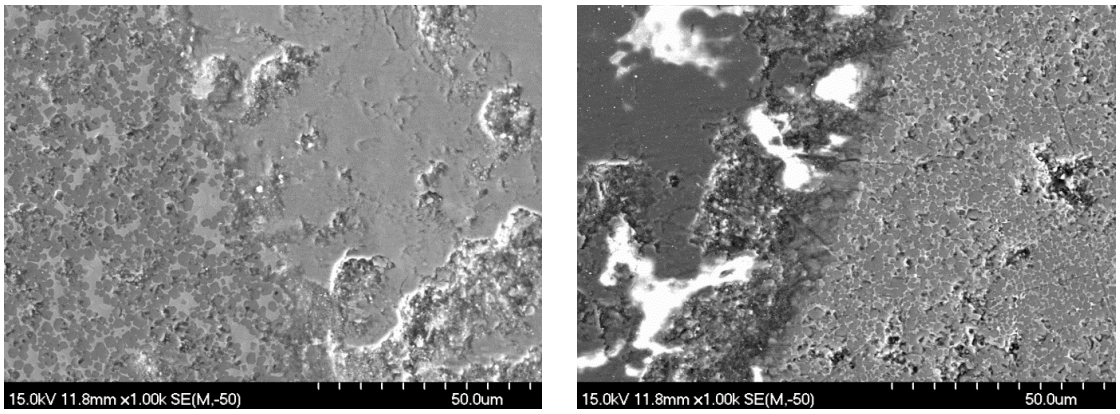

(c)

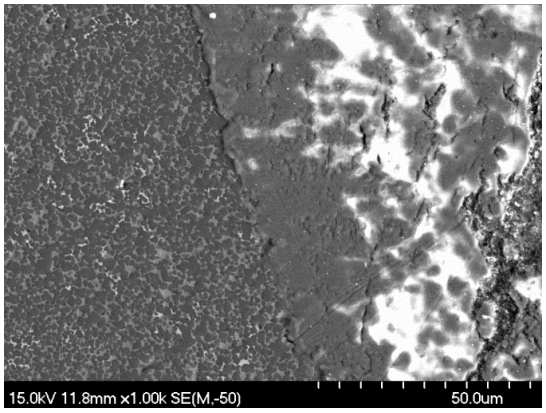

(d)

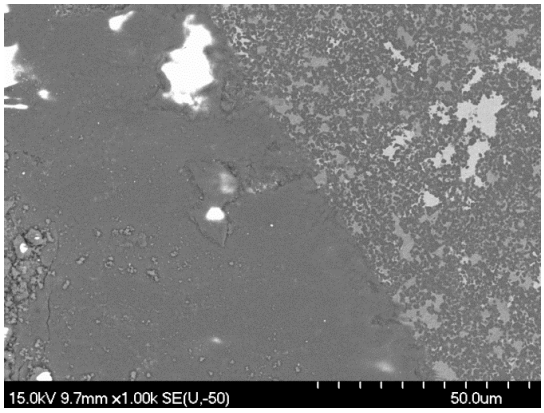

(e)

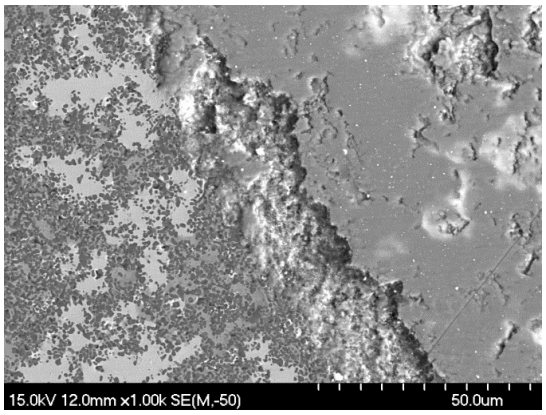

Figure 47. Representative SEM images demonstrating the effects of Mo_2C additions on the severity of the wear suffered for $Ti(C_{0.3},N_{0.7})$-20 vol% Ni_3Al samples at 60 N applied load: (a) 0 vol%, (b) 1.25 vol%, (c) 2.5 vol%, (d) 5 vol%, and (e) 10 vol% Mo_2C.

In cermet systems the tribolayer is the region that is formed after three-body debris has undergone substantial attrition due to the wear process [14,33]. It is predominantly composed of oxides from the components that make up the structure of the tribo-pair. Table 7 shows the chemical composition of the various tribolayers formed in the $Ti(C_{0.3},N_{0.7})$ cermets as the amount of Mo_2C was varied, while using an applied load of 60 N, determined using EDS. It is apparent that the O content for all the different compositions remained fairly constant at ~50 at%. The amount of material transferred from the counter face wear ball is also presented in Table 7, which confirms that adhesive wear has occurred during the frictional sliding process.

Table 7. The effects of Mo_2C content on the chemical compositions of the tribolayers formed for $Ti(C_{0.3},N_{0.7})$-20 vol% Ni_3Al at an applied load of 60 N; all compositions are given in atomic %.

Element (KLM Line)	0 vol%	1.25 vol%	2.5 vol%	5 vol%	10 vol%
O (K)	51.78	44.74	55.70	52.50	49.79
C (K)	11.21	12.66	10.23	13.67	17.31
Ti (K)	25.65	24.60	23.89	21.10	16.83
Ni (K)	8.65	6.73	7.15	7.89	10.48
Al (K)	2.40	1.90	2.04	2.25	3.09
W (M)	0.31	0.18	0.17	0.27	0.22
Mo (L)	-	0.30	0.82	2.07	4.37

Figure 48 demonstrates an EDS elemental map for a sample with 10 vol% Mo_2C, subjected to an applied load of 40 N. A distinct transitional boundary of O concentration exists between the wear track and the undamaged microstructure. Outside of the wear track there is no measurable O content in the material. This observation confirms that the O is incorporated into the tribolayer through mechanical attrition, rather than frictional heating leading to oxidation; this is further supported by the relatively low temperature rises (up to ~110°C) noted when testing similar materials in the absence of Mo_2C additions [15,36]. The clean boundary between the wear track and the microstructure indicates that there was no structural damage to the cermet beyond the wear groove itself, which is beneficial for the integrity of the composite. Distinct regions of Mo-rich material are observed in the microstructure, as noted earlier. However, there are also Mo-rich regions apparent within the tribolayer itself. This may suggest that mixing of the constituents may not have been fully complete, resulting in an inhomogeneous tribolayer structure. However, it is also possible that this is simply due to the tribolayer being relatively thin in these regions, with the Mo-rich regions sitting just below the thin tribolayer film. The high average atomic number of this region then still contributes a reasonable X-ray yield during EDS analysis. In support of this latter scenario, the other elemental species do not show such significant evidence of segregation within the tribolayer, while the Mo-rich regions also appear continuous with areas just outside of the wear track.

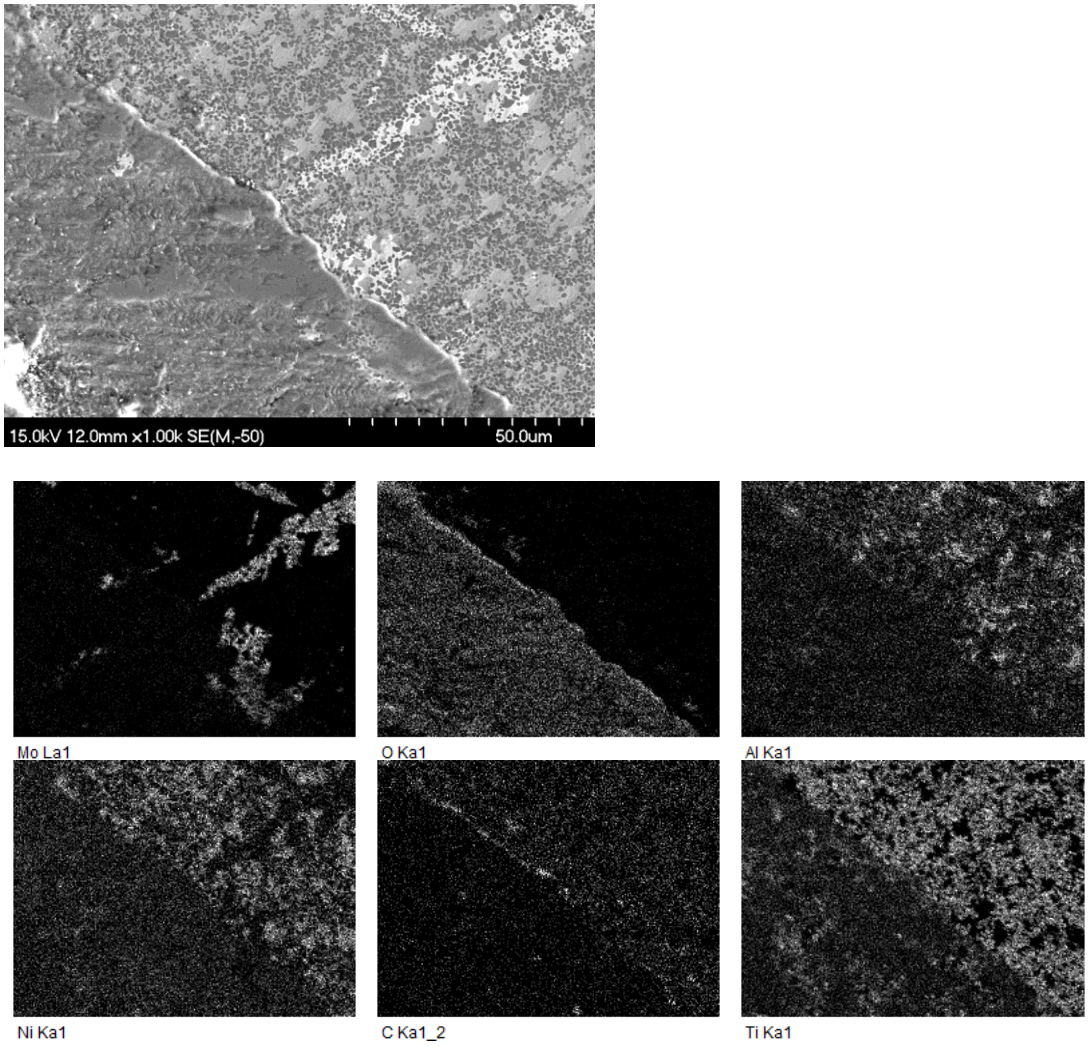

Figure 48. Typical examples of the EDS elemental maps obtained at the edge of a wear track. The cermet composition in this instance was $Ti(C_{0.3},N_{0.7})$-40 vol% Ni_3Al-10 vol% Mo_2C, tested under an applied load of 40 N.

The effect of the applied load on the amount of wear the samples experienced can be seen in Figure 49. While increasing the applied load from 20 to 60 N it can be noticed that the amount of the tribolayer that formed becomes more distinct, along with the amount of spallation that occurs increases. In Figure 49(a) the tribolayer is discontinuous and the boundary is not clear, however as the load is increased to 40 N as seen in Figure 12(b) the layer covers the wear track region clearly and cracking can be noticed within the somewhat smooth layer, with clear areas of spallation occurring. In Figure 49(c) the

amount of cracking inside the tribolayer and the roughness increases dramatically indicating that a more severe amount of wear occurred.

(a) (b)

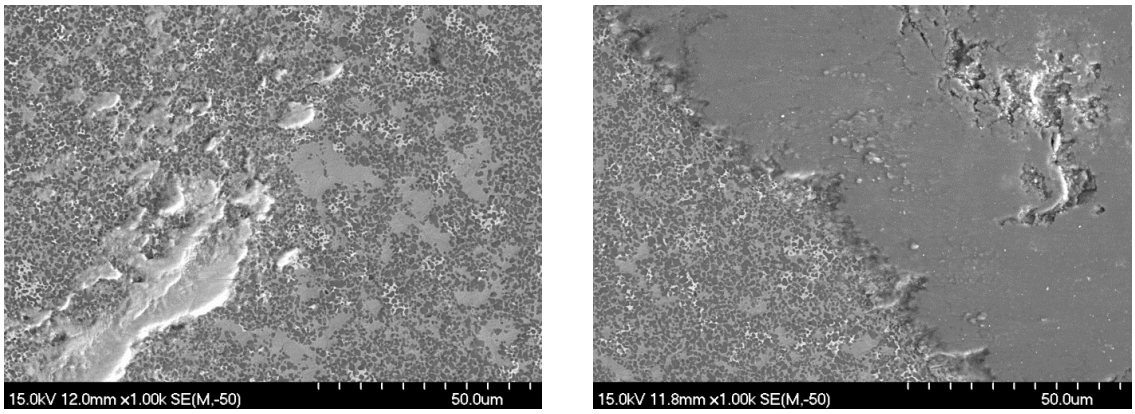

(c)

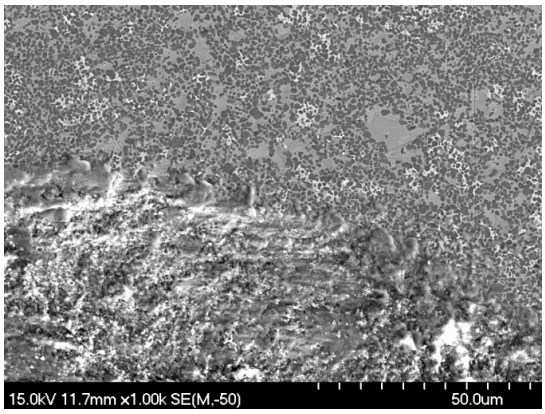

Figure 49. The evolution of the tribolayer while increasing the applied load in samples with 40 vol% Ni_3Al-5 vol% Mo_2C: (a) 20N, (b) 40N, and (c) 60N.

To both quantify the thickness of the tribolayer and assess the presence of subsurface cracking in the microstructure upon wear testing FIB microstructural analysis was completed on a representative sample. In Figure 50 the cross section of a sample with 40 vol% Ni_3Al-10 vol% Mo_2C that was subjected to an applied load of 60N can be seen. Figure 50(a) displays a relatively low magnification back scattered image where the protective W strip along with remnants of the WC-Co wear ball can be noticed spread throughout the tribolayer, which is an indication of adhesive wear. In Figure 50(b) a high magnification image that displays both the thickness of the brittle tribolayer phase and the formation of subsurface cracking in the microstructure of the cermet. This subsurface

cracking further validates the claim that a more severe type of wear occurred in the samples with Mo_2C added when compared to those without as noted in previous work [15].

(a) (b)

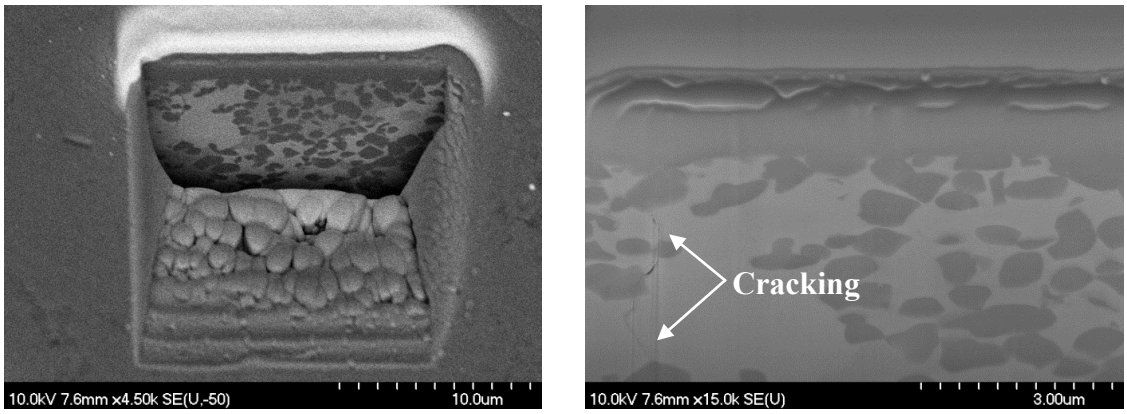

Figure 50. FIB generated section through the tribolayer in $Ti(C_{0.3},N_{0.7})$-40 vol% Ni_3Al-10 vol% Mo_2C after wear testing under a load of 60 N for 120 minutes: (a) Low magnification BSE image showing the staircase cut and remnant W protective layer. (b) Higher magnification, mixed SE/BSE image of the end of the cut showing the tribolayer thickness, wear track profile and cracking in the tribolayer and microstructure.

The WC-6Co counter face spheres were also examined for surface modification after wear testing. Table 8 shows typical examples of the surface compositions of the wear balls, determined using EDS, following testing over the full range of applied loads; for these examples the cermet had 30 vol% Ni_3Al with 2.5 vol% Mo_2C. There is clear evidence of both Ni and Ti transferred over from the cermet samples to the WC-6Co counter face for the higher applied loads (i.e. 40 and 60 N). There are also increasing amounts of O present on the surface of the WC-Co as the applied load is raised. This transfer of material, combined with an increasing O content, presents further evidence of an adhesive wear mechanism becoming dominant during the latter stages of testing.

Table 8. The effects of applied load on the chemical compositions of the tribolayers formed on the WC-6Co counter face sphere. The cermet composition for each test was $Ti(C_{0.3},N_{0.7})$-30 vol% Ni_3Al-2.5 vol% Mo_2C; all compositions are given in atomic %.

Element (KLM Line)	**20N**	**40N**	**60N**
C (K)	49.47	44.81	48.08
O (K)	10.60	22.47	22.69
W (M)	29.79	21.33	18.11
Co (K)	5.40	3.52	2.99
Ni (L)	-	2.76	2.80
Ti (K)	-	1.88	2.13

In terms of the effects of Mo_2C addition on the observed wear modes, the amount added did not appear to have a significant impact. From Table 8 it can be seen that at the applied load of 20 N adhesive wear was not a major factor in the damage to the cermets, as there is essentially no Ni and Ti transferred to the counter face material. However, as the load is increased, to 40 and then 60 N, adhesive wear does become more of a factor, with the presence of transferred material on both the WC-Co balls and the carbonitride cermets, as displayed in Tables 1 and 2. From Figure 49 it is apparent that the transition from two- to three-body abrasive wear primarily occurs between 20 and 40 N, with significantly lower amounts of tribolayer generated at the lowest load. At 60 N adhesive wear is more prevalent, and eventually spalled regions of the relatively thick tribolayer arise in the samples subjected to 40 and 60 N. The overall progression of wear therefore one of two- to three-body wear at the lowest loads, with increasing amounts of adhesive wear at the highest loads due to binder extrusion and fragmentation of the carbonitride grains contributing the formation of a tribolayer.

6.4 Conclusions

High-density $Ti(C_{0.3},N_{0.7})$-Ni_3Al-Mo_2C cermets were successfully manufactured by vacuum sintering. The addition of Mo_2C improved the wettability and densification of the system, as samples prepared in the absence of Mo_2C with 20 vol% Ni_3Al had a relatively poor densification response (~94 % of theoretical). In contrast, the addition of just 1.25 wt% Mo_2C led to sintered densities in excess of 99 % of theoretical. The Mo_2C additions also significantly reduced the average $Ti(C_{0.3},N_{0.7})$ grain size, by lowering the solubility of the carbonitride phase into the Ni_3Al binder. However, with higher Mo_2C contents, an inhomogeneous microstructure developed, with $Ti(C_{0.3},N_{0.7})$-free regions and the formation of a Mo-rich phase whose size depended broadly on the amount of Mo_2C added.

The improved densification from the addition of low volume fractions of Mo_2C also enhanced the hardness and IFR. The hardness of low binder content cermets was predominantly improved through the removal of residual porosity. Some solid solution strengthening of the binder phase may also arise, as there was a small increase in hardness with increasing Mo_2C content for the highest Ni_3Al binder contents. However, this effect disappeared with lower binder contents, and the 20 vol% Ni_3Al cermets actually showed a significant decrease in hardness at the highest Mo_2C contents. This was attributed to progressive replacement of the higher hardness $Ti(C_{0.3},N_{0.7})$ phase. The IFR demonstrated a significant benefit from the addition of low volume fractions of Mo_2C, especially in samples with the higher binder levels. This may again relate to potential solid solution strengthening, increasing the binder yield stress, in combination with slightly improved densification. However, for the highest Ni_3Al content cermets, a further increase in Mo_2C above 2.5 vol% resulted in a significant decrease in the IFR, as the microstructure became less homogeneous, there was an increasing amount of the more brittle Mo-rich phase, and a reduction in the carbonitride grain sizes. Larger grains are normally related to higher IFR values due to the increase in the binder ligament dimensions.

The addition of Mo_2C was demonstrated to have a predominantly detrimental effect on the wear response of the cermets. While the COF was largely independent of Mo_2C volume fraction, the specific wear rates were consistently increased, with the exception of

the most porous cermets prepared without Mo_2C. It was observed that the wear resistance of the samples decreased as the amount of Mo_2C was increased. Initially a transition between two- and three-body abrasive wear was observed, with a subsequent further transition to an adhesive wear mechanism, and the formation of a high O containing tribolayer on both the Ti(C,N) cermets and the WC-6Co counter face. The extent of tribolayer formation increased with applied load.

6.5 References

1] Liao, H., Normand, B., & Coddet, C. (2000). Influence of Coating Microstructure on the Abrasive Wear Resistance of WC/Co Cermet Coatings. *Surface and Coatings Technology*, *124*(2), 235-242.

[2] Zhang, S. (1993). Titanium Carbonitride-Based Cermets - Processes and Properties. *Mat Sci Eng A-Struct. 163*(1), 141-148.

[3] Chuanxian, D., Bingtang, H., & Huiling, L. (1984). Plasma-Sprayed Wear-Resistant Ceramic and Cermet Coating Materials. *Thin Solid Films*, *118*(4), 485-493.

[4] German, R. M. (1985). The Contiguity of Liquid Phase Sintered Microstructures. *Metallurgical Transactions A*, *16*(7), 1247-1252.

[5] Gurland, J. (1966). An Estimate of Contact and Continuity of Dispersions in Opaque Samples. *AIME MET SOC TRANS*, *236*(5), 642-646.

[6] Moskowitz, D., & Humenik Jr, M. (1995). Cemented Titanium Carbide Cutting Tools. *Modern Developments in Powder Metallurgy*. 83-94.

[7] Park, J. K., & Park, S. T. (1999). Densification of TiN-Ni Cermets by Improving Wettability of Liquid Nickel on TiN Grain Surface with Addition of Mo_2C. *International Journal of Refractory Metals and Hard Materials*, *17*(4), 295-298.

[8] Wang, X., He, X., & Guo, H. (2010). Influence of Mo on the Microstructure and Mechanical Properties of TiC-based Cermets. *Rare Metals*, *29*(4), 346-350.

[9] Guo, Z., Xiong, J., Yang, M., Wang, J., Sun, L., Wu, Y., & Xiong, S. (2009). Microstructure and Properties of Ti(C,N)–Mo_2C–Fe Cermets. *International Journal of Refractory Metals and Hard Materials*, *27*(4), 781-783.

[10] LaSalvia, J. C., Kim, D. K., & Meyers, M. A. (1996). Effect of Mo on Microstructure and Mechanical Properties of TiC-Ni-Based Cermets Produced by Combustion Synthesis-Impact Forging Technique. *Materials Science and Engineering: A*, *206*(1), 71-80.

[11] Deevi, S. C., & Sikka, V. K. (1996). Nickel and Iron Aluminides: An overview on Properties, Processing, and Applications. *Intermetallics. 4*(5), 357-375.

[12] Plucknett, K. P., & Becher, P. F. (2001). Processing and Microstructure Development of Titanium Carbide–Nickel Aluminide Composites Prepared by Melt Infiltration/Sintering (MIS). *Journal of the American Ceramic Society*, *84*(1), 55-61.

[13] Lofaj, F., & Kaganovskii, Y. S. (1995). Kinetics of WC-Co Oxidation Accompanied by Swelling. *Journal of materials science*, *30*(7), 1811-1817.

[14] Buchholz, S., Farhat, Z. N., Kipouros, G. J., & Plucknett, K. P. (2013). Reciprocating Wear Response of Ti(C,N)-Ni_3Al Cermets. *Canadian Metallurgical Quarterly*, *52*(1), 69-80.

[15] Stewart,T.,Plucknett,K.P.(2014). The Sliding Wear of TiC and Ti(C,N) Cermets Prepared with a Stoichiometric Ni_3Al Binder. Manuscript submitted for publication.

[16] Mendelson, M. I. (1969). Average Grain Size in Polycrystalline Ceramics. *Journal of the American Ceramic Society, 52*(8), 443-446.

[17] Gurland, J., & Bardzil, P. (1955). Relation of Strength, Composition, and Grain Size of Sintered WC-Co alloys. *J. Metals*, *7*.

[18] Niihara, K., Morena, R., & Hasselman, D. P. H. (1982). Evaluation of KiC of Brittle Solids by the Indentation Method with Low Crack-to-Indent Ratios. *Journal of Materials Science Letter. 1*(1), 13-16.

[19] Lancaster, J. K. (1967). The Influence of Substrate Hardness on the Formation and Endurance of Molybdenum Disulphide Films. *Wear. 10*(2), 103-117.

[20] Giannuzzi, L. A., & Stevie, F. A. (1999). A Review of Focused Ion Beam Milling Techniques for TEM Specimen Preparation. *Micron*, *30*(3), 197-204.

[21] Li, Y., Liu, N., Zhang, X., & Rong, C. (2008). Effect of Mo Addition on the Microstructure and Mechanical Properties of Ultra-Fine Grade TiC–TiN–WC–Mo_2C–Co Cermets. *International Journal of Refractory Metals and Hard Materials*, *26*(3), 190-196.

[22] Liu, N., Xu, Y., Li, Z., Chen, M., Li, G., & Zhang, L. (2003). Influence of Molybdenum Addition on the Microstructure and Mechanical Properties of TiC-Based Cermets with Nano-TiN Modification. *Ceramics International*, *29*(8), 919-925.

[23] Mari, D., Bolognini, S., Feusier, G., Cutard, T., Verdon, C., Viatte, T., & Benoit, W. (2003). TiMoCN Based Cermets: Part I. Morphology and Phase Composition. *International Journal of Refractory Metals and Hard Materials*, *21*(1), 37-46.

[24] Matsubara, H., Shin, S. G., & Sakuma, T. (1991). Growth of Carbide Particles in TiC-Ni and TiC-Mo2C-Ni Cermets During Liquid Phase Sintering. *Materials Transactions JIM*, *32*(10), 951-956.

[25] Engqvist, H., Jacobson, S., & Axén, N. (2002). A Model for the Hardness of Cemented Carbides. *Wear*, *252*(5), 384-393.

[26] Li, Y., Liu, N., Zhang, X., & Rong, C. (2008). Effect of Mo Addition on the Microstructure and Mechanical Properties of Ultra-Fine Grade TiC–TiN–WC–Mo_2C–Co Cermets. *International Journal of Refractory Metals and Hard Materials*, *26*(3), 190-196.

[27] Russias, J., Cardinal, S., Aguni, Y., Fantozzi, G., Bienvenu, K., & Fontaine, J. (2005). Influence of Titanium Nitride Addition on the Microstructure and Mechanical Properties of TiC-Based Cermets. *Int J Refract Met H*. *23*(4), 358-362.

[28] Li, Z. H., Xu, Y. D., & Zhao, Y. (2001). Cutting Properties and Abrasion Mechanism of Ti(C,N) Cermet Cutters. *Journal of Hefei University of Technology*, *24*(6), 1040-1045.

[30] Liu, N., Chao, S., & Huang, X. (2006). Effects of TiC/TiN Addition on the Microstructure and Mechanical Properties of Ultra-Fine Grade Ti (C, N)–Ni Cermets. *Journal of the European Ceramic Society*, *26*(16), 3861-3870.

[31] You, X. Q., Si, T. Z., Liu, N., Ren, P. P., Xu, Y. D., & Feng, J. P. (2005). Effect of Grain Size on Thermal Shock Resistance of Al_2O_3–TiC Ceramics. *Ceramics International*, *31*(1), 33-38.

[32] Ozdemir, O., Zeytin, S., & Bindal, C. (2012). Tribological Properties of Ni_3Al Produced by Pressure-Assisted Volume Combustion Synthesis. *Tribology International*, *53*, 22-27.

[33] Gong, K., Zhou, Z., Shum, P. W., Luo, H., Tian, Z., & Li, C. (2011). Tribological Evaluation on Ni_3Al-Based Alloy and its Composites Under Unlubricated Wear Condition. *Wear*, *270*(3), 195-203.

[34] Onuoha, C. C., Kipouros, G. J., Farhat, Z. N., & Plucknett, K. P. (2013). The Reciprocating Wear Behaviour of TiC-304L Stainless Steel Composites Prepared by Melt Infiltration. *Wear*, *303*(1-2), 321-333.

[35] Bhattacharya, B., & Ray, R. K. (2000). Deformation Behavior of a Ni_3Al (B, Zr) Alloy During Cold Rolling: Part I. Changes in Order and Structure. *Metallurgical and Materials Transactions A*, *31*(12), 3001-3010.

[36] Sikka, V. (1989). Nickel Aluminides-New Advanced Alloys. *Materials and Manufacturing Processes, 4*(1), 1-24.

[37] Pirso, J., Viljus, M., & Letunovits, S. (2004). Sliding Wear of TiC–NiMo Cermets. *Tribology International. 37*(10), 817-824.

7 Conclusions

In the present study the physical properties of TiC and Ti(C,N)-Ni_3Al based cermets, manufactured through a simple reaction sintering process, were examined. Particular attention was given to the wear behavior of the new materials, for the purpose of determining the ideal composition of the bulk powder phase to be later used as a thermal spray coating. Cermets were prepared with the ceramic phases of TiC, Ti($C_{0.7}$,$N_{0.3}$), Ti($C_{0.5}$,$N_{0.5}$) and Ti($C_{0.3}$,$N_{0.7}$), and were sintered at 1550°C for one hour with 20 to 40 vol% Ni_3Al. Using this general processing approach gave cermets with final densities in excess of 98% of theoretical. However, the highest N content Ti(C,N) ceramic phase suffered from relatively poor wetting characteristics, resulting in degraded densification upon sintering for the 20 vol% Ni_3Al binder sample. To alleviate this problem in the high N content samples, a sintering aid was incorporated, in the form of Mo_2C. The Mo_2C was added in various volume percentages (1.25, 2.5, 5 and 10 vol%) and the characteristics of the samples were studied.

The Vickers hardness of the various cermets were determined by applying a 5 kgf load normal to a polished surface, while the indentation fracture resistance (IFR) was determined through the analysis of the cracks formed in the samples after applying loads from 5 to 30 kgf, and assuming a Palmqvist type cracking system, which is typically seen in relatively ductile materials beneath the surface. In general, as the amount of C in the ceramic phase was decreased the hardness of the samples also decreased, for a given vol% of Ni_3Al. In addition, as the amount of the ceramic phase decreased, the hardness also decreased in a nominally linear fashion. In the highest N content samples, the addition of Mo_2C increased the hardness of cermets, reaching a maximum at 2.5 vol% Mo_2C. The increase in hardness was believed to be a combination of two separate phenomena, first the addition of Mo_2C acted as a strengthening aid in the form of solid solution strengthening, secondly the improved densification behavior reduced the porosity seen throughout the samples with the lowest amount of Ni_3Al added. In contrast to the hardness, the IFR increased as the amount of the ceramic phase decreased, this was due to the increasing amount of ductile metallic binder present, which is able to bridge any cracks that form through the microstructure during loading. With the addition of

Mo_2C, the IFR was further increased due to increased bond strength of the phases present in the samples.

The wear responses of the cermets were determined by using a ball on flat sliding geometry, with a WC-Co (6 wt%) counter face. Wear tests were performed at a frequency of 20 Hz, over a range of applied loads from 20 to 60 N, for a test duration of two hours. The predominant modes of wear that were noticed to be occurring in the samples were a combination of two- and three-body abrasive wear, along with adhesive wear. Two-body abrasive wear occurs when two separate bodies come into contact with one another, and where one body is usually harder which wears away the other; in the current system the polished surface of the Ti(C,N)-Ni_3Al cermet was the softer material, while the WC-Co ball was the material that wore away the microstructure. Three-body abrasive wear is very similar to that of two-body, but there is a third separate object introduced into the system, usually a contaminant that slides in between the two solid bodies. A transition from two- to three-body abrasive wear, as the dominant mechanism of wear, was seen to occur between the applied loads of 40 to 60N, after examining the specific wear rates of the materials. Adhesive wear was confirmed through EDS analysis, which showed the transfer of material from one face to the other; small amounts of W were observed throughout the tribolayer on the cermet, and traces of Ni and Ti were also found to be transferred to the surface of the wear balls. The specific wear rates seen in the samples were as low, or lower, when compared to the more conventional cemented carbide systems (i.e. WC-Co) and other TiC based cermet systems, achieving wear rates between 0.5 and $3x10^{-7}$ mm^3/Nm.

In order to quantify the depth of tribolayer that was formed during the wear tests, focused ion beam (FIB) microstructural analysis was performed on several samples; FIB allows site specific micro-machining of the samples, to cut small sections through the tribolayer. It was found that as the applied load was increased, so too did the thickness of the tribolayer that formed. The general structure of the tribolayer was also observed following FIB micro-machining, where it was seen that the tribolayer forms in subsequent plate-like layers, which become more and more compact as the depth of the layer increases.

The addition of Mo_2C had a negative effect on the wear resistance of the materials, where the specific wear rates were seen to increase by nearly an order of magnitude in some cases. The increase in the wear rate was thought to be because of an increasing inhomogeneity in the distribution of the carbonitride phase throughout the microstructure. This occurred in combination with the introduction of a third, Mo-rich, phase, thus helping to generate the inhomogeneous structure in the cermets. The increased severity of wear in the samples with Mo_2C can be seen not only through the increase in specific wear rates, but also from the examination of the cross section wear tracks, where sub-surface cracking was observed that was not seen in the Mo-free samples.

7.1 Suggestions for Future Work

In order to fully understand the wear mechanisms and the transitions that occur in the current cermets, the evolution of the wear tracks should be studied over time, and not only dependent upon the applied load. The duration of the wear testing should be varied from short duration of ~15 minutes to longer times (i.e. several hours), in order to simulate use in service and to create a wear mechanism map where the various transitions of two- to three-body abrasive wear, and adhesive wear, can be clearly seen over time. Another aspect that could be examined to simulate the conditions these materials may be immersed in while in service is that the wear response of the cermets should be tested over a range of elevated temperatures. Since one of the major benefits of using Ni_3Al as the binder phase is the increased strength the intermetallic phase experiences as the temperature is increased from ambient conditions to up to ~1100°C, while other metallic materials would typically see a decrease in their physical properties as the temperature was increased. In addition to the high temperature wear tests, the wear behavior of the samples should be tested in corrosive environments, where it is expected the wear rates would increase but the severity of which is not yet known. Since the ultimate goal of this research was to develop a protective coating to be thermally sprayed on substrates the techniques that should be followed to create a stoichiometrically correct composite particle also need to be determined, in order to create a feedstock powder production method that is both reproducible and low cost. The integrity of this system as a thermal spray coating should then also be observed, in terms of the uniformity and stability of the phases, with particular attention given to the carbonitride phase. In addition to the

microstructural observations, determining the optimal spraying conditions, including the ideal temperature, stand-off distance, fuel mixture, and spraying speed should be determined. Once the processing stages necessary to develop high quality coatings have been established, the properties of the coatings should also be evaluated. This includes the tribological and corrosion responses of the coatings, as well as the physical properties, such as the hardness and the IFR of the coatings. In addition, it will be important to evaluate the fatigue performance of the coated substrates in comparison with uncoated equivalents.

Works Cited

[1] Humenik, M., & Parikh, N. (1956). Cermets, 1. Fundamental concepts related to microstructure and physical properties of cermet systems. *Journal of the American Ceramic Society, 39*(2), 60-63.

[2] Stewart, T., Collier, R. B., Farhat, Z. N., Kipouros, G. J. and Plucknett, K. P. (2010). Melt-infiltration processing of titanium carbide-stainless steel cermets. *Ceramic Engineering and Science Proceedings 31*(8), 97-104.

[3] Pierson, H. O. (1996). *Handbook of Refractory Carbides & Nitrides: Properties, Characteristics, Processing and Apps*. Access Online via Elsevier.

[4] Nuilek, K., Memongkol, N., & Niyomwas, S. (2008). Production of titanium carbide from ilmenite. *Journal of Materials Science*, *30*, 3083-3093.

[5] European Food Safety Authority. (2008). Scientific opinion of the panel of food contact materials, enzymes, flavourings, and processing aids *The ESFA Journal,* (888-890), 1-14.

[6] Koc, R., & Glatzmaier, G. C. (1995). *U.S. Patent No. 5,417,952*. Washington, DC: U.S. Patent and Trademark Office.

[7] LaSalvia, J. C., Kim, D. K., Lipsett, R. A., & Meyers, M. A. (1995). Combustion synthesis in the Ti-C-Ni-Mo system: Part: Micromechanisms. *Metallurgical and Materials Transactions A*, *26*(11), 3001-3009.

[8] Davidson, C. F., Shirts, M. B., & Harbuck, D. D. (1989). *U.S. Patent No. 4,812,301*. Washington, DC: U.S. Patent and Trademark Office.

[9] Zhang, S. (1993). Titanium carbonitride-based cermets: processes and properties. *Materials Science and Engineering: A*, *163*(1), 141-148.

[10] Woo, Y. C., Kang, H. J., & Kim, D. J. (2007). Formation of TiC particle during carbothermal reduction of TiO_2. *Journal of the European Ceramic Society*, *27*(2), 719-722.

[11] Wattanachit W. (2004). *Upgrading ilmenite ore by hydrochloric acid leaching.* (Unpublished MASc). Prince of Songkla University, Hat Yai Thailand.

[12] Yi, H. C., & Moore, J. J. (1990). Self-propagating high-temperature (combustion) synthesis (SHS) of powder-compacted materials. *Journal of materials Science*, *25*(2), 1159-1168.

[13] Gaskell, D. R. (1981). *Introduction to metallurgical thermodynamics* (Vol. 492). New York, NY: Hemisphere Publishing Corporation.

[14] Yeh, C. L., & Chen, Y. D. (2005). Direct formation of titanium carbonitrides by SHS in nitrogen. *Ceramics international*, *31*(5), 719-729.

[15] Yang, Q., Lengauer, W., Koch, T., Scheerer, M., & Smid, I. (2000). Hardness and elastic properties of Ti(C_xN_{1-x}), Zr(C_xN_{1-x}) and Hf(C_xN_{1-x}). *Journal of alloys and compounds*, *309*(1), L5-L9.

[16] Sikka, V. K. (1999). Intermetallic-based high-temperature materials. *CORROSION 99*

[17] Deevi, S. C., & Sikka, V. K. (1996). Nickel and iron aluminides: an overview on properties, processing, and applications. *Intermetallics*, *4*(5), 357-375.

[18] Liu, C. T., & Sikka, V. K. (1986). Nickel aluminides for structural use. *JOM*, *38*(5), 19-21.

[19] Dey, G., Tewari, R., Rao, P., Wadekar, S., & Mukhopadhyay, P. (1993). Precipitation Hardening in Nickel-Copper Base Alloy Monel K 500. *Springer Boston. 24***,** 2709-2719

[20] Liu, C. T., & White, C. L. (1984, January). Design of Ductile Polycrystalline Ni3 Al Alloys. In *MRS Proceedings* (Vol. 39, No. 1). Cambridge University Press.

[21] George, E. P., Liu, C. T., Lin, H., & Pope, D. P. (1995). Environmental Embrittlement and Other Causes of Brittle Grain Boundary Fracture in Ni_3Al. *Materials Science and Engineering: A, 192–193, Part 1*(0), 277-288.

[22] Liu, C., White, C., & Lee, E. (1985). Effect of test environment on ductility and fracture-behaviour of boron doped Ni_3Al at 600°C. *Scripta Metallurgica, 19*(10), 1247-1250.

[23] Liu, C. T., White, C. L., & Horton, J. A. (1985). Effect of boron on grain-boundaries in Ni_3Al. *Acta metallurgica*, *33*(2), 213-229.

[24] P. H. Thornton, R. G. Davies and T. L. Johnston. (1970). The temperature dependence of the flow stress of the γ′ phase based upon Ni_3Al. *Metallurgical and Materials Transactions B, 1*(1), 207-218.

[25] Okamoto, H. (2004). Al-Ni (Aluminum-Nickel). *Journal of Phase Equilibria and Diffusion, 25*(4), 394-394.

[26] Stoloff, N. (1989). Physical and Mechanical Metallurgy of Ni_3Al and its Alloys. *International Materials Reviews, 34*(4), 153-183.

[27] Dey, G. K. (2003). Physical metallurgy of nickel aluminides. *Sadhana*, *28*(1-2), 247-262.

[28] Russias, J., Cardinal, S., Aguni, Y., Fantozzi, G., Bienvenu, K., & Fontaine, J. (2005). Influence of titanium nitride addition on the microstructure and mechanical properties of TiC-based cermets. *International Journal of Refractory Metals and Hard Materials 23*(4), 358-362.

[29] Qi, F., & Kang, S. (1998). A study on microstructural changes in Ti(CN)–NbC–Ni cermets. *Materials Science and Engineering A 251*(1), 276-285.

[30] Nishimura, T. (1985). Some properties of cermet sintered in nitrogen gas. *International Journal of Refractory Metals Hard Materials, 4*(1), 31.

[31] Zhang, H., Yan, J., Zhang, X., & Tang, S. (2006). Properties of titanium carbonitride matrix cermets. *International Journal of Refractory Metals and Hard Materials 24*(3), 236-239.

[32] Cardinal, S., Malchère, A., Garnier, V., & Fantozzi, G. (2009). Microstructure and mechanical properties of TiC-TiN based cermets for tools application. *International Journal of Refractory Metals and Hard Materials 27*(3), 521-527.

[33] Gee, M. G., Reece, M. J., & Roebuck, B. (1992). High resolution electron microscopy of Ti (C, N) cermets. *Journal of Hard Materials(UK)*, *3*(2), 119-142.

[34] Lindahl, P., Mainert, T., Jonsson, H., & Andrén, H. O. (1993). Microstructure and mechanical properties of a (Ti, W, Ta, Mo)(C, N)-(Co, Ni) type cermet. *J. Hard Mater*, *4*, 187-204.

[35] Warren, R. (1968). Microstructural development during the liquid-phase sintering of two-phase alloys, with special reference to the NbC/Co system. *Journal of Materials Science*, *3*(5), 471-485.

[36] Qi, F., & Kang, S. (1998). A study on microstructural changes in Ti(CN)–NbC–Ni cermets. *Materials Science and Engineering A 251*(1), 276-285.

[37] German, R. (1985). The contiguity of liquid phase sintered microstructures. *Metallurgical Transactions A, 16*(7), 1247-1252. [37] Gurland, J. (1966). An estimate of contact and continuity of dispersions in opaque samples. *AIME MET SOC TRANS, 236*(5), 642-646.

[38] Kim, C. S. (2004). *Microstructural-Mechanical Property Relationships in WC-Co Composites* (Doctoral dissertation, Ph. D Tesis. University Pittsburgh, USA. 2004, 214p).

[39] Li, Y., Liu, N., Zhang, X., & Rong, C. (2008). Effect of Mo addition on the microstructure and mechanical properties of ultra-fine grade TiC–TiN–WC–Mo_2C–Co cermets. *International Journal of Refractory Metals and Hard Materials*, *26*(3), 190-196.

[40] LaSalvia, J. C., Kim, D. K., & Meyers, M. A. (1996). Effect of Mo on microstructure and mechanical properties of TiC—Ni-based cermets produced by combustion synthesis—impact forging technique. *Materials Science and Engineering: A*, *206*(1), 71-80.

[41] Mari, D., Bolognini, S., Feusier, G., Cutard, T., Verdon, C., Viatte, T., & Benoit, W. (2003). TiMoCN Based Cermets: Part I. Morphology and Phase Composition. *International Journal of Refractory Metals and Hard Materials*, *21*(1), 37-46.

[42] Engqvist, H., Jacobson, S., & Axén, N. (2002). A Model for the Hardness of Cemented Carbides. *Wear*, *252*(5), 384-393.

[43] Liu, N., Xu, Y., Li, Z., Chen, M., Li, G., & Zhang, L. (2003). Influence of molybdenum addition on the microstructure and mechanical properties of TiC-based cermets with nano-TiN modification. *Ceramics International*, *29*(8), 919-925.

[44] Takagi, K. I. (2001). High tough boride base cermets produced by reaction sintering. *Materials chemistry and physics*, *67*(1), 214-219.

[45] Aoki, K., & Izumi, O. (1979). Improvement in room temperature ductility of the L 12 type intermetallic compound Ni_3Al by boron addition. *Journal of the Japan institute of metals*, *43*(12), 1190-1196.

[46] Koch, C. C., Horton, J. A., Liu, C. T., Cavin, O. B., & Scarbrough, J. O. (1983). Rapid solidification processing, principles and technologies III, R. *National Bureau of Standards*, 264-69.

[47] Schulson, E. M., Weihs, T. P., Baker, I., Frost, H. J., & Horton, J. A. (1986). Grain boundary accommodation of slip in Ni_3Al containing boron. *Acta Metallurgica*, *34*(7), 1395-1399.

[48] Baker, I., Schulson, E. M., Michael, J. R., & Pennycook, S. J. (1990). The effects of both deviation from stoichiometry and boron on grain boundaries in Ni3Al. *Philosophical Magazine B*, *62*(6), 659-676.

[49] George, E. P., Liu, C. T., & Pope, D. P. (1996). Mechanical behavior of Ni_3Al: Effects of environment, strain rate, temperature and boron doping. *Acta materialia*, *44*(5), 1757-1763.

[50] Baker, I., Huang, B., & Schulson, E. M. (1988). The effect of boron on the lattice properties of Ni_3Al. *Acta Metallurgica*, *36*(3), 493-499.

[51] Lee, C., Han, G., Smallman, R., Feng, D., & Lai, J. (1999). The influence of boron-doping on the effectiveness of grain boundary hardening in Ni3Al. *Acta Materialia, 47*(6), 1823-1830.

[52] Schulson, E. M., Weihs, T. P., Baker, I., Frost, H. J., & Horton, J. A. (1986). Grain boundary accommodation of slip in Ni_3Al containing boron. *Acta Metallurgica, 34*(7), 1395-1399.

[53] Upadhyaya, G. S. (1998). Cemented Tungsten Carbides: Production. *Properties, and Testing, Noyes Publication, Westwood, NJ*.

[54] G. H. S. Price, C. J. Smithells, & S. V. Williams. (1938). Sintered alloys: I, copper-nickel-tungsten alloys sintered with a liquid phase present. *J. Inst. Metals,* (62), 239-254.

[55] Parikh, N. M., & Humenik, M. (1957). Cermets: II, Wettability and microstructure studies in liquid-phase sintering. *Journal of the American Ceramic Society*, *40*(9), 315-320.

[56] Gong, J., Wu, J., & Guan, Z. (1999). Examination of the indentation size effect in low-load Vickers hardness testing of ceramics. *Journal of the European Ceramic Society*, *19*(15), 2625-2631.

[57] Vander Voort, G. F., & Lucas, G. M. (1998). Microindentation hardness testing. *Advanced materials & processes*, *154*(3), 21-25.

[58] Shetty, D. K., Wright, I. G., Mincer, P. N., & Clauer, A. H. (1985). Indentation fracture of WC-Co cermets. *Journal of Materials Science*, *20*(5), 1873-1882.

[59] Pickens, J. R., & Gurland, J. (1978). The fracture toughness of WC-Co alloys measured on single-edge notched beam specimens precracked by electron discharge machining. *Materials Science and Engineering*, *33*(1), 135-142.

[60] Frank, F. C., & Lawn, B. R. (1967). On the theory of Hertzian fracture. *Proceedings of the Royal Society of London. Series A. Mathematical and Physical Sciences*, *299*(1458), 291-306.

[61] Anstis, G. R., Chantikul, P., Lawn, B. R., & Marshall, D. B. (1981). A critical evaluation of indentation techniques for measuring fracture toughness: I, direct crack measurements. *Journal of the American Ceramic Society*, *64*(9), 533-538.

[62] Palmqvist, S. (1962). Occurrence of crack formation during Vickers indentation as a measure of the toughness of hard materials. *Arch Eisenhuettenwes*, *33*, 629-333.

[63] Lawn, B. R., Evans, A. G., & Marshall, D. B. (1980). Elastic/plastic indentation damage in ceramics: the median/radial crack system. *Journal of the American Ceramic Society*, *63*(9-10), 574-581.

[64] Warren, R., & Matzke, H. (1983). Indentation testing of a broad range of cemented carbides. In *Science of Hard Materials* (pp. 563-582). Springer US.

[65] Palmqvist, S. (1962). Occurrence of crack formation during vickers indentation as a measure of the toughness of hard metals. *Arch Eisenhuttenwes, 33*, 629-633.

[66] Niihara, K., Morena, R., & Hasselman, D. (1982). Evaluation of Kic of brittle solids by the indentation method with low crack-to-indent ratios. *Journal of Materials Science Letters, 1*(1), 13-16.

[67] Chattopadhyay, R. (2001). *Surface wear: analysis, treatment, and prevention*. ASM International.

[68] Bisson, E. E. (1969). Various modes of wear and their controlling factors. *Evaluation of Wear Testing, ASTM STP*, *446*, 1-22.

[69] Williams, J. A. (2005). Wear and wear particles—some fundamentals. *Tribology International*, *38*(10), 863-870.

[70] Merchant, M. E. (1940). The mechanism of static friction. *Journal of Applied Physics*, *11*(3), 230-230.

[71] Zhao, Y., Maietta, D. M., & Chang, L. (2000). An asperity microcontact model incorporating the transition from elastic deformation to fully plastic flow. *Journal of Tribology*, *122*(1), 86-93.

[72] Friedrich, K. (1986). Erosive wear of polymer surfaces by steel ball blasting. *Journal of materials science*, *21*(9), 3317-3332.

[73] Padhy, M. K., & Saini, R. P. (2008). A review on silt erosion in hydro turbines. *Renewable and Sustainable Energy Reviews*, *12*(7), 1974-1987.

[74] Tewari, U. S., Harsha, A. P., Häger, A. M., & Friedrich, K. (2003). Solid particle erosion of carbon fibre–and glass fibre–epoxy composites. *Composites Science and Technology*, *63*(3), 549-557.

[75] Sınmazçelik, T., & Taşkıran, İ. (2007). Erosive wear behaviour of polyphenylenesulphide (PPS) composites. *Materials & design*, *28*(9), 2471-2477.

[76] Hutchings, I. M., Winter, R. E., & Field, J. E. (1976). Solid particle erosion of metals: the removal of surface material by spherical projectiles. *Proceedings of the Royal Society of London. Series A, Mathematical and Physical Sciences*, 379-392.

[77] Krakhmalev, P. V., Sukumaran, J., & Gåård, A. (2007). Effect of microstructure on edge wear mechanisms in WC–Co. *International Journal of Refractory Metals and Hard Materials*, *25*(2), 171-178.

[78] Pirso, J., Viljus, M., Juhani, K., & Letunovitš, S. (2009). Two-body dry abrasive wear of cermets. *Wear*, *266*(1), 21-29.

[79] Archard, J. F. (1953). Contact and rubbing of flat surfaces. *Journal of applied physics*, *24*(8), 981-988.

[80] Lancaster, J. K. (1967). The influence of substrate hardness on the formation and endurance of molybdenum disulphide films. *Wear*, *10*(2), 103-117.

[81] Gee, M., Gant, A., & Roebuck, B. (2007). Wear mechanisms in abrasion and erosion of WC/Co and related hardmetals. *Wear, 263*(1), 137-148.

[82] Archard, J., & Hirst, W. (1956). The wear of metals under unlubricated conditions. *Proceedings of the Royal Society of London.Series A.Mathematical and Physical Sciences, 236*(1206), 397-410.

[83] Pirso, J., Letunovitš, S., & Viljus, M. (2004). Friction and wear behaviour of cemented carbides. *Wear, 257*(3), 257-265.

[84] Onuoha, C. C., Kipouros, G. J., Farhat, Z. N., & Plucknett, K. P. (2013). The reciprocating wear behaviour of TiC-304L stainless steel composites prepared by melt infiltration. *Wear*.

[85] Buchholz, S., Farhat, Z. N., Kipouros, G. J., & Plucknett, K. P. (2013). Reciprocating wear response of Ti (C, N)-Ni 3 Al cermets. *Canadian Metallurgical Quarterly*, *52*(1), 69-80.

[86] Picraux, S. T., & Pope, L. E. (1984). Tailored surface modification by ion implantation and laser treatment. *Science*, *226*(4675), 615-622.

[87] Bémer, D., Régnier, R., Subra, I., Sutter, B., Lecler, M. T., & Morele, Y. (2010). Ultrafine particles emitted by flame and electric arc guns for thermal spraying of metals. *Annals of occupational hygiene*, *54*(6), 607-614.

[88] Kuroda, S., Kawakita, J., Watanabe, M., & Katanoda, H. (2008). Warm spraying—A novel coating process based on high-velocity impact of solid particles. *Science and technology of advanced materials*, *9*(3), 033002.

[89] Pawlowski, L. (2008). *The science and engineering of thermal spray coatings*. John Wiley & Sons.

[90] DeMasi-Marcin, J. T., & Gupta, D. K. (1994). Protective coatings in the gas turbine engine. *Surface and Coatings Technology*, *68*, 1-9.

[91] Chuanxian, D., Bingtang, H., & Huiling, L. (1984). Plasma-sprayed wear-resistant ceramic and cermet coating materials. *Thin Solid Films*, *118*(4), 485-493.

[92] Schwetzke, R., & Kreye, H. (1999). Microstructure and properties of tungsten carbide coatings sprayed with various high-velocity oxygen fuel spray systems. *Journal of thermal spray technology*, *8*(3), 433-439.

[93] Zum Gahr, K. H. (1987). *Microstructure and wear of materials* (Vol. 10). Elsevier.

[94] Liao, H., Normand, B., & Coddet, C. (2000). Influence of coating microstructure on the abrasive wear resistance of WC/Co cermet coatings. *Surface Coatings Technology, 124*(2-3), 235-242.

[95] Hawthorne, H. M., Arsenault, B., Immarigeon, J. P., Legoux, J. G., & Parameswaran, V. R. (1999). Comparison of slurry and dry erosion behaviour of some HVOF thermal sprayed coatings. *Wear*, *225*, 825-834.

[96] Bolelli, G., Lusvarghi, L., Manfredini, T., Mantini, F. P., & Polini, R. (2007). Comparison between plasma- and HVOF-sprayed ceramic coatings. part I: Microstructure and mechanical properties. *International Journal of Surface Science and Engineering, 1*(1), 38-61.

[97] Mendelson, M. I. (1969). Average grain size in polycrystalline ceramics. *Journal of the American Ceramic Society*, *52*(8), 443-446.